New engine concept development-Multi-body dynamic of valvetrain system and friction assessment

Antonio Turturro – Supervisors: Prof. C. Delprete and L. Magro

contact conjunction in a single analysis framework. This approach is termed by Teodorescu and Votsios [51] 'multi-physics' and they [51] show that this approach yields predictions that conform much closer to experimental findings than the traditional rigid-body dynamics, even at modest camshaft speeds.

On the other hand, the transient analysis works directly with a multi-physical multi-body dynamic model where the rehology model of the oil lubricant is accounted inside the equations of motion. The reason is that the quasi-static solutions, whilst providing valuable design information are insufficient to account for the magnitudes of lubricant films present in regions of zero entraining motion, where the elastic squeeze film motion should be considered which depends on the inclusion of the film thickness history under transient conditions. Therefore, a more complex transient form of analysis is required, such as those reported by Mei and Xie [83], Dowson et al [74] and Ai and Yu [84, 85]. However, all these solutions have been carried out under non-steady conditions, assuming infinite line contact conjunctions between the cam and the follower. Most solutions have been carried out for polynomial cams used in the valve trains in the internal combustion engines, where the speed of entraining motion diminishes at two symmetric locations on either side of the cam nose to the flat-follower contact. At these locations, the inlet lubrication boundary reverses in direction as the speed of entraining motion increases to a finite value. These locations, therefore, are significant in the study of cam to follower lubrication, because the retention of a coherent lubricant film is largely dependent on the squeeze film motion and the entrapment of a volume of lubricant. Furthermore, it has been shown by all the aforementioned authors that the transit time through these regions is very short indeed, resulting in a rapid lubricant replenishment. The analysis carried out by Kushwaha and Ranejat [86] makes use of a modified cycloidal cam, the characteristics of which are described below. A comprehensive study of such a cam has been carried out by Flesser and Ham [87]. They have employed the Dowson and Higginson's [88] regression formula for the central oil film thickness to predict the lubricant film thickness at various locations in a cam cycle, superimposing the effect of pure squeeze action in an infinite line contact solution. The authors have shown that under such quasi-static conditions, the zero films obtained by the latter increase marginally to a finite value. Fessler and Ham [87] have shown that for the modified cycloidal cams, four

New engine concept development-Multi-body dynamic of valvetrain system and friction assessment

Antonio Turturro – Supervisors: Prof. C. Delprete and L. Magro

values of central film thickness minima are obtained. This has been shown in the Kushwaha and Rahnejat [86] transient analysis.

Kushwaha and Rahnejat [86] have been presented a combined solution for multi-body dynamics of a modified cycloidal cam to flat follower with transient lubricated finite line contact conjunction. The solution to the dynamics of the valve train system is undertaken in the Euler frame of reference, which includes valve surge due to the non-linear behaviour of the spring. The elasto-hydrodynamic transient contact conjunction in analysed in each integration step time by simultaneous solution of the Reynolds' equation in space-time co-ordinates with the instantaneous elastic film shape equation, taking into account the generalized contact elasticity for finite line contact geometry. Therefore, the Kushwaha and Rahnejat [86] analysis provides, for the first time, a full transient elasto-hydrodynamic solution of the finite line conjunction of cam to flat-follower, also including the effect of valve spring surge. There are two important elements in the analysis highlighted in that paper: multi-body dynamic analysis of the valve-train system, and the transient elasto-hydrodynamic analysis of cam-flat-follower contact.

III-II Valvetrain characterization

The new engine concept uses a new valvetrain system layout and it need to be analysed. After an in-depth investigation into the engine design environment and the presentation of the integrated methodology to design an exact engine concept to meet the customer requirements, it is quite important to analyse the engine configuration. The engines of the next 15 years have to be able to meet the stringent severe emission regulation with a drastic reduction in the break specific fuel consumption.

At the same time, these future engines should retain their performance level desired in the market. Therefore, the automotive industry will be under pressure to find new technical

New engine concept development-Multi-body dynamic of valvetrain system and friction assessment

Antonio Turturro – Supervisors: Prof. C. Delprete and L. Magro

solutions for enhanced efficiency of the internal combustion engine. One of the most important objectives to increase the efficiency of an internal combustion engine is through reduction of friction. This requires more attention to be paid to conjunctional surface materials and lubricant rheology, in particular, its viscosity. The current strategy is based on moderate contact pressure on the main mechanical couplings. Unfortunately, in the case of the valvetrain system, this strategy is rather dated, because higher performance translates to significant elasto-hydrodynamic pressures, for examples, in the roller-cam lobe contact. These high pressures, in certain case, can lead to fatigue spalling damage of the conjunction. For these reasons, the engine sub-system chosen to analyze in this thesis is the valve train system. The reasons also extend to the multi-scale nature of valve train system and the opportunity to work with multi-body dynamic analysis. Furthermore, the valve train system is one of the key areas to achieve reduction of friction in an engine. It invariably accounts for 6-10% of parasitic losses in an engine, which itself accounts for 1-3% of fuel energy [3]. This is quite significant.

Unfortunately, the valve train analysed in this thesis will only be prototyped after the current work. Therefore, precise data is still not available. Consequently, the data used here is from an existing engine. The valvetrain analyzed is that of the GM 2 litre Euro 4 engine, which is a 4-cylinder, 4-stroke with 4 valves per cylinder. The maximum intermittent, three seconds, engine speed is 5500 rpm and the maximum continuous engine speed is 4500 rpm. The purpose of the analysis is to check kinematic and dynamic behaviour of the valvetrain system. Furthermore, more attention is paid to the contact between the cam lobe and the rocket pivot roller and for this contact some tribology aspects are evaluated. In addition, the mechanical behaviour of the bodies in contact are evaluated.

New engine concept development-Multi-body dynamic of valvetrain system and friction assessment

Antonio Turturro – Supervisors: Prof. C. Delprete and L. Magro

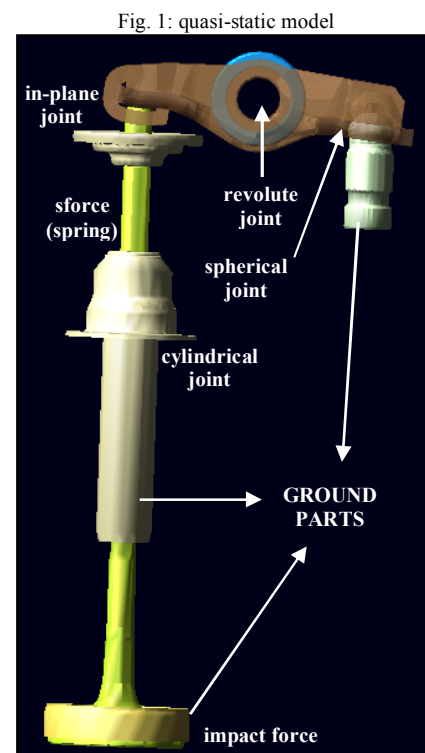## III-III Valvetrain modelling

The valvetrain of GM 2 litre Euro 4 has been modelled both in quasi-static and dynamic modes, using commercially available multi-body dynamic software; MSC ADAMS VIEW 2005 R2. The quasi-static analysis is indispensable in order to decouple from the dynamic inertial effects. This enables appreciation of parameter variations in isolation throughout the engine speed range of $0 - 5500$ rpm.

A quasi-static model and a dynamic model of the valve train system have been made. For academic purposes, only a kinematic and dynamic analysis of the exhaust side is made, with two simplifications with regards to the hydraulic lash adjuster (HLA) and the rocker pivot roller. The HLA has been replaced with a fixed fulcrum and the rocker pivot roller has been replaced with its external ring only. The inertial properties of the original design are kept constant as shown in Figure 1. Moreover, in both the models the back pressure is not taken into account, because this form a part of future model validation though experimentation.

A suitable CAD model of the cam lobe was not available at the time of these analyses. A cam-lobe model was designed in crude, but suitable for purpose of the analyses in the MSC ADAM VIEW 2005 R2 and UGS NX7.5 CAD environments. Further investigation of this aspect will be required later in a proper location.

Fig. 1: quasi-static model

III-IV Quasi-static model

The valve train modelling activity starts with the construction of a quasi-static model. This is depicted in Figure 1. This model is without the cam lobe and determines the motion of the valve through the valve lift profile. In the multi-body model, the

New engine concept development-Multi-body dynamic of valvetrain system and friction assessment

Antonio Turturro – Supervisors: Prof. C. Delprete and L. Magro

ground part constitutes the assembly of: valve ring, valve guide, lower retainer and HLA. The contact between the valve ring and the poppet valve is modelled with as an impact function [89].
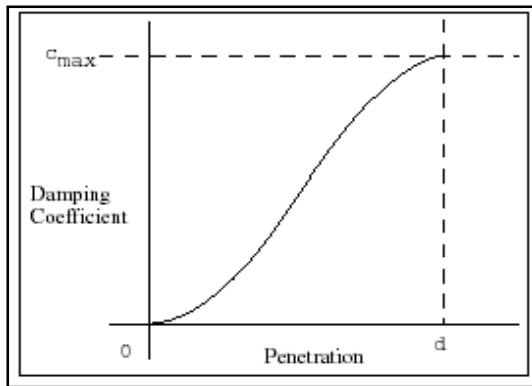
Fig. 2: example illustrating the impact function
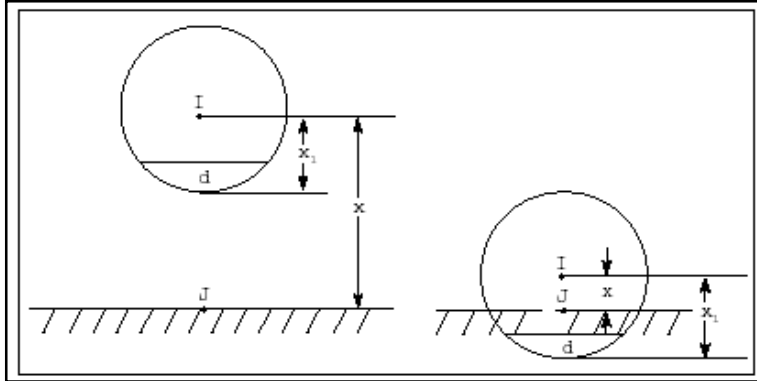
The impact function is activated when the distance between the marker I, the exhaust poppet valve and the marker J: the valve ring falls below a nominal free length: $x_1 = 1.32$

Fig. 3: damping coefficient versus penetration

mm. This constitutes the impact of the two parts. As long as the distance between the I and J markers is greater than x_1, the force remains zero. The force has two components, a spring or stiffness component and a damping or viscous component. The stiffness component is proportional to the stiffness, and it is a function of penetration of the I marker within the free length distance from the J marker. The stiffness component opposes the penetration. The damping component of the force is a function of the speed of penetration (rate of change of deflection). The damping opposes the direction of relative motion. To prevent a discontinuity in the damping force at contact, the damping coefficient is, by definition, a cubic step function of the penetration. Thus, at zero penetration, the damping coefficient is always zero. The damping coefficient achieves its maximum values at a user-defined penetration.

Fig. 4: Adams View interface about the impact function

213

New engine concept development-Multi-body dynamic of valvetrain system and friction assessment

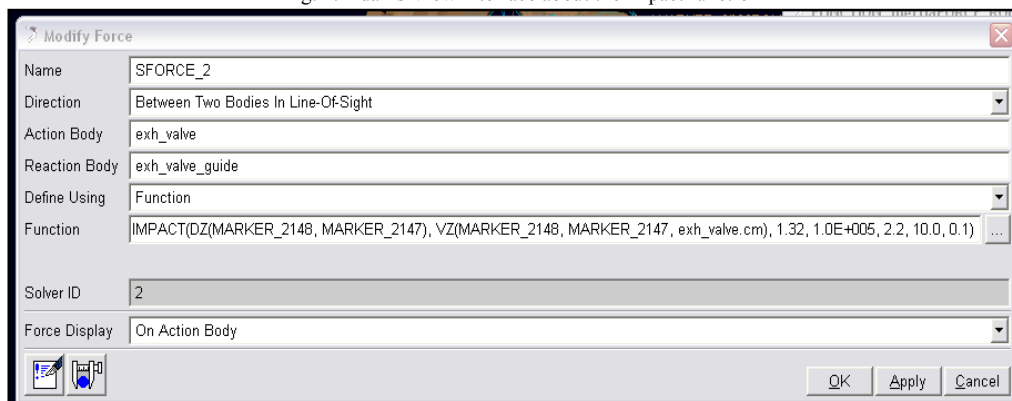Antonio Turturro – Supervisors: Prof. C. Delprete and L. Magro
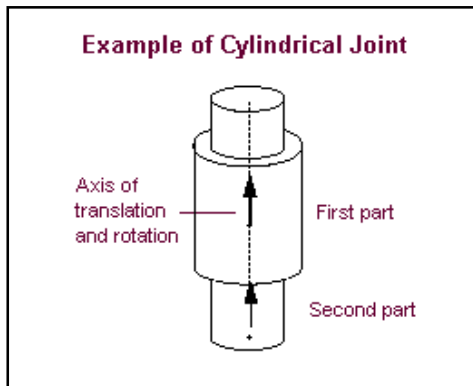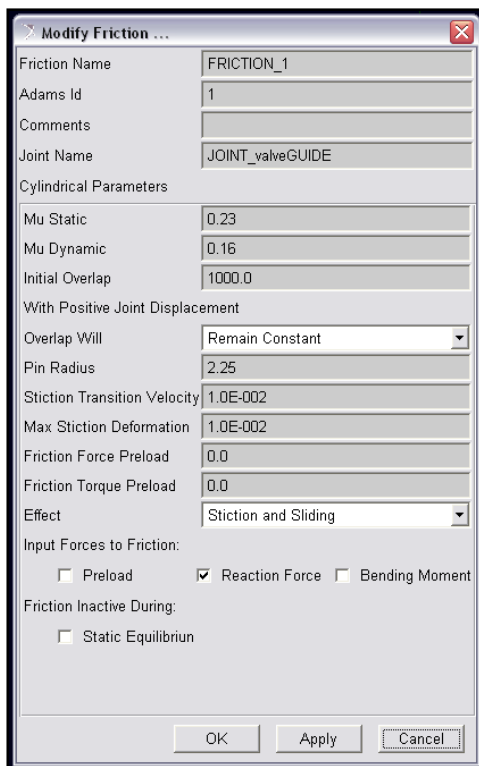
Fig. 5: example of cylindrical joint

Figure 3 is a plot of the damping coefficient versus penetration. The ADAMS View window to define the impact function is shown in the Figure 4. The contact between the valve stem and the valve guide is modelled with a cylindrical joint [90]. This kind of joint allows both relative rotation as well as relative translation of one part with respect to the other (see Figure 5). At cylindrical joint it is added the ADAMS Coulomb friction model to account the friction around the stem valve. Figure 6 depicts the ADAMS View window for the friction parameters in the cylindrical joint. The exhaust valve part includes the poppet valve, the upper retainer and one third of the valve spring mass. The valve spring is a variable pitch coil spring where its mass is significant. Simple analysis shows that one third of its mass should be taken into account in any dynamic analysis. The contact between the rocker pivot pad and the valve tip is modelled with an in-plane joint [90].

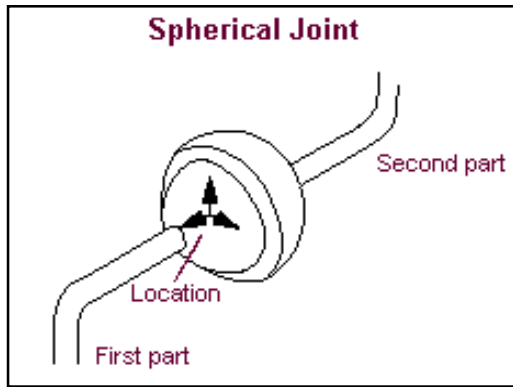Fig. 6: Adams View window for cylindrical joint friction option

Fig. 7: in-plane primitive joint tool
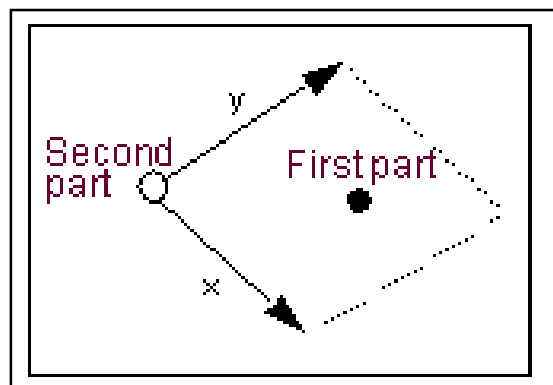
The in-plane joint is a primitive joint and constrains one part so that it can only move in a plane of a second part, as shown in the Figure 7. The solid circle indicates the first part that the joint connects and the hollow circle indicates the second part that the joint connects. Unfortunately, the primitive joints do not allow the lift-off between the rocker pivot pad and the valve tip. However, this type of primitive is used because it is well known that this valve train system is not affected by the lift-off at 5500 rpm engine.

New engine concept development-Multi-body dynamic of valvetrain system and friction assessment

Antonio Turturro – Supervisors: Prof. C. Delprete and L. Magro

Fig. 8: Adams View window to set in-plane joint

Fig. 9: spherical joint tool
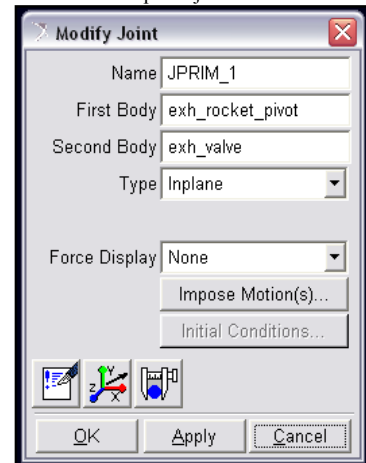
This will be verified with the dynamic model. Figure 8 depicts the ADAMS View window to set the in-plane joint parameters. The motion between the rocker pivot and the roller is modelled by a cylindrical joint as well. Indeed, the motion between the HLA ball and the rocket pivot is modelled with a spherical joint [90]. This kind of joint allows free rotation about a common point of one part with respect to the other part. Figure 9 and Figure 10 depict the spherical joint tool and the ADAMS View window to set the parameters. As it can see in the Figure 10, the spherical joint window has set up the parameters about the friction joint and they correspond to a greased steel surface while the stiction transition velocity and the maximum stiction

Fig. 10: Adams View spherical joint window


deformation are set up as the ADAMS View Solver guidelines. Furthermore, there is also the ball radius and the possibility to use the preload and the reaction force to calculate the spherical joint friction. The ADAMS View Solver uses a relatively simple velocity-based friction model for contact. Figure 11 shows how the

Fig. 11: coefficient of friction varying with slip velocity

New engine concept development-Multi-body dynamic of valvetrain system and friction assessment

Antonio Turturro – Supervisors: Prof. C. Delprete and L. Magro

coefficient of friction varies with slip velocity. The end time of simulation is set as 0.0082 s and the number of steps of simulation is 676. The simulation time takes account the time to complete a cam rotation when the engine speed is 5500 rpm. At this regime the simulation has more than 5 steps every for each cam degree of rotation. The Figure 12 depicts the solver setting about the equation motion integrator.

The dynamic simulations involve the solution of differential and algebraic equations. A basic type of algorithms available in Adams Solver to perform the numerical integration required for dynamic analysis is the stiff solution methods that uses implicit backward difference formulations. The integrator used in this project is the Gear (GSTIFF) that uses backward differentiation formulae and uses fixed coefficients for prediction and correction. The formulation that the GSTIFF work in this project is the SI2 that takes into account constraint derivatives when solving for equations of motion. This process enables the GSTIFF integrator to monitor the integration error of velocity variables, and, therefore, renders highly accurate simulations. Furthermore, the Jacobian matrix remains stable at small step sizes, which in turn increases the stability and robustness of the

Fig. 12: Adams View dynamic solver settings window
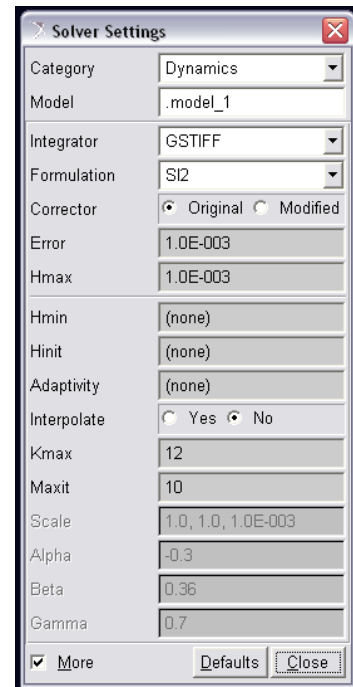
corrector at small step sizes. To sum up the benefits of GSTIFF integrator are: high speed, high accuracy of the system displacements and robust in handling a variety of analysis problems. On the other hand its limitations are: velocity and especially accelerations can have errors - an easy way to minimize these errors is to control HMAX so that the integrator runs at a constant step size and runs consistently at a high order; it can encounter corrector failures at small step sizes - these occur because the Jacobian matrix is a function of the inverse of the step size and becomes ill-conditioned at small steps. About the benefits of SI2 formulation, they are: gives very accurate results especially for velocities and accelerations, usually allows an ERROR that is approximately 10 to 100 times larger than regular GSTIFF to produce the same quality of results, is very robust and stable at small step size, corrector failures that small step sizes cause occur less frequently than with other formulations, corrector failures are typically indicative of a modelling problem and not of a numeric deficiency in the ADAMS Solver software, tracks high frequency oscillations very accurately. On the other

New engine concept development-Multi-body dynamic of valvetrain system and friction assessment

Antonio Turturro – Supervisors: Prof. C. Delprete and L. Magro

hand, the limitations of SI2 formulation are: is typically 25% to 100% slower for most problems than regular GSTIFF, when run with the same error, requires that all velocity inputs be differentiable [91].

The quasi-static model can be summed up by the Tables 1 and 2. The Table 1 highlights the parts that form the quasi-static model, their mass, their inertia and how the parts in the model are defined. The Table 2 highlights the constraints used in the model and, for each link, it shows the number of degree of freedom constrained.

Tab. 1: parts, masses and inertias in the model

Part	Mass	Inertia
Valve ring – ground	-	-
Valve guide and lower retainer- ground	-	-
HLA body – ground	-	-
Exhaust valve and upper retainer + 33% mass spring	49.37 g	IXX 80.52 kg-mm^2 IYY 80.52 kg-mm^2 IZZ 1.42 kg-mm^2
End-pivot rocket arm	33.62 g	IXX 9.80 kg-mm^2 IYY 8.97 kg-mm^2 IZZ 1.60 kg-mm^2
Roller	9.74 g	IXX 0.52 kg-mm^2 IYY 0.35 kg-mm^2 IZZ 0.35 kg-mm^2

Tab. 2: parts, constrains description

Part 1	Part 2	Type	Constrain
Exhaust valve	Valve guide	Cylindrical joint	4
End-pivot rocket arm	Valve guide	Spherical joint	3
End-pivot rocket arm	Valve	In-plane joint	3
Roller	End-pivot rocker arm	Revolute joint	5
			15

Constraints in ADAMS View remove the degrees of freedom from the model by adding algebraic constraint equations to the governing system of differential and algebraic equations.

New engine concept development-Multi-body dynamic of valvetrain system and friction assessment

Antonio Turturro – Supervisors: Prof. C. Delprete and L. Magro

The different constraints in the ADAMS View constraints library remove different types and numbers of degree of freedom. Joints can remove anywhere from one to six degree of freedom, depending on their type. The model verification tool calculates the number of degrees of freedom left in the model. It gives two separate calculations: the Gruebler count by the equation (1), which is a rough estimate of the number of degree of freedom in the model using the Gruebler equation to add up the number of degree of freedom introduced by parts and to subtract the number of degrees of freedom removed through constraints; and the actual number and type of movable parts and constraints in the model that ADAMS Solver determines, after it formulates the model's equations of motion.

$$(1) \qquad nDOF = 6(n-1) - \sum const$$

where: *nDOF* is the number of degrees of freedom of the model or mechanical system; *n* is the number of the parts plus the ground; and *constant* is the number of constraints present in the model. Figure 13 shows the results of the model verification tool and in particular the information about the degrees of freedom and the redundant constraints.

Fig. 13: verify model tool results

```
VERIFY MODEL: .model_1

   4 Gruebler Count (approximate degrees of freedom)
   4 Moving Parts (not including ground)
   1 Cylindrical Joints
   1 Revolute Joints
   1 Spherical Joints
   1 Fixed Joints
   1 Inplane Primitive_Joints
   1 Motions

   4 Degrees of Freedom for .model_1

There are no redundant constraint equations.
```

New engine concept development-Multi-body dynamic of valvetrain system and friction assessment

Antonio Turturro – Supervisors: Prof. C. Delprete and L. Magro

III-V Quasi-static model – Results and discussion

The first group of parameters about the valve train characterization are the valve displacement, the valve velocity and the valve acceleration as shown in the Figure 14.

Fig. 14: exhaust valve displacement, velocity and acceleration
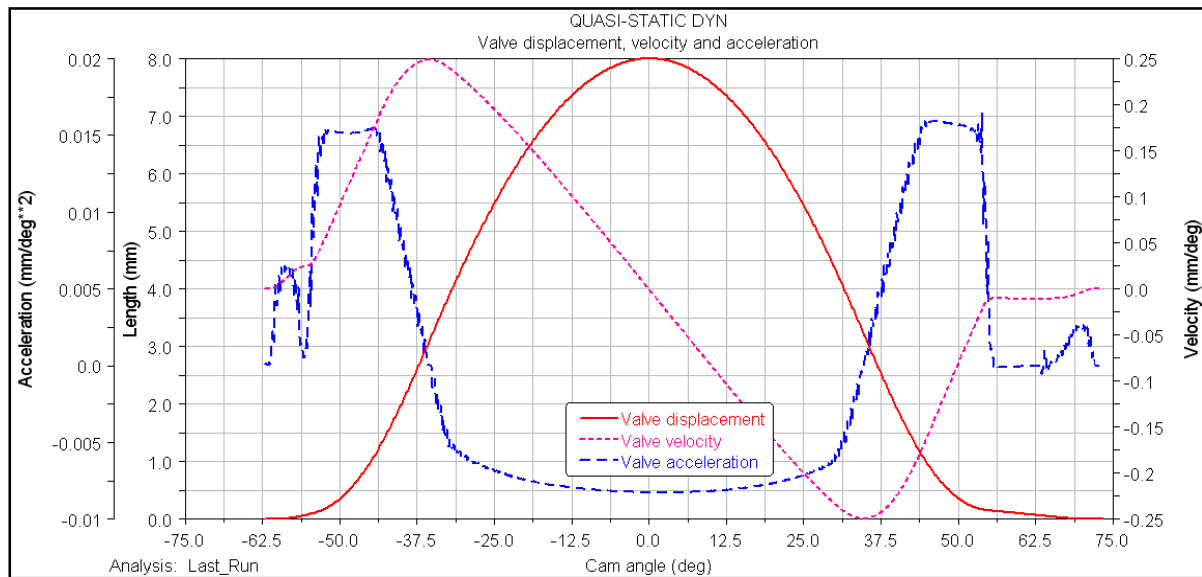
These parameters were calculated at the centre of mass of the exhaust valve. The exhaust valve event takes place between −62 cam degrees and 72 cam degrees. The maximum valve lift is 8 mm at 0 cam degree (representing the nose) in line with the system requirement. The maximum velocity on the open ramp is 0.2485 mm/deg at −35.18 cam deg, while the maximum velocity on the closed ramp is −0.2493 mm/deg at 34.67 cam deg. The maximum velocity on the height opening and closing ramps are, respectively, 0.0240 mm/deg at −55.60 cam deg and −0.0109 mm/deg at 63.69 cam deg. The exhaust valve acceleration at maximum lift is −0.0083 mm/deg^2 at 0 cam deg. The maximum acceleration on valve opening and closing ramps are, respectively, 0.0154 mm/deg^2 at −44.59 cam deg and 0.0160 mm/deg^2 at 45.28 cam deg. Indeed, the maximum acceleration on the opening and closing height ramps are, respectively, 0.0066 mm/deg^2 at −58.79 cam deg and 0.0027 mm/deg^2 at 69.70 cam deg. The valve acceleration changes sign at −35.98 cam deg from positive to negative and vice-versa at 34.77 cam deg. The valve motion respects the requirements. Table 3 provides a summary of all the kinematic and dynamic values of the valve motion.

New engine concept development-Multi-body dynamic of valvetrain system and friction assessment

Antonio Turturro – Supervisors: Prof. C. Delprete and L. Magro

Tab. 3: valve motion parameters

Parameter	Value	Angle [cam deg]
Exhaust event	134 cam deg	−62 to 72
Max valve lift	8 mm	0
Max open height ramp velocity	0.0240 mm/deg	−55.60
Max open ramp velocity	0.2485 mm/deg	−35.18
Max closed ramp velocity	0.2493 mm/deg	34.67
Max closed height ramp velocity	−0.0109 mm/deg	63.69
Max open height ramp acceleration	0.0066 mm/deg^2	−58.79
Max open ramp acceleration	0.0154 mm/deg^2	−44.59
Acceleration at max valve lift	−0.0083 mm/deg^2	0
Max closed ramp acceleration	0.0160 mm/deg^2	45.28
Max closed height ramp acceleration	0.0027 mm/deg^2	69.70

The next group of parameters are related to the force acting on the system, including the spring force, the inertia force of valve body and the contact load at the valve tip. The spring force comprises both the elastic load and the preload. It is inserted in the model as an Akima spline, as shown in the Figure 15. In this way, the spring behaviour reflects exactly the real spring characteristics. The theoretical working range length of the spring is from 24 mm at the valve opening position to 32 mm at valve closing position. The inertia force F_i is evaluated with the equation (2):

$$(2) \qquad F_i = a\left(m_V + \frac{1}{3}m_S\right)$$

where a is the valve acceleration, $m_V = 40.23$ g is the valve mass and $m_S = 27.42$ g is the spring mass. The valve mass comprises its mass and that of the upper retainer and semi-cones mass. Then, using the spring F_S and the inertia force F_i, and this is the contact load at valve tip W is obtained from the equation (3):

New engine concept development-Multi-body dynamic of valvetrain system and friction assessment

Antonio Turturro – Supervisors: Prof. C. Delprete and L. Magro

(3) $$W = F_s - F_i$$
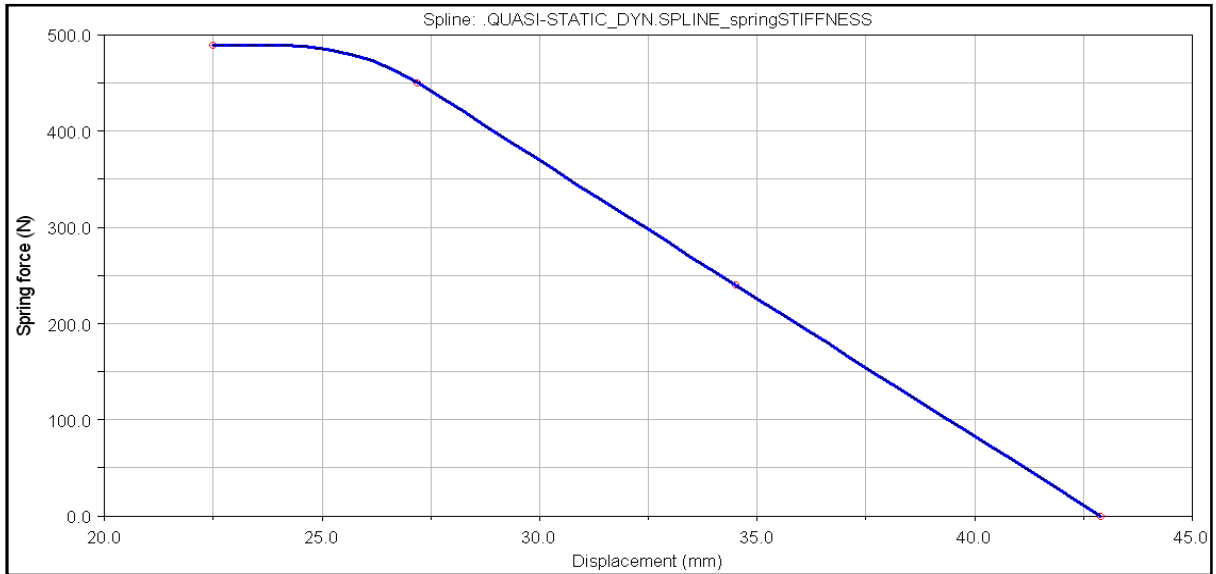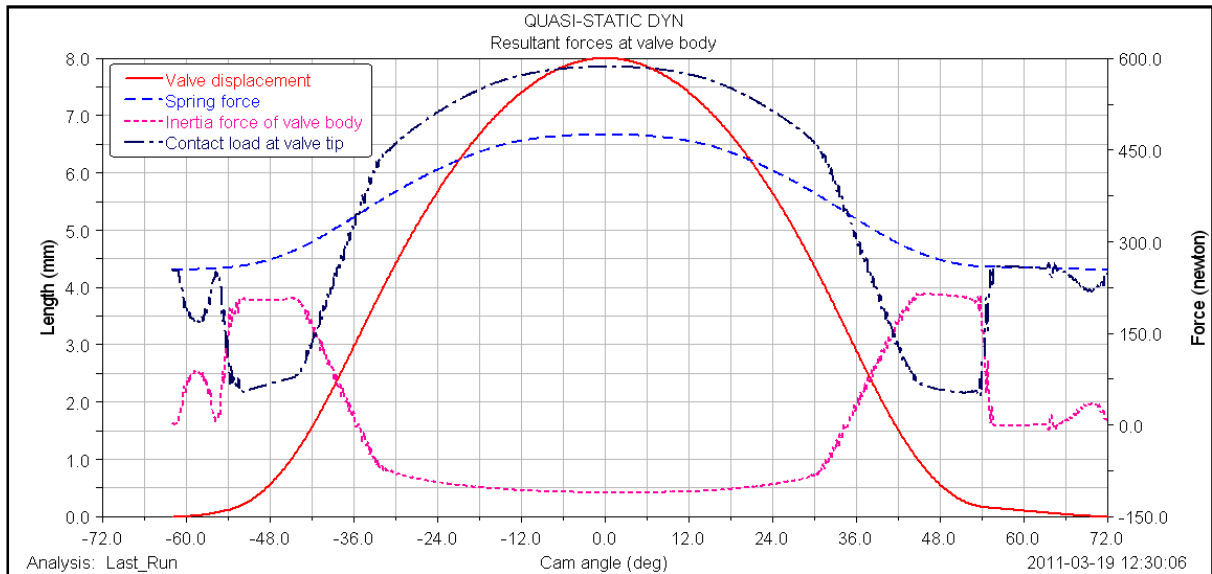
Fig. 15: spring characterization

Fig. 16: force resultant at valve body

The results of this group of parameters are depicted in the Figure 16. First of all, Figure 16 highlights the marginal force of the spring that graphically corresponds at the area amid the spring force (blue line) and the inertia force at valve surface (magenta line). The spring force for valve closing and opening positions are, respectively, 254.15 N and 475.18 N. Unfortunately, these values are slightly over the requirements: the spring force at the closing position is 0.85% over the specification and the spring force at opening position

New engine concept development-Multi-body dynamic of valvetrain system and friction assessment

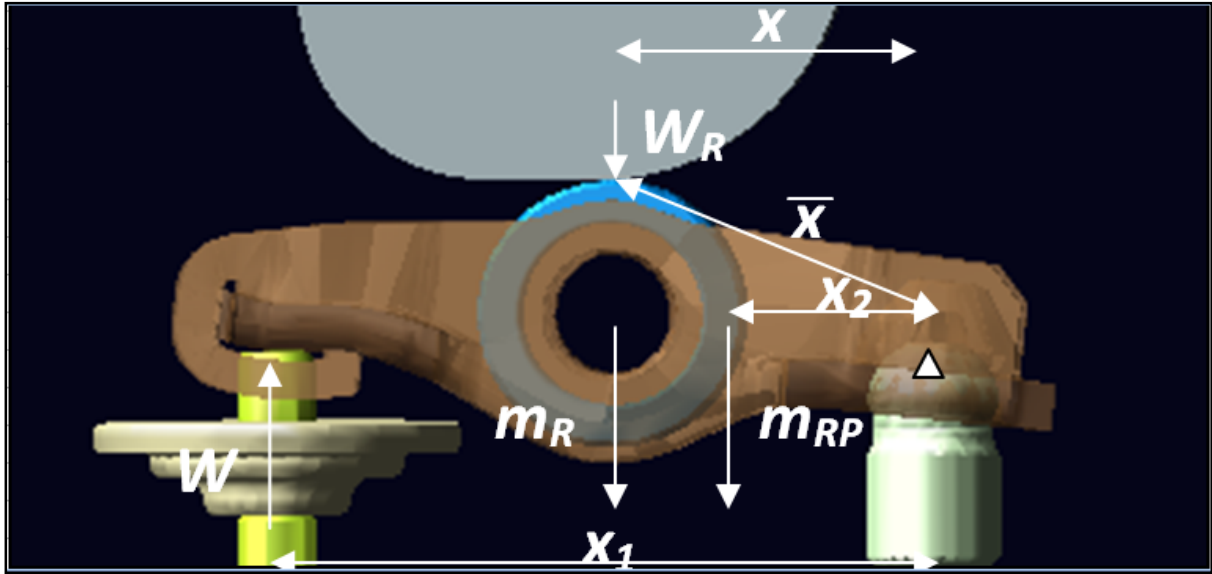Antonio Turturro – Supervisors: Prof. C. Delprete and L. Magro

correspondingly is 1.10% over the specification. The maximum valve inertial force on the valve opening and closing height ramps are, respectively, 88.14 N at -58.80 cam deg and 35.96 N at 69.70 cam deg, while the maximum inertia force on the valve opening and closing ramps are, respectively, 207.56 N at −44.59 cam deg and 215.38 N at 45.28 cam deg. At the end, the inertia force at maximum valve lift is −110.76 N at 0 cam deg, negative indicating direction of force. The inertia force changes sign at −35.98 cam deg from positive to negative and vice-versa at 34.77 cam deg, as ascertained from the valve acceleration curve. The maximum contact load at valve tip is 586.18 N at maximum valve lift. The Table 4 sums up the values of the forces acting on the valve body.

Tab. 4: valve body resultant force parameters

Parameter at valve body	Value	Angle [cam deg]
Spring force at valve closed position	254.15 N	Outside 73 to −63
Spring force at valve open position	475.18 N	0
Max inertia force at open height ramp	88.14 N	−58.80
Max inertia force at open ramp	207.56 N	−44.59
Max inertia force at max valve lift	−110.76 N	0
Max inertia force at closed ramp	215.38 N	45.28
Max inertia force at closed height ramp	35.96 N	69.70
Inertia changes sign	Positive to negative	−35.98
Inertia changes sign	Negative to positive	34.77

The next step and parameters group is the contact load at the rocker pivot roller. It is calculated by a free body equation of the rocker pivot as seen in the Figure 17.

New engine concept development-Multi-body dynamic of valvetrain system and friction assessment

Antonio Turturro – Supervisors: Prof. C. Delprete and L. Magro

Fig. 17: free body scheme of end-rocket pivot

The contact load at the valve tip W by a free body diagram of the rocker pivot is moved onto the roller where physically there is the generated force. So the contact force at roller is W_R [92]:

$$(4) \qquad W_R \bar{x} = W x_1 - m_R x^2 \ddot{\theta} - m_{RP} x_2^2 \ddot{\theta}$$

where m_R = 21.49 g is the mass of the roller, m_{RP} = 33.62 g the mass of the rocker pivot, x_1 = 41.63 mm the distance between HLA fulcrum (centre of the HLA sphere) and valve tip, x = 20.10 mm the distance between HLA fulcrum and roller centre, x_2 = 18.87 mm the distance between HLA fulcrum and the rocket pivot centre of mass, $\bar{x}$ the distance between the contact point and the HLA fulcrum and it is a variable value with the pressure angle α, $\ddot{\theta}$ the rocker pivot angular acceleration. The mass of the roller m_R is the same as the original one, with the central and radial pins. Actually, the distance between the HLA fulcrum and the valve tip x_1 is variable, as it is stated by Wang [93], due to the fact that the valve stem follows a line while the end-pivot rocker arm follows a circumferential arc. However, its variability is around 0.4 mm and for this reason, it is decided to keep it constant. The distance between the contact point and the HLA fulcrum $\bar{x}$ is introduced in the quasi-static model as an input by a spline as depicted in the Figure 18.

New engine concept development-Multi-body dynamic of valvetrain system and friction assessment

Antonio Turturro – Supervisors: Prof. C. Delprete and L. Magro

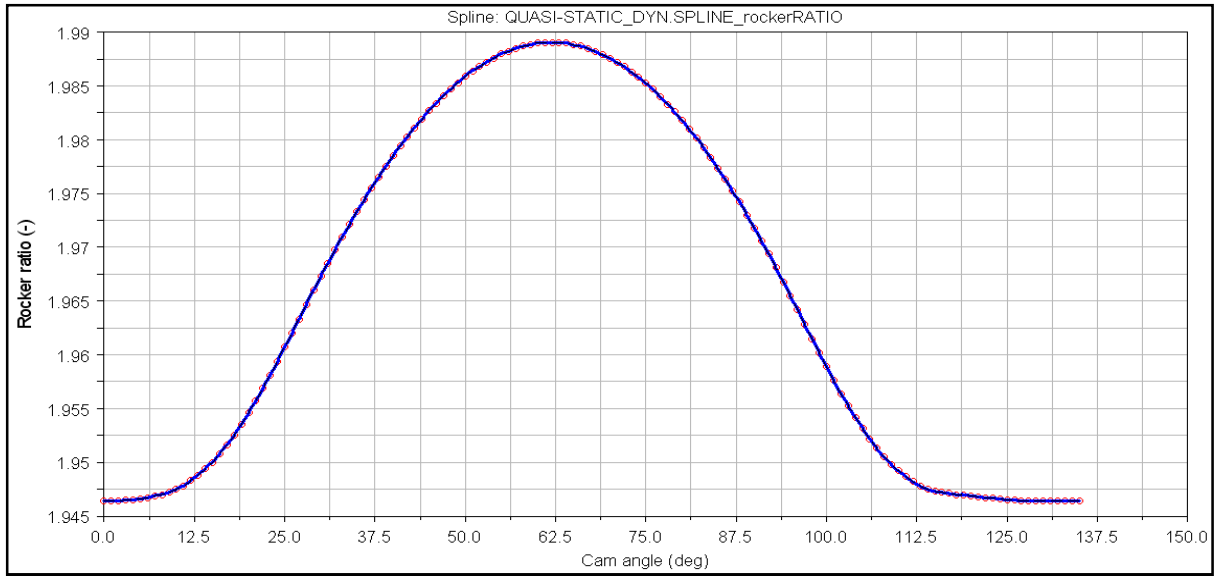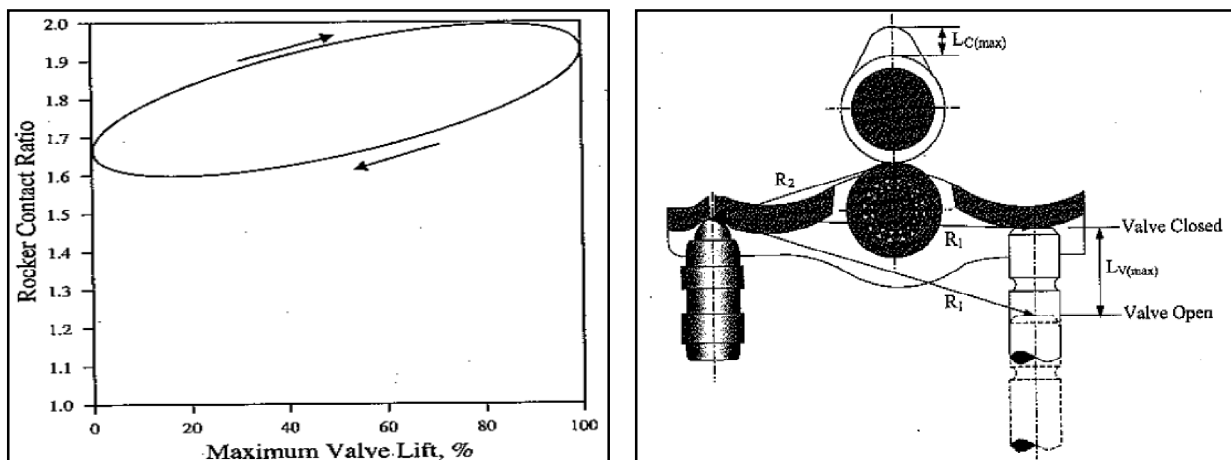Fig. 18: rocker ratio versus cam angle of valve event

Figure 18 shows the rocker arm ratio versus the cam angle of the valve event. The rocker ratio is the ratio between the valve lift and the cam lift, or in the same way, the ratio between the distance from the rocker pivot centre to the valve centreline at valve tip x_1 and the distance from the rocker pivot centre to the cam/follower contact point $\bar{x}$ (see Figure 19).

$$(5) \qquad Rocker\ ratio = \frac{x_1}{\bar{x}}$$

Fig. 19: instantaneous rocker ratios for end-pivot arms – (right) end-pivot rocker arm, (left) change of rocker ratio versus percentage of valve

New engine concept development-Multi-body dynamic of valvetrain system and friction assessment

Antonio Turturro – Supervisors: Prof. C. Delprete and L. Magro

Usually, the rocker ratio is plotted as a function of the percentage of the valve lift, but in this case, it is used as the rocker arm ratio versus the cam angle event. Finally, the resultant forces at roller/cam contact are depicted in the Figure 20.
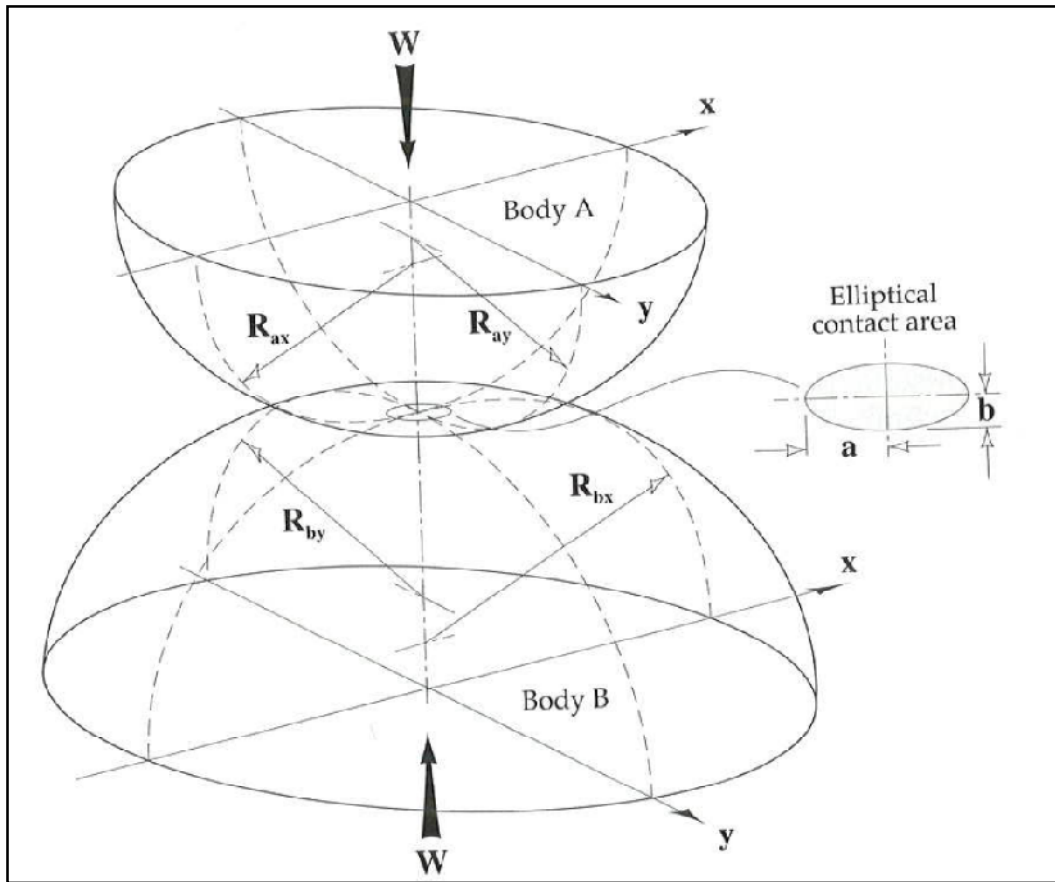
Fig. 20: resultant forces at end-pivot rocker arm
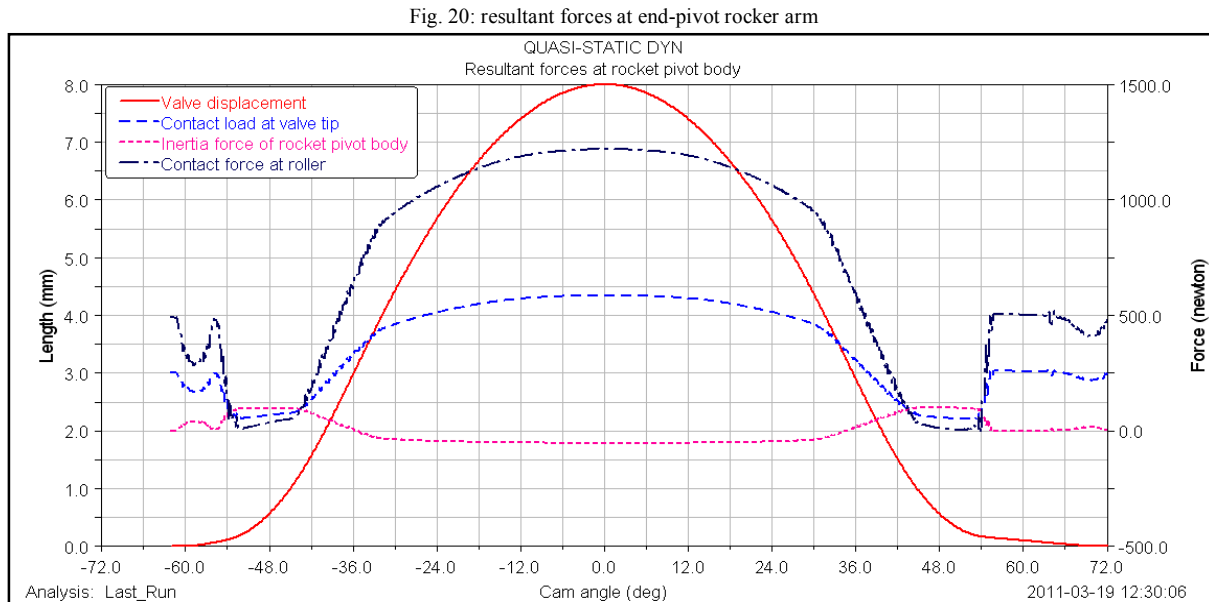
The maximum inertia force at rocker arm on the opening and closing height ramps are, respectively, 41.41 N at −58.80 cam deg and 16.86 at 69.90 cam deg. Indeed, the maximum inertia force on rocker arm on the opening and closing ramp are, respectively, 97.79 N at −44.59 cam deg and 101.43 N at 45.28 cam deg. While the maximum inertia force on rocker arm at the maximum cam lift is −53.18 N at 0 cam deg. The peaks of the inertia force at rocker arm follow that one of the inertia force of the valve body and, of course, the valve acceleration curve. The maximum contact load at roller cam interface is 1219 N at the maximum cam lift. Table 5 sums up the resultant forces values at end-pivot rocket arm.

New engine concept development-Multi-body dynamic of valvetrain system and friction assessment

Antonio Turturro – Supervisors: Prof. C. Delprete and L. Magro

Tab. 5: end-pivot rocker arm force values

Parameter at rocker arm	Value	Angle [cam deg]
Max inertia force at open height ramp	41.41 N	−58.80
Max inertia force at open ramp	97.79 N	−44.59
Max inertia force at max cam lift	−53.18	0
Max inertia force at closed ramp	101.43 N	45.28
Max inertia force at height closed ramp	16.86 N	69.90
Inertia change sign	Positive to negative	−35.98
Inertia change sign	Negative to positive	34.77
Max contact load at max cam lift	1219 N	0

The equivalent or reduced radius of curvature is analysed [91, 94]. The shape of the contact area depends on the shape (curvature) of the both surfaces in mutual approach. The curvature of this body could be convex, flat or concave: it depends on the instantaneous radius of curvature of the two surfaces of the contacting body. The convention to evaluate the sign of equivalent radius of curvature is that convex surfaces possess positive curvatures and concave surfaces possess negative curvatures. There is a general rule that can be applied to discriminate the sign of surfaces curvature: if the centres of curvatures lie in the opposite sides of the line of contact then the curvature is positive, if they lie in the same side of the contact then the concave radius is negative. The general case of two elastic bodies with convex surfaces in contact was originally considered by Hertz in 1881 and is shown in the Figure 21.

New engine concept development-Multi-body dynamic of valvetrain system and friction assessment

Antonio Turturro – Supervisors: Prof. C. Delprete and L. Magro

Fig. 21: geometry of two elastic bodies with convex surfaces in contact
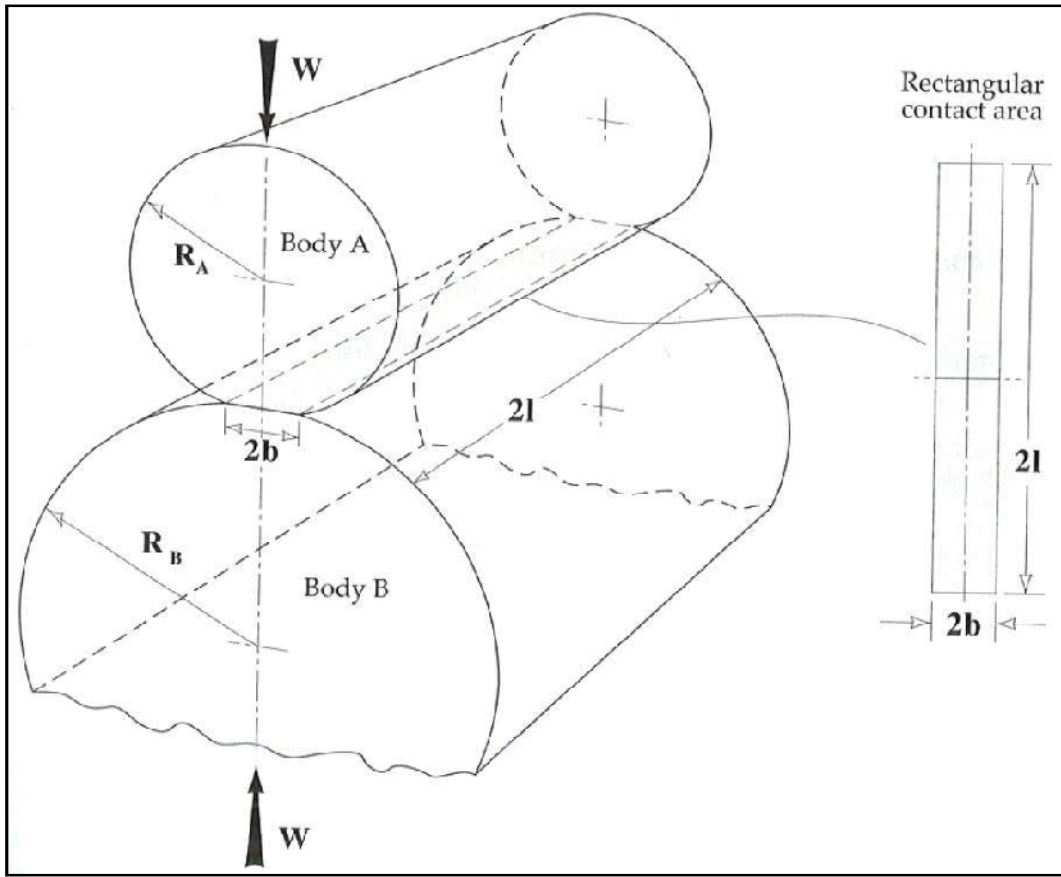

In this case, the reduced radius of curvature is defined as:

$$(6) \qquad \frac{1}{R} = \frac{1}{R_x} + \frac{1}{R_y} = \frac{1}{R_{ax}} + \frac{1}{R_{bx}} + \frac{1}{R_{ay}} + \frac{1}{R_{by}}$$

where: R_x is the reduced radius of curvature in the x direction in m, R_y the reduced radius of curvature in the y direction in m, R_{ax} the radius of curvature of body a in the x direction in m, R_{ay} the radius of curvature of body a in the y direction in m, R_{bx} the radius of curvature of body b in the x direction in m, R_{by} the radius of curvature of body b in the y direction in m.

In our case, the body geometry of the cam lobe and the end-pivot rocker arm roller is idealized, for every step, as two instantaneous cylinders in contact. Than the case considered to calculate the equivalent radius of curvature is the contact between two parallel cylinders [94]. The geometry of parallel cylinders in contact is shown in Figure 22.

New engine concept development-Multi-body dynamic of valvetrain system and friction assessment

Antonio Turturro – Supervisors: Prof. C. Delprete and L. Magro

Fig. 22: geometry of the contact between two parallel cylinders

Substituting into equation (6) yields:

(7)
$$\frac{1}{R} = \frac{1}{R_x} + \frac{1}{R_y} = \frac{1}{R_r} + \frac{1}{R_l} + \frac{1}{\infty} + \frac{1}{\infty} = \frac{1}{R_r} + \frac{1}{R_l}$$

and

(8)
$$\frac{1}{R_x} = \frac{1}{R_r} + \frac{1}{R_l}$$

(9)
$$\frac{1}{R_y} = 0$$

where: R_r the radius of curvature of the roller as 8.5 mm; R_l the radius of curvature of the cam lobe in mm.

As it can be seen one can suppose the radius of curvature of both the roller and the cam lobe in the y direction to be infinite; i.e. perfectly flat surface. The quasi-static model works

New engine concept development-Multi-body dynamic of valvetrain system and friction assessment

Antonio Turturro – Supervisors: Prof. C. Delprete and L. Magro

without the cam lobe, then the radius of curvature of the cam lobe is introduced into the model as an input by a cubic spline, fitted by the Akima method as shown in Figure 23.

Fig. 23: instant radius of curvature of the cam lobe
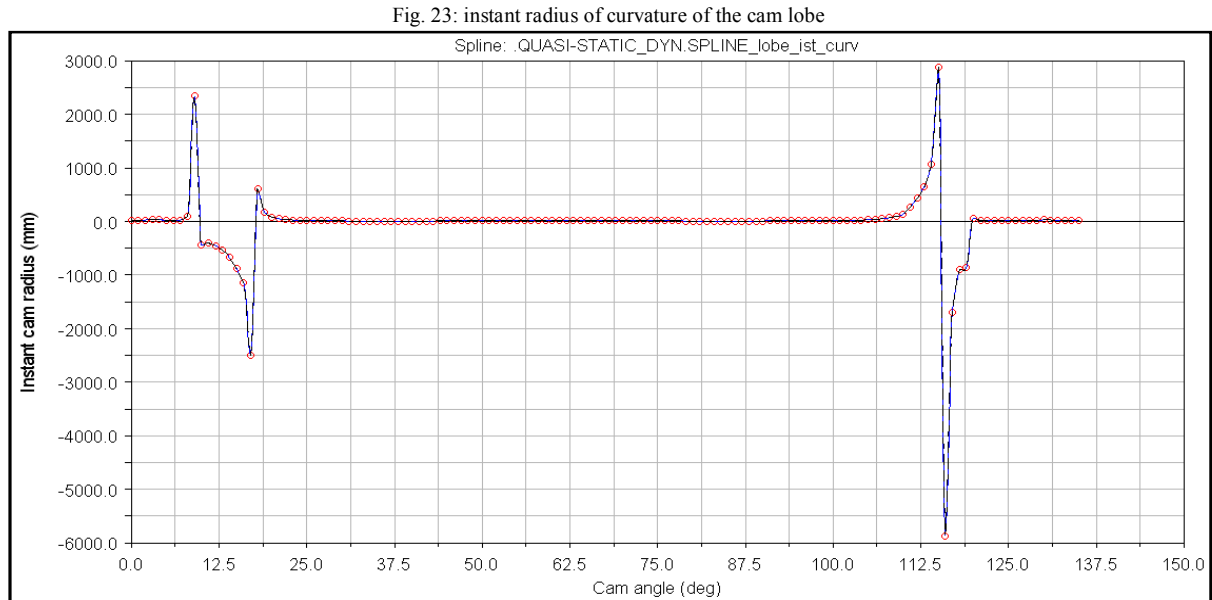
As it can see, the cam lobe profile present two areas where the surface is concave and it happens, respectively, at the end of the opening and closing ramps. It can be supposed that the function of the concave surface is strongly related to the oil film formation, where inlet reversals would otherwise result in the depletion of an oil film. It should be noted that were it not for these concavities, the surface velocity would go through a reversal in these locations. This means no entraining motion, and one can see from Grubin's equation that no film would form. The maximum positive and negative radii of curvature of the height opening ramp are, respectively, 2352.88 mm at −53 cam deg and −2500.85 mm at −44.97 cam deg. Indeed, the maximum positive and negative radii of curvature of the height closing ramps are, respectively, 2873.92 mm at 53 cam deg and −5875.33 mm at 54 cam deg. At the end, the radius of curvature at max cam lift is 10.96 mm at 0 cam deg. The radius of curvature of the cam lobe at height open ramp changes its sign from positive to negative at −52.27 cam deg and vice-versa at −44.3 cam deg. While the radius of curvature of the cam lobe at height closing ramp changes its sign from positive to negative at 53.41 cam deg and vice-versa at 57.86 cam deg. The Table 6 sums up the relevant radius of curvature of the cam lobe.

New engine concept development-Multi-body dynamic of valvetrain system and friction assessment

Antonio Turturro – Supervisors: Prof. C. Delprete and L. Magro

Tab. 6: relevant cam lobe radius of curvature

Radius of curvature	Value [mm]	Angle [cam deg]
Max positive radius at height open ramp	2352.88	−53
Max negative radius at height open ramp	−2500.85	−44.97
Radius at max cam lift	10.96	0
Max positive radius at height closed ramp	2873.92	53
Max negative radius at height closed ramp	−5875.33	54
Radius changes sign at height open ramp	Positive to negative	−52.27
Radius changes sign at height open ramp	Negative to positive	−44.3
Radius changes sign at height closed ramp	Positive to negative	53.41
Radius changes sign at height closed ramp	Negative to positive	57.86

The equivalent or reduced radius of the contact is evaluated and plotted in the Figure 24.

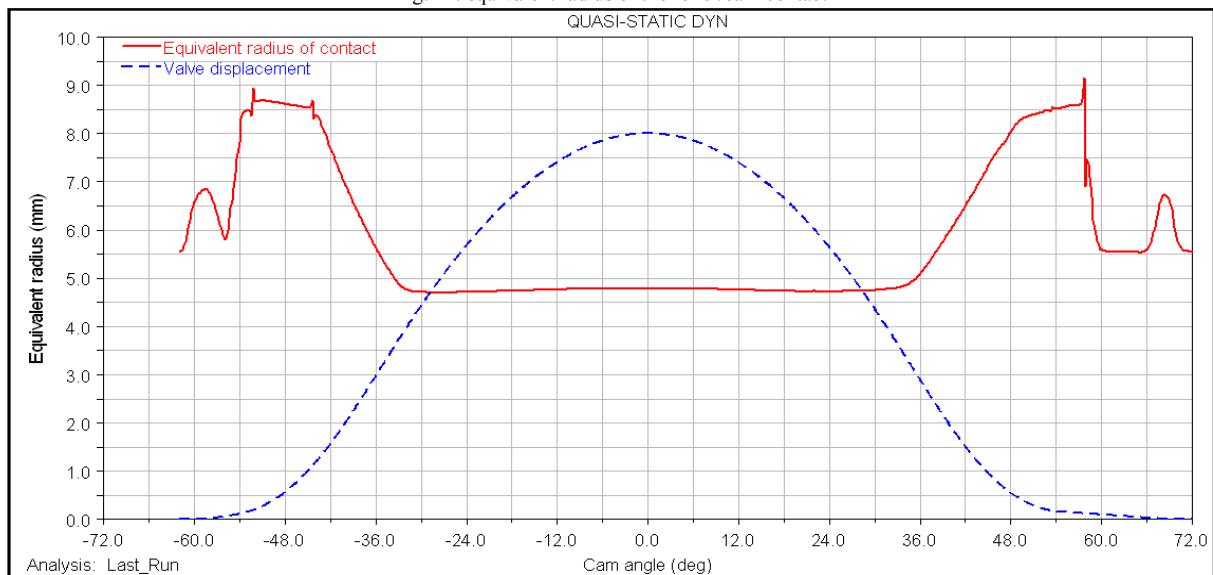Fig. 24: equivalent radius of the roller/cam contact

Figure 24 presents both the equivalent radius of contact and the valve displacement for comparison purposes. The equivalent radius of curvature at maximum valve lift is 4.79 mm at 0 cam deg and it keeps pretty constant. The maximum radii of curvature of both the opening and closing ramps are, respectively, 8.67 at −52.19 cam deg and 8.94 at 57.69 cam deg. Indeed, the maximum equivalent radii of contact, respectively, at height opening ramp and at

New engine concept development-Multi-body dynamic of valvetrain system and friction assessment

Antonio Turturro – Supervisors: Prof. C. Delprete and L. Magro

height closing ramp are: 6.84 mm at −59 cam deg and 6.72 mm at 68.30 cam deg. Table 7 sums up the relevant equivalent radii of the roller cam contact.

Tab. 7: relevant equivalent radius of roller/cam lobe contact

Reduced radius of curvature	Value [mm]	Angle [cam deg]
Max radius at height open ramp	6.84	−59
Max radius at open ramp	8.67	−52.19
Radius at max cam lift	4.79	0
Max radius at closed ramp	8.94	57.69
Max radius at height closed ramp	6.72	68.30

The reduced Young's modulus E is calculated by the equation (10):

(10)
$$\frac{1}{E} = \frac{1-\nu_l^2}{E_l} + \frac{1-\nu_r^2}{E_r}$$

where: E_l and E_r are respectively the Young's modules of the cam lobe and the roller. In particular, this data are unknown and according to Wang [93] it is decided to set them up at 207000 MPa; ν_l and ν_r are respectively the Poisson's ratio for the cam and the roller. These are, according to Wang [93] 0.28. Finally, the reduced Young's modulus for the contact becomes 224609 MPa.

The full length of the roller - cam contact L is the net length of the roller that means the width of the roller minus the edge chamfer. This is 10.5 mm.

The next group of parameters are related to the contact area A [73, 93, 94]. First of all, the contact between the roller and the cam lobe is modelled by the contact of two cylinders which a constant roller radius and the cam with a radius that changes every cam deg, i.e. the cam lobe. The area of the contact that this two bodies produce is a rectangular strip area with the same length of the net roller, without chamfer, and the semi width dimension a evaluated through Hertzian theory by equation (11):

New engine concept development-Multi-body dynamic of valvetrain system and friction assessment

Antonio Turturro – Supervisors: Prof. C. Delprete and L. Magro

(11) $$a = \sqrt{4\frac{W_R R}{L\pi E}}$$

The area of contact A is evaluated by the equation (12):

(12) $$A = 2aL$$

Figure 25 depicts the semi width dimension a and the area of the contact A.

Fig. 25: semi width and area of the roller – cam lobe contact
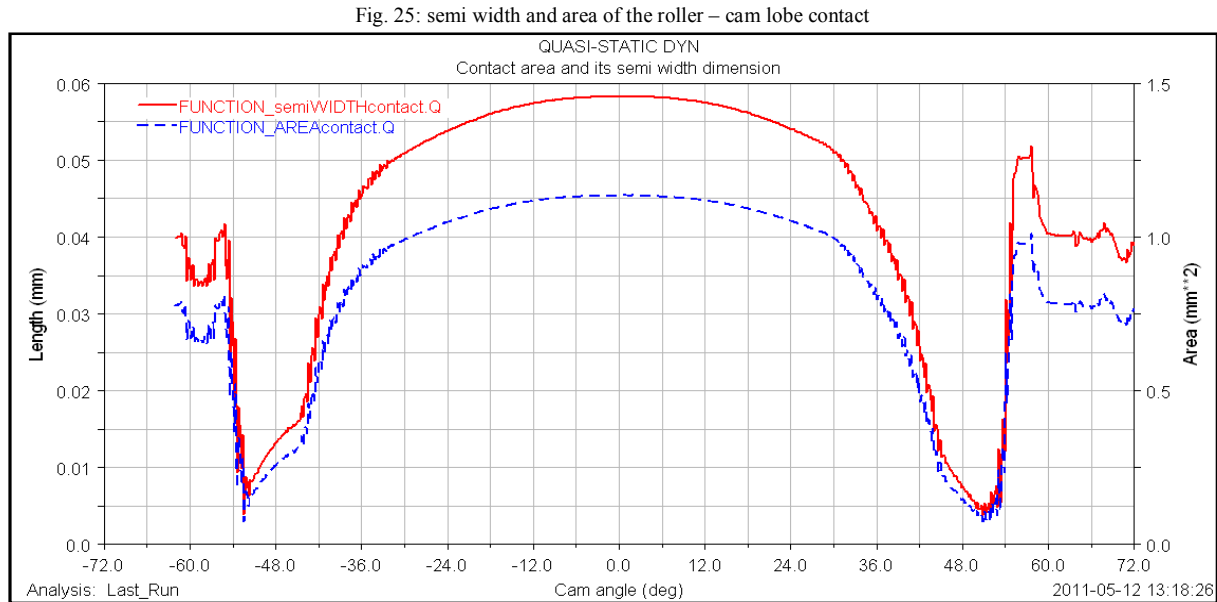
The contact area trend is in accord with the contact load trends. The minimum area of the contact is at the end of the height opening ramp 0.16 mm^2 at -51.99 cam deg and at the beginning of the height closing ramp 0.09 mm^2 at 51.48 cam deg while the maximum is 1.14 mm^2 at the maximum cam lift.

The next group of parameters are related to the contact centre deflection δ and the contact stiffness K_C [73]. According with the elasticity theory by Hertz and the elastic line contact theory, the total deflection at the centre of the contact δ is evaluated by the equation (13):

New engine concept development-Multi-body dynamic of valvetrain system and friction assessment

Antonio Turturro – Supervisors: Prof. C. Delprete and L. Magro

(13)
$$\delta = \frac{W_R}{\pi L E}\left[\ln\left(\frac{L^3 \pi E}{2RW_R}\right) + 1\right]$$

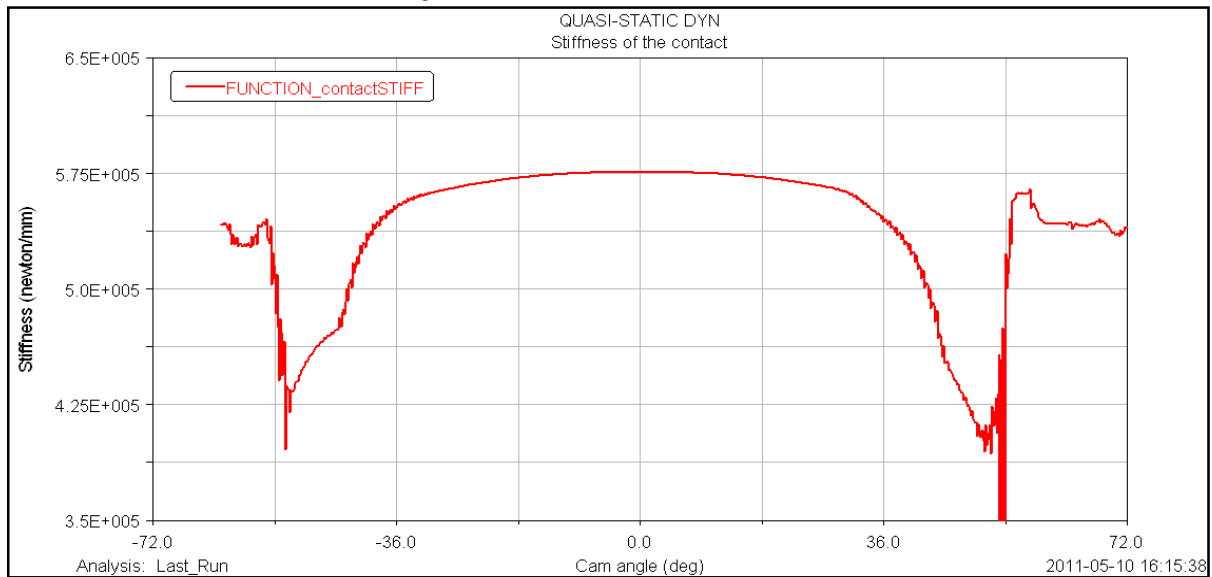where W_R is the contact force at roller cam lobe interface. Figure 26 depicts the contact central deflection δ.

Fig. 26: total central deflection of the roller – cam lobe contact
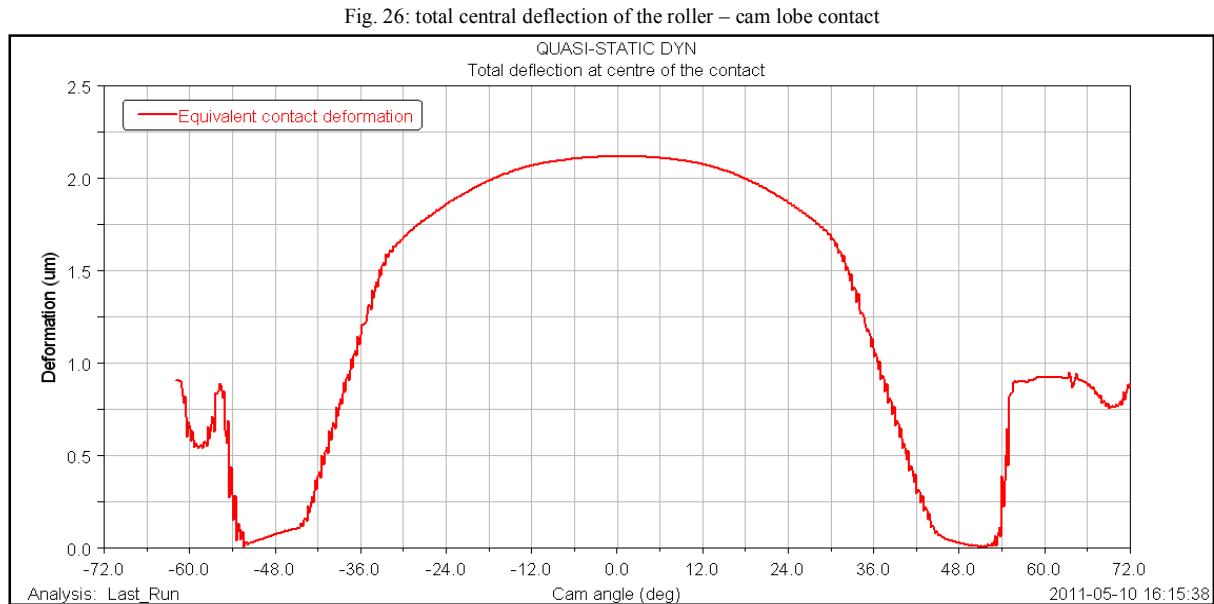
As it can see in Figure 26, the total central deflection trend follow properly the contact load at roller cam lobe contact curves. The maximum total deflection starts with 0.91 µm at −62 cam deg in the beginning of the height open ramp and after an oscillation it arrives almost to 0. Then it increases again on the open ramp to reach its peak of 2.12 µm slightly after the maximum cam lift at 1.05 cam deg. The behaviour of the total central deflection on the close side is specular about the open side. At the beginning of the height closed ramp, it reaches 0.93 µm at 59.89 cam deg. Using the total central deflection, it is possible evaluate the contact stiffness K_C by the equation (14) and depicts in Figure 27:

(14)
$$K_C = \frac{W_R}{\delta}$$

Figure 27 describes the stiffness of the contact by its definition of rate between the applied load and the deflection produced.

New engine concept development-Multi-body dynamic of valvetrain system and friction assessment

Antonio Turturro – Supervisors: Prof. C. Delprete and L. Magro

Fig. 27: stiffness of the roller – cam lobe contact

This parameter is extremely important to set up the feature contact in Adams View to develop the fully dynamic model. The maximum and minimum contacts stiffness are, respectively, $4.33\ 10^5$ N/mm at -51.39 cam deg at the end of the height open ramp, $4.05\ 10^5$ N/mm at 51.29 cam deg at the beginning of the height closed ramp, and $5.76\ 10^5$ N/mm at 0.05 cam deg at maximum cam lift.

The next group of parameters are related to the Hertzian stress on the contact [73, 93, 94]. For the study of the Hertzian stress system, the cam lobe roller contact is modelled by the parallel rolling cylinder that adds the sliding effect. The effect of the sliding component is to distort the Hertzian pressure distribution modelled by two parallel cylinders in pure rolling introducing a tangential stress system. This tangential stress system a tensile component on the whole stress distribution and enlarge the zone of stress actions. However, as it could find in the literature the percentage of sliding is at last around 2% and the effects on the stress system are negligible. So, in this way, it is decided to approach the Hertzian stress evaluation by the two parallel cylinders in pure rolling motion. The most important parameter is the maximum Hertzian contact pressure $\bar{p}_0$ evaluated by the equation (15):

(15) $$\bar{p}_0 = \sqrt{\frac{W_R E}{L \pi R}}$$

New engine concept development-Multi-body dynamic of valvetrain system and friction assessment

Antonio Turturro – Supervisors: Prof. C. Delprete and L. Magro

Inside the material the Hertzian pressure produces a stress system composed by a tensile stress with the same value of the Hertzian pressure and a shear stress τ_{max} evaluated by the equation (16):

(16) $\qquad \tau_{max} = 0.304\bar{p}_0$

The maximum shear stress τ_{max} acts in the centreline of the contact at a depth of $0.786\ a$. The maximum Hertzian pressure or tensile stress $\bar{p}_0$ and the maximum Hertzian shear stress are shown respectively in Figures 28 and 29.

Fig. 28: maximum Hertzian pressure

New engine concept development-Multi-body dynamic of valvetrain system and friction assessment

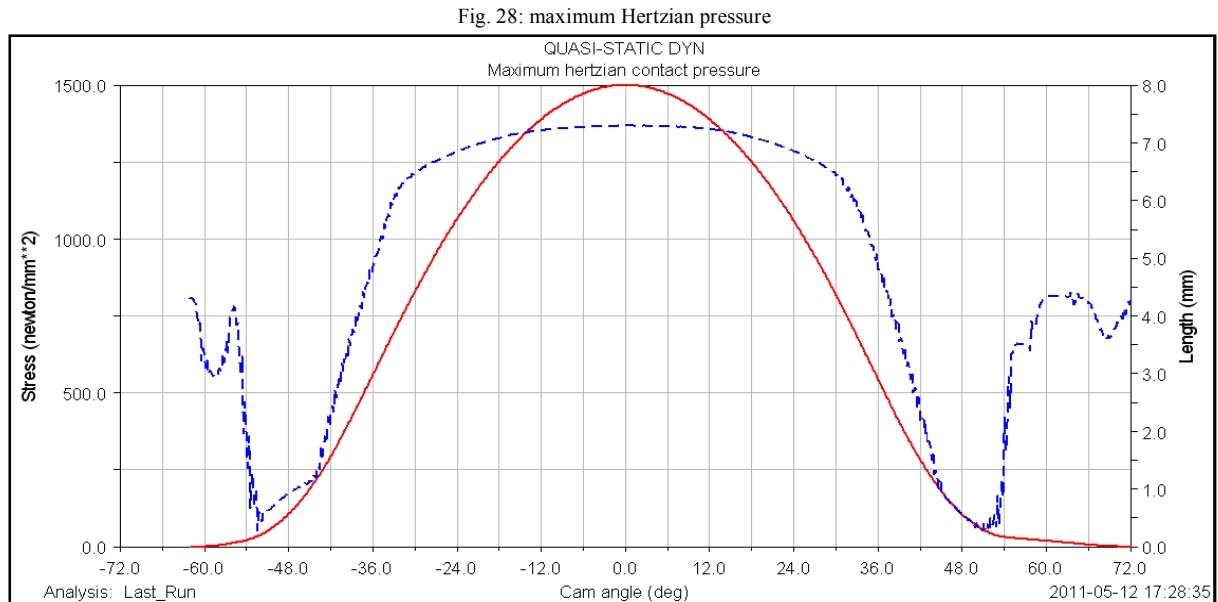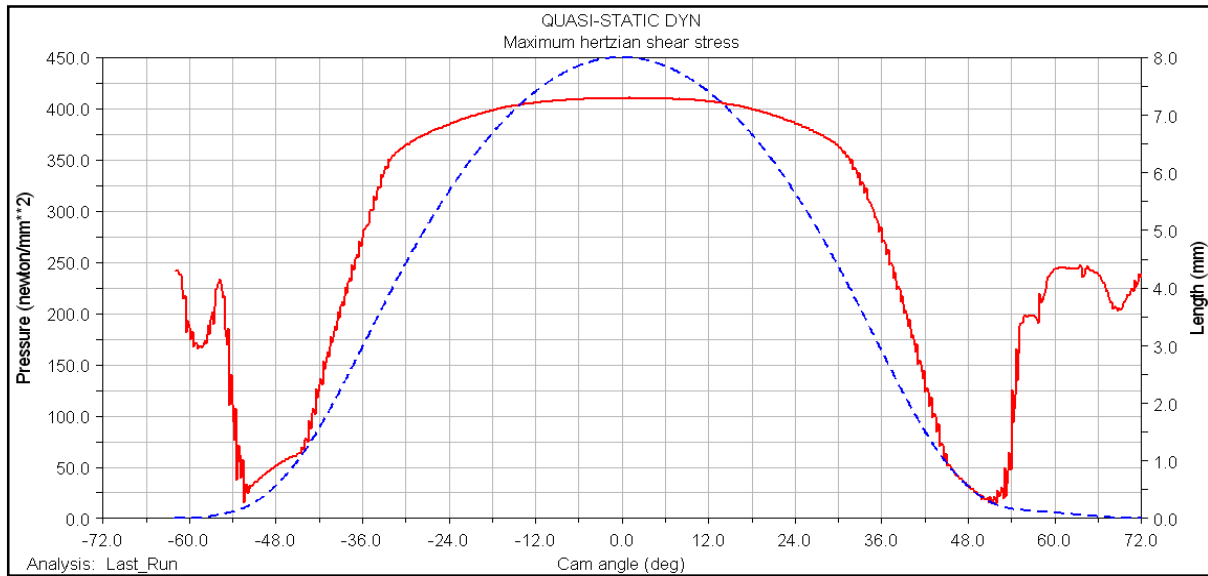Antonio Turturro – Supervisors: Prof. C. Delprete and L. Magro

Fig. 29: maximum Hertzian shear stress

The Hertzian stresses depend strictly on the contact load at roller - cam lobe and they have three main values: at the beginning of the height open ramp where $\bar{p}_0$ = 806.48 MPa and τ_{max} = 241.94 MPa; at the maximum valve lift where $\bar{p}_0$ = 1367.50 MPa and τ_{max} = 410.22 MPa; at the beginning of the height closed ramp where $\bar{p}_0$ = 814.95 MPa and τ_{max} = 244.48 MPa. The material of the cam lobe and the roller in contact on this project is assumed to be iron steel. According with Wang [93] and other literature material, an average Hertzian limit for this kind of material is 1724 MPa for the Hertzian pressure and 862 MPa for the Herztian shear stress. So, the cam lobe and the roller respect that limit.

New engine concept development-Multi-body dynamic of valvetrain system and friction assessment

Antonio Turturro – Supervisors: Prof. C. Delprete and L. Magro

III-VI Dynamic model

Fig. 30: Adams View dynamic model

The construction of the dynamic model starts from the quasi-static model plus several improvements but the most important difference with the previous model is the motion of the cam lobe that acts every other part in the model. In fact, the cam lobe is linked to the ground with a revolute joint by the centre of rotation that is different from the centre o mass which Adams View usually use to locate the joint. The cam lobe rotates at 16500 degrees cam per second that means 5500 rpm engine. The analysis of the top point of the end-rocker pivot arm by the point trace tool of Adams View 2005 R2, allow having a two dimensional cam lobe profile. Then this profile was exported to UGS NX7.5 and it was extruded. When the cad part was ready and it had the best surface achievable, it was imported in Adams View and built up in the model with a revolute joint. Now, the contact between the roller and the cam lobe was born up and it was modelled with the solid-to-solid feature. With the same feature it was modelled the contact between the valve tip and the rocker pivot as well. Figure 31 depicts the Adams View interface window for the solid-to-solid contact. The main characteristics of this feature are: the lift-off of the valve and of the rocker pivot as well; and the behaviour of the solid-to-solid feature that have a force of 0 N if the bodies in contact are simply backed to each other or a force of the value of the resultant forces applied to the two bodies engaged in the contact. The first step to define a solid-to-solid contact force is to set up the geometry that comes into the contact [90]. Two models for normal force calculations are available in ADAMS Solver [89]: impact function
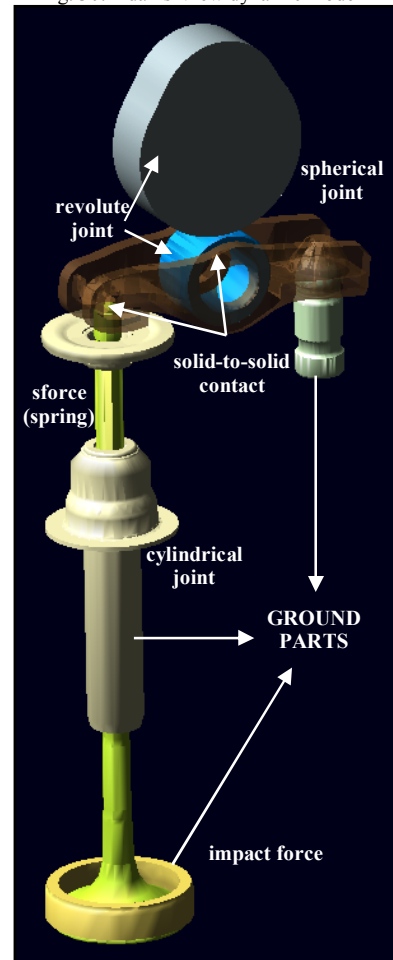
Fig. 31: Adams View solid-to-solid contact force interface window

237

New engine concept development-Multi-body dynamic of valvetrain system and friction assessment

Antonio Turturro – Supervisors: Prof. C. Delprete and L. Magro

model, and coefficient of restitution or the Poisson model. Both force models result from a penalty regularization of the normal contact constraints. Penalty regularization is a modelling technique in mechanics, in which a constraint is enforced mathematically by applying forces along the gradient of the constraint. The force magnitude is a function of the constraint violation. For this project the normal force based on the impact function is the most suitable way to evaluate it. The normal force based on an impact function used the impact function is based on four key parameters: stiffness, force exponent, damping and penetration depth. The stiffness specifies a material stiffness that is to be used to calculate the normal force for the impact model. In general, the higher the stiffness, the more rigid or hard the bodies in contact are. About the force exponent, Adams Solver models normal force as a nonlinear spring – damper. If the damper penetration is the instantaneous penetration between the contacting geometry, the software calculates the contribution of the material stiffness to the instantaneous normal force as:

(17) $\qquad$ *normal force = stiffness (penetration)^{exponent}*

The value of the damping defines the damping properties of the contacting material. A good rule of thumb is that the damping coefficient is about 1% of the stiffness coefficient. In this project, it was used this rule as first attempt but with that damping value the height ramp, in particular, the end one does not follow properly the valve lift profile, so it is decided to use a value that allow a good height closed ramp profile. The penetration depth defines the value of the penetration at which Adams Solver turns on full damping. The solver uses a cubic step function to increase the damping coefficient from zero, at zero penetration, to full damping when the penetration reaches the damping penetration. A reasonable value for this parameter is 1E−2 mm. Indeed, in this project, it is used a penetration depth of 5E−5 mm for the same reason of the damping value and to be nearer to the reality of the roller cam lobe contact. The friction effects at the contact locations using the Coulomb friction model and it is the same described in the quasi-static model. This model models dynamic friction but not stiction. The Coulomb friction model can be set to dynamic only to define that the friction effects are to be included only on dynamic behaviour of the contact. The static coefficient specifies the

New engine concept development-Multi-body dynamic of valvetrain system and friction assessment

Antonio Turturro – Supervisors: Prof. C. Delprete and L. Magro

coefficient of friction at a contact point when the slip velocity is smaller than the value for the static transition velocity and its value is 0.23 as suggested from the Adams View guidelines for a greasy steel-steel contact. Excessively large values of static coefficient can cause integration difficulties. The dynamic coefficient specifies the coefficient of friction at a contact point when the slip velocity is larger than the value for friction transition velocity and its value is 0.16 as suggested from the Adams View guidelines for a greasy steel-steel contact. Excessively large values of dynamic coefficient can cause integration difficulties. The static transition velocity and the friction transition velocity are depicted in Figure 11. About the dynamic solver, the end time is 0.022 s and the number of steps is 1818. The simulation time takes account the time to complete a cam rotation when the engine speed is 5500 rpm. At this regime the simulation has more than 5 steps every cam degree. The dynamic model can be summed up by Table 8 and Table 9. Table 8 highlights the parts that form the dynamic model, their mass, their inertia and how the parts in the model are collected and work.

Tab. 8: parts, masses and inertias in the model

Part	Mass	Inertia
Valve ring	ground	ground
Valve guide and lower retainer	ground	ground
HLA body	ground	ground
Exhaust valve and upper retainer + 33% mass spring	49.37 g	IXX 80.52 kg-mm^2 IYY 80.52 kg-mm^2 IZZ 1.42 kg-mm^2
End-pivot rocket arm	33.62 g	IXX 9.80 kg-mm^2 IYY 8.97 kg-mm^2 IZZ 1.60 kg-mm^2
Roller	9.74 g	IXX 0.52 kg-mm^2 IYY 0.35 kg-mm^2 IZZ 0.35 kg-mm^2
Cam lobe	68.64 g	IXX 9.72 kg-mm^2 IYY 6.06 kg-mm^2 IZZ 4.81 kg-mm^2

New engine concept development-Multi-body dynamic of valvetrain system and friction assessment

Antonio Turturro – Supervisors: Prof. C. Delprete and L. Magro

Table 9 highlights the constrains used in the model and, for each link, it shows the number of degree of freedom blocked from the relative constrain.

Tab. 9: parts, constrains description

Part 1	Part 2	Type	Constrain
Exhaust valve	Valve guide	Cylindrical joint	4
End-pivot rocker arm	Valve guide	Spherical joint	3
End-pivot rocker arm	Valve	Solid-to-solid contact force	-
Roller	End-pivot rocker arm	Revolute joint	5
Roller	Cam lobe	Solid-to-solid contact force	-
Cam lobe	Ground	Revolute joint	5
			17

Figure 32 shows the results of the model verify tool and in particular the information about the degrees of freedom and the redundant constraints.

Fig. 32: verify model tool results

```
VERIFY MODEL: .model_1

   6 Gruebler Count (approximate degrees of freedom)
   5 Moving Parts (not including ground)
   1 Cylindrical Joints
   2 Revolute Joints
   1 Spherical Joints
   1 Fixed Joints
   1 Motions


   6 Degrees of Freedom for .model_1

There are no redundant constraint equations.
```

New engine concept development-Multi-body dynamic of valvetrain system and friction assessment

Antonio Turturro – Supervisors: Prof. C. Delprete and L. Magro

III-VII Dynamic model – Results and discussion

The first parameters of the ADAMS View dynamic model about the valve train characterization are the valve displacement, the valve velocity and the valve acceleration as shown in Figures 33 and 34.

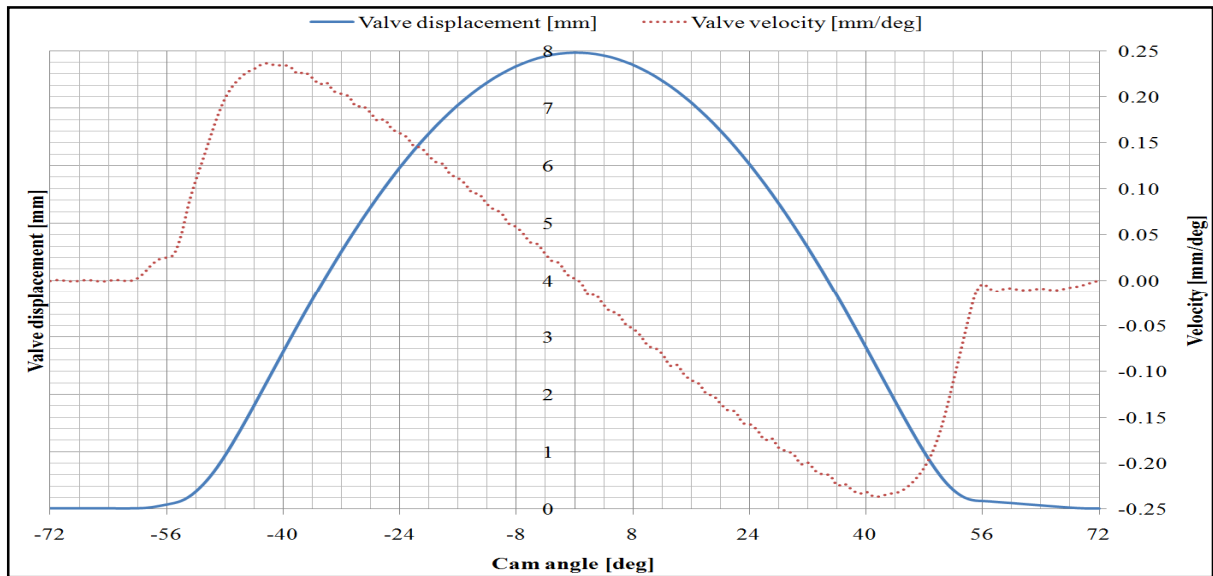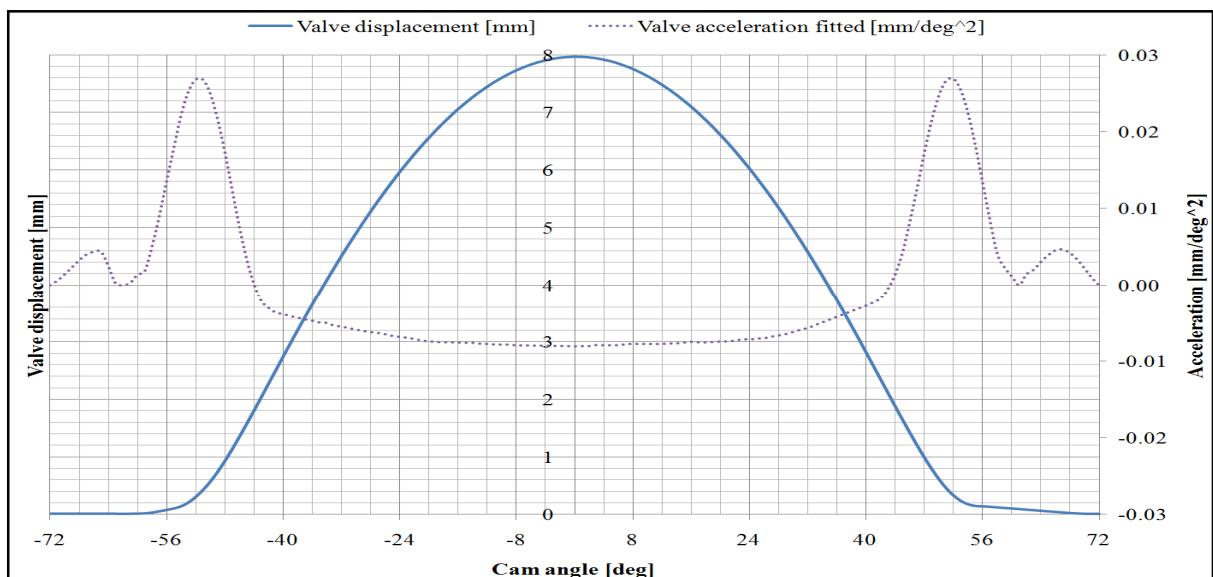Fig. 33: exhaust valve displacement and velocity for the dynamic model

Fig. 34: fitted exhaust valve acceleration data for the dynamic model

These parameters were calculated at the centre of mass of the exhaust valve as in the quasi-static model. The exhaust valve event takes place between −62 cam degrees and 72 cam

New engine concept development-Multi-body dynamic of valvetrain system and friction assessment

Antonio Turturro – Supervisors: Prof. C. Delprete and L. Magro

degrees. The maximum valve lift is 7.97 mm at 0 cam degree in line with the system requirement. The maximum velocity on the opening ramp is 0.2364 mm/deg at −41.88 cam deg, whilst that on the closing ramp is −0.2360 mm/deg at 40.78 cam deg. The maximum velocity on the height open and closed ramp are, respectively, 0.0265 mm/deg at −55.46 cam deg and −0.0112 mm/deg at 57.95 cam deg. The valve acceleration showed a noise response on the cam flank and on the base circle due to discrepancies in numerical approximation of the cam lobe surface. So, it was necessary to fit the valve acceleration data by MatLab and Excel to have a noise free representation (filtering the noise). The exhaust valve acceleration at maximum lift is −0.0081 mm/deg^2 at 0 cam deg. The maximum acceleration on the opening and closing ramps are, respectively, 0.0268 mm/deg^2 at −52.03 cam deg and 0.0268 mm/deg^2 at 52.00 cam deg. Indeed, the maximum acceleration on the opening and closing height ramps are, respectively, 0.0044 mm/deg^2 at −60.79 cam deg and 0.0046 mm/deg^2 at 66.99 cam deg. The valve acceleration changes sign at −44.05 cam deg from positive to negative and vice-versa at 42.98 cam deg. The valve motion conforms to the requirements. Table 10 summarises the kinematics and dynamics of the valve motion.

Tab. 10: valve motion parameters for the dynamic model

Parameter	Value	Angle [cam deg]
Exhaust event	134 cam deg	−62 to 72
Max valve lift	7.97 mm	0
Max open height ramp velocity	0.0265 mm/deg	−55.46
Max open ramp velocity	0.2364 mm/deg	−41.88
Max closed ramp velocity	0.2360 mm/deg	40.78
Max closed height ramp velocity	−0.0112 mm/deg	57.95
Max open height ramp acceleration	0.0066 mm/deg^2	−58.79
Max open ramp acceleration	0.0268 mm/deg^2	−52.03
Acceleration at max valve lift	−0.0081 mm/deg^2	0
Max closed ramp acceleration	0.0268 mm/deg^2	52.00
Max closed height ramp acceleration	0.0027 mm/deg^2	69.70

The next group of parameters are related to the forces acting on the valve body. In particular, these are the spring force and the contact load at valve tip. The spring force comprises the elastic force and the preload. This is inserted into the model as described in the quasi-static

New engine concept development-Multi-body dynamic of valvetrain system and friction assessment

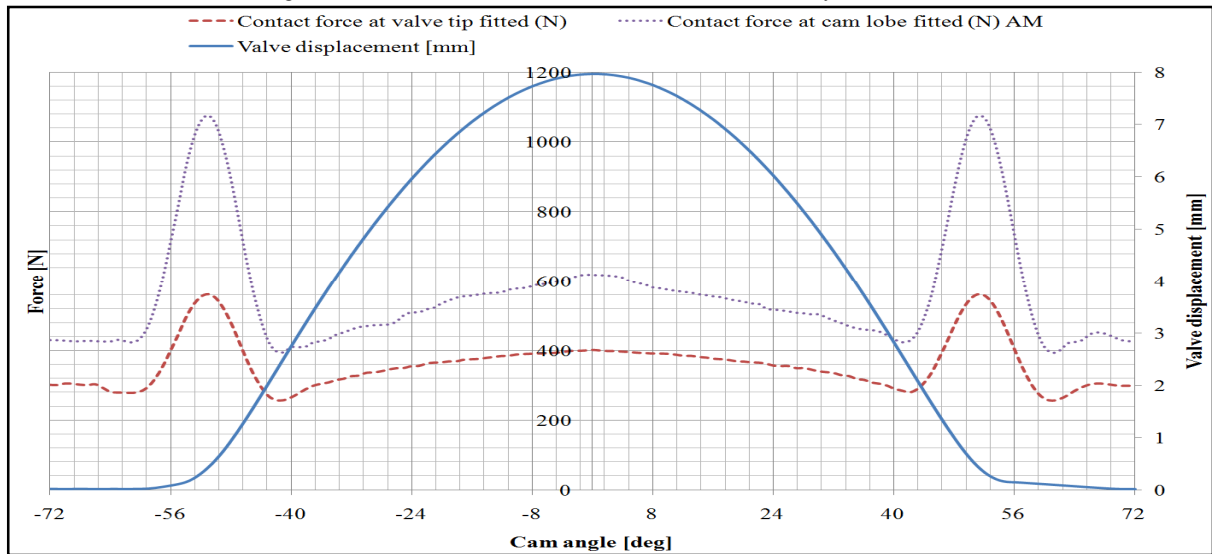Antonio Turturro – Supervisors: Prof. C. Delprete and L. Magro

model and shown in Figure 15. The contact load at valve tip in the dynamic model is evaluated directly from the solid-to-solid contact force between the valve tip and the rocker pad as depicted in Figure 35.

Fig. 35: fitted contact forces at valve tip for the dynamic model
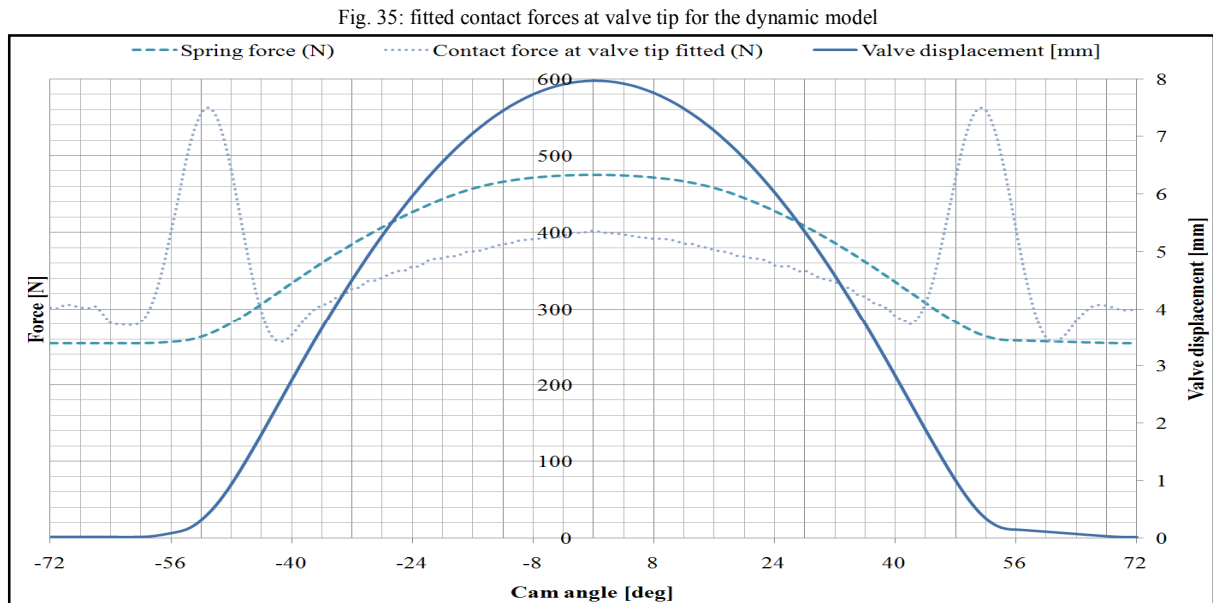
The spring force at valve closing and opening positions is, respectively, 254.63 N and 474.66 N. Unfortunately, these values are slightly over the specifications: the spring force at the valve closure is 1.04% over and the spring force at valve opening is 0.14% over the specified values. The maximum contact loads at valve tip are at the beginning of the opening ramp and at the end of the closing ramp, and their values are respectively, 562.76 N at −51.02 cam deg and 561.86 N at 51.01 cam deg. The contact load at maximum valve lift is 402.24 N.

The next step is to determine the contact load at rocker pivot roller that is depicted in Figure 36.

New engine concept development-Multi-body dynamic of valvetrain system and friction assessment

Antonio Turturro – Supervisors: Prof. C. Delprete and L. Magro

Fig. 36: fitted contact forces at cam lobe – roller contact for the dynamic model

The maximum contact load at roller-cam interface is, as in the case of the force at valve tip-rocker pad contact, at the transition point between the cam event and the flanks on the both side of the cam lobe, and at the maximum cam lift. The values are: 1076 N at -51.02 cam deg on the open side, about 1073 N at 51.01 cam deg on the closed side, and approximately 619 N at maximum cam lift.

The next group parameters are related to the oil film thickness in the cam-roller conjunction. This is an important parameter, which determines friction and hence the main losses from the valve train system. It is evaluated by the Grubin's equation in case of elastohydrodynamic lubrication condition [73, 94]. The properties of the lubricating oil which separates the opposing surfaces of a concentrated contact, typically 2 µm thick and 400 µm across, and which is subjected to extremes of pressure and shear, determine the efficiency of the lubrication mechanism under rolling contact. The effects contributing to the generation of elastohydrodynamic films are: the hydrodynamic film formation, the modification of the film formation by elastic deformation, and the transformation of the lubricant's viscosity and rheology under pressure. These three effects play together and cause the generation of elastohydrodynamic films. The basic principles of hydrodynamic lubrication apply, but with some major differences: both contact geometry and lubricant viscosity are a function of hydrodynamic pressure. It is impossible to specify precisely a film geometry and viscosity before proceeding to solve the Reynolds equation. The principal effect of elastic deformation by Hertzian contact on the lubricant film profile is to interpose a central region of quasi-

New engine concept development-Multi-body dynamic of valvetrain system and friction assessment

Antonio Turturro – Supervisors: Prof. C. Delprete and L. Magro

parallel surfaces between inlet and outlet wedges. With regard to the transformation of lubricant viscosity and rheology under pressure, one can state that when a liquid separates two surfaces, extreme pressures many times higher than those encountered in hydrodynamic lubrication are inevitable. Consequently, the viscosity of oil increases dramatically with pressure. This phenomenon is known as piezoviscosity. The viscosity-pressure relationship is usually described by the Barus law:

(18) $$\eta_p = \eta_0 e^{\alpha p}$$

where: η_p is the lubricant viscosity at pressure p and temperature θ in Pa s, $\eta_0 = 0.007$ Pa s is the viscosity at atmospheric pressure and temperature θ, and $\alpha = 10^{-8}$ Pa^{-1} the pressure-viscosity coefficient.

The Grubin equation takes account only about the main factors that influence the oil film thickness as the sliding velocity U and the contact load W_R. The derivation of the film thickness equation begins with the one-dimensional form of Reynolds equation without the squeeze film effects as:

(19) $$\frac{dp}{dx} = 6U\eta \left(\frac{h-h_0}{h^3}\right)$$

where: p is the hydrodynamic pressure in Pa, U is the entraining velocity in m/s, η the lubricant viscosity in Pa s, h the film thickness in m, h_0 the film thickness where the pressure gradient is 0 in m, and x the distance in rolling direction in m.
Substituting into Reynolds equation the expression for viscosity according to the Barus law yields:

(20) $$\frac{dp}{dx} = 6U\eta_0 e^{\alpha p} \left(\frac{h-h_0}{h^3}\right)$$

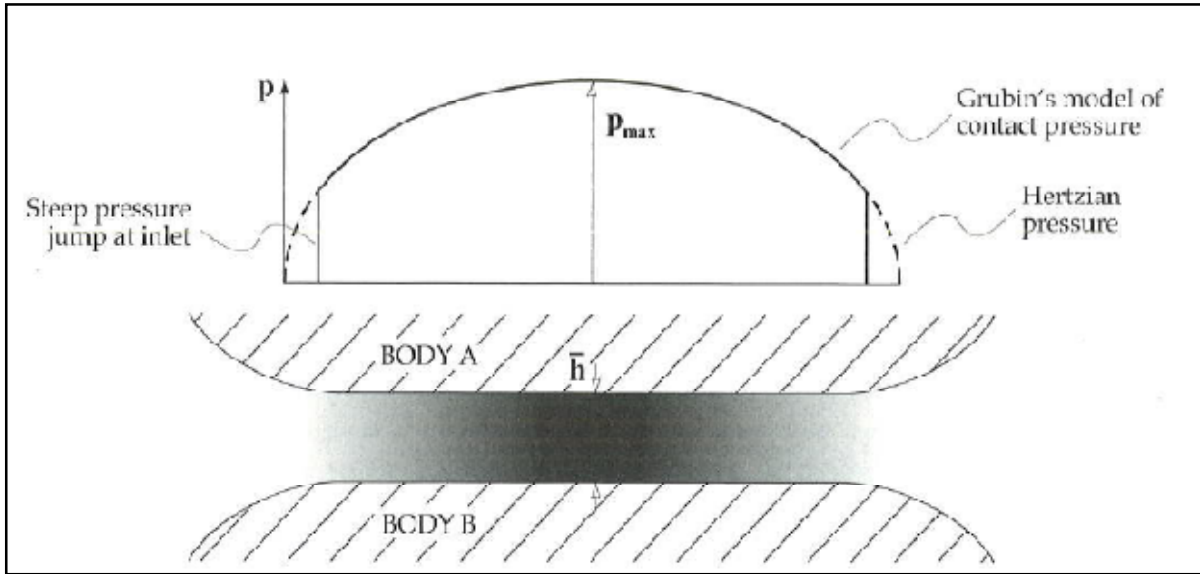To solve this equation, Grubin introduced an intermediate variable, known as the "reduced pressure", defined as:

New engine concept development-Multi-body dynamic of valvetrain system and friction assessment

Antonio Turturro – Supervisors: Prof. C. Delprete and L. Magro

(21) $$q = \frac{1}{\alpha}(1 - e^{-\alpha p})$$

After differentiating with respect to x and substituted into the Reynolds equation (20), the separation of pressure and film thickness is achieved:

(22) $$\frac{dq}{dx} = 6U\eta_0 \left(\frac{h-h_0}{h^3}\right)$$

Two independent controlling variables still remain and for a solution one requires the replacement of either of these variables by the other. Grubin observed that at the inlet conjunction of the Elastic Hydrodynamic Lubrication - EHL contact, the contact pressures sharply rise as predicted by the Hertzian contact theory. If a hydrodynamic oil film is established, then the hydrodynamic pressures should follow the Hertzian pressure profile and, of course, also rise sharply at inlet wedge of the contact. This sharp rise of the pressure can approximate as a step jump to a certain value of the same magnitude of the Hertzian contact pressure. Now, it is extremely important to understand the behaviour of the reduced pressure equation (9). When the pressure is large enough, then the term $e^{-\alpha p} \ll 1$ and $q \approx \frac{1}{\alpha}$. Grubin reasoned that since the stress and the deformations in the EHL contacts were substantially identical to the classical Hertzian, the opposing surfaces must follow an almost parallel conjunction and thus the film thickness is approximately uniform within the contact. Then inside the contact, the film thickness h is constant so that $h = h_0$. Since h_0 occurs where p_{max} takes place, Grubin deduced that there must be a sharp increase in pressure in the inlet zone to the contact with a corresponding rise in lubricant viscosity, as shown in Figure 37.

New engine concept development-Multi-body dynamic of valvetrain system and friction assessment

Antonio Turturro – Supervisors: Prof. C. Delprete and L. Magro

Fig. 37: Grubin's approximation to film thickness within an EHL contact

It is, therefore, in accord with the model $q \approx \frac{1}{\alpha} = constant, \frac{dq}{dx} = 0, h = h_0$ within the contact. After replacing one variable for the other, the differential equation is solved numerically by assuming that the value of the film thickness h is equal to the distance separating the surfaces plus the film thickness within the EHL contact. The constant of integration is 0 for the selected limits of the next integral since at any position remote from the contact, $p = 0$ and therefore $q = 0$. The following approximation was calculated numerically for the integral as applied to a line contact:

(23)
$$\int_{h_\infty}^{h_1} \left(\frac{h-h_0}{h^3}\right) dx = 0.131 \left(\frac{W}{LER}\right)^{-0.625} \left(\frac{a}{R^2}\right) \left(\frac{h_0}{R}\right)^{-1.375}$$

where: h_1 is the inlet film thickness to the EHL contact in m, h_∞ the film thickness at a distance "infinitely" far ahead of the contact in m, R the reduced or equivalent radius of contact in m, E the reduced Young's module in Pa, L the full length of the EHL contact, a the half-width of the EHL contact in m, h_0 the film thickness where the pressure gradient is 0, i.e., Grubin's EHL film thickness as shown in the Figure 37, in m, W the contact load in N. Expressing the equation (22) in the non-dimensional form $\frac{h_0}{R}$ and substituting the semi-half width of the contact a with the Hertzian contact formula for parallel cylinders yields a more convenient Grubin's expression for film thickness in the elastohydrodynamic contact, as shown by Stachowiack and Batchelor [94]:

New engine concept development-Multi-body dynamic of valvetrain system and friction assessment

Antonio Turturro – Supervisors: Prof. C. Delprete and L. Magro

(24)
$$\left(\frac{h_0}{R}\right) = 1.657 \left(\frac{U\eta_0\alpha}{R}\right)^{0.7273} \left(\frac{W}{LER}\right)^{-0.0909}$$
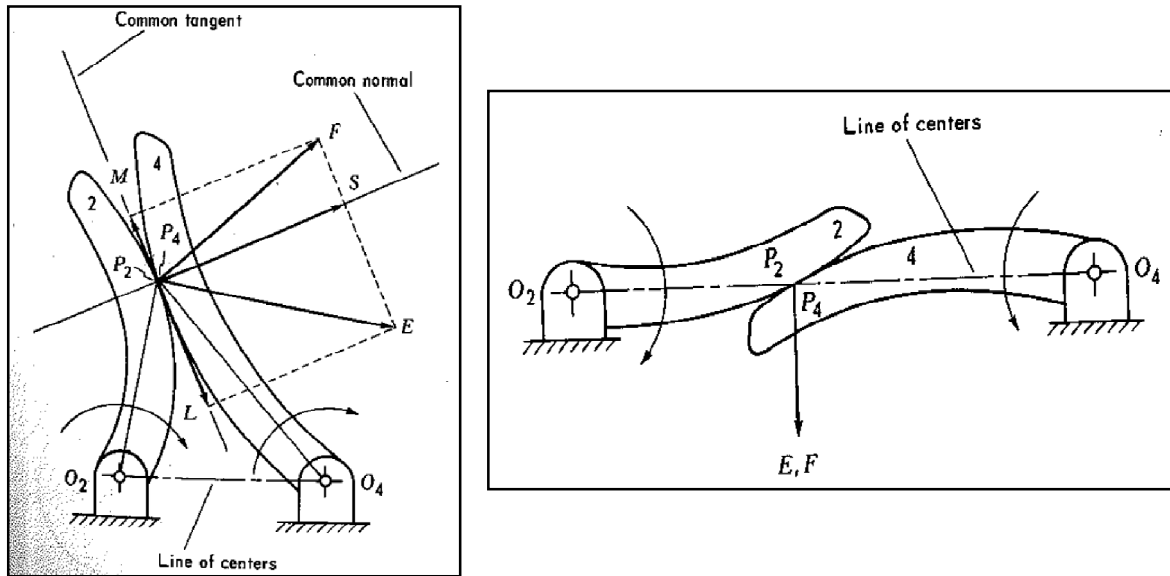
It can be seen that all the variables are combined in dimensionless groups making it easier for the interpretation of the irrational exponents. However, the evaluation of oil film thickness for this project, the contact between the roller and cam lobe of an end-pivot rocker arm valve train, is executed by the expression proposed by Gohar and Rahnejat [73]:

(25)
$$\frac{h_0}{R} = 2.076 \left(\frac{\alpha\eta_0 U}{R}\right)^{\frac{8}{11}} \left(\frac{ERL}{W}\right)^{\frac{1}{11}}$$

Equation (25) predicts approximately the parallel film thickness in terms of piezoviscous properties of the lubricant, entraining velocity, geometry of the contact and load. The solution of Reynolds equation under piezoviscous condition proposed by Rahnejat has some important characteristics: the film thickness depends strongly on the product of lubricant viscosity and entraining velocity, but there is a weak correlation to the contact load. This is because the parallel shape of the EHL film widens as the load increases. Equation (25) is quite accurate at high loads and/or low speeds.
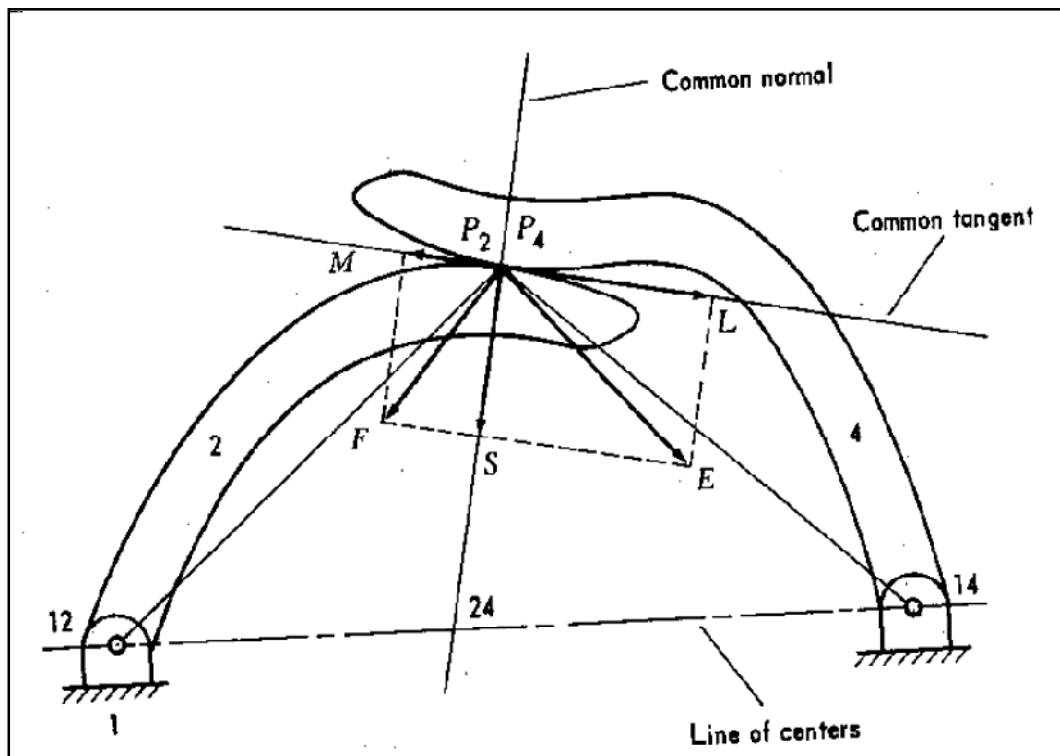
The sliding velocity is also calculated [95]. The roller-cam lobe contact is defined as a pure rolling contact out of the valve lift event and sliding contact within the valve event. The method to classify the form of contact kinematics requires the determining whether the contact point lies on the line of the centres of contacting bodies or not. If true, then is a rolling contact, otherwise some degree of sliding occurs as shown in Figure 38.

New engine concept development-Multi-body dynamic of valvetrain system and friction assessment

Antonio Turturro – Supervisors: Prof. C. Delprete and L. Magro

Fig. 38: sliding and rolling contact

An instantaneous centre is a point in a body about which some other body rotates either permanently or at the instant of time; a point common to two both bodies having the same linear velocity in both magnitude and direction. The instantaneous centre of rotation for the two aforementioned forms of is different. For a sliding contact, the instantaneous centre of two bodies is defined by the conjunction between the common normal at the two surfaces in contact and the line of their centres (point 24) as shown in Figure 39.

Fig. 39: instant centre for sliding contact

New engine concept development-Multi-body dynamic of valvetrain system and friction assessment

Antonio Turturro – Supervisors: Prof. C. Delprete and L. Magro

A way to analyse easily the kinematics of the end-pivot rocker arm is to replace it by an equivalent linkages mechanism as shown in Figure 40.

Fig. 40: equivalent linkages mechanism for pivot rocker arm valve train
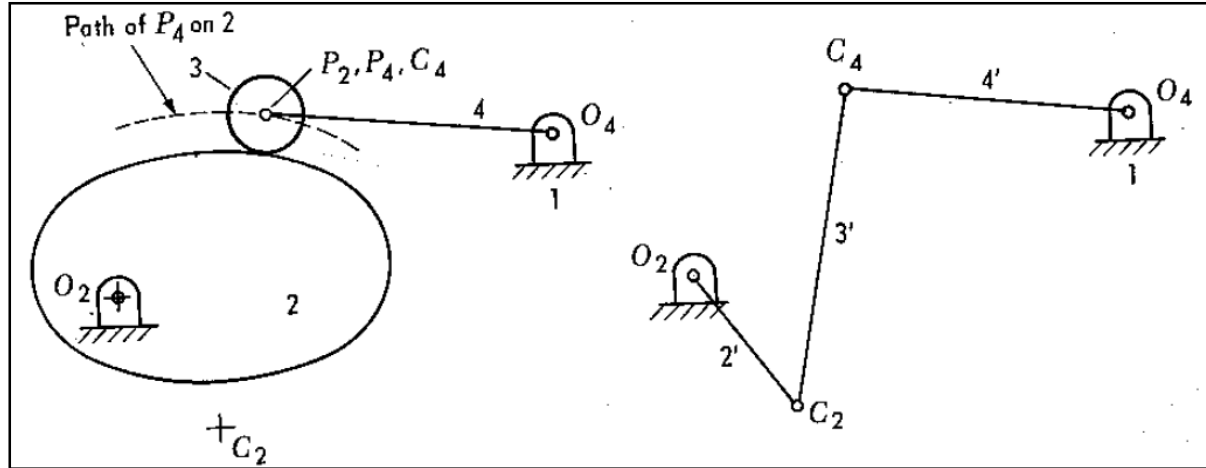
The bar *2'* changes its length with the radius of curvature of the cam lobe and then the velocity of point *C4*. To calculate the contact velocity between the roller and cam lobe, it is needed to consider an incremental step forward, because in assuming equivalent linkage mechanisms the roller is defined as a redundant kinematic constraint. It is possible to calculate the surface velocity of the cam lobe both through determination of the instantaneous centre or by its components as stated by Martin [95]. Here with the available data, it is decided to calculate the instantaneous cam lobe velocity through components. Then, a UGS NX7.5 file is built and both the roller and cam lobe were schematically located. From a previous analysis, the pressure angle α between the roller and cam lobe was introduced as an input into the CAD file and for every cam degree, the angle γ between the normal at the line that links the centre of rotation of the cam lobe and the point of contact was evaluated, as well as the normal to the line that links the centre of roller and the contact point. Figure 41 depicts the pressure angle α versus the cam angle for the exhaust valve, while Figure 42 shows the schematic model of the roller-cam lobe location.

New engine concept development-Multi-body dynamic of valvetrain system and friction assessment

Antonio Turturro – Supervisors: Prof. C. Delprete and L. Magro

Fig. 41: roller pressure angle versus cam angle for the exhaust side of the valve train
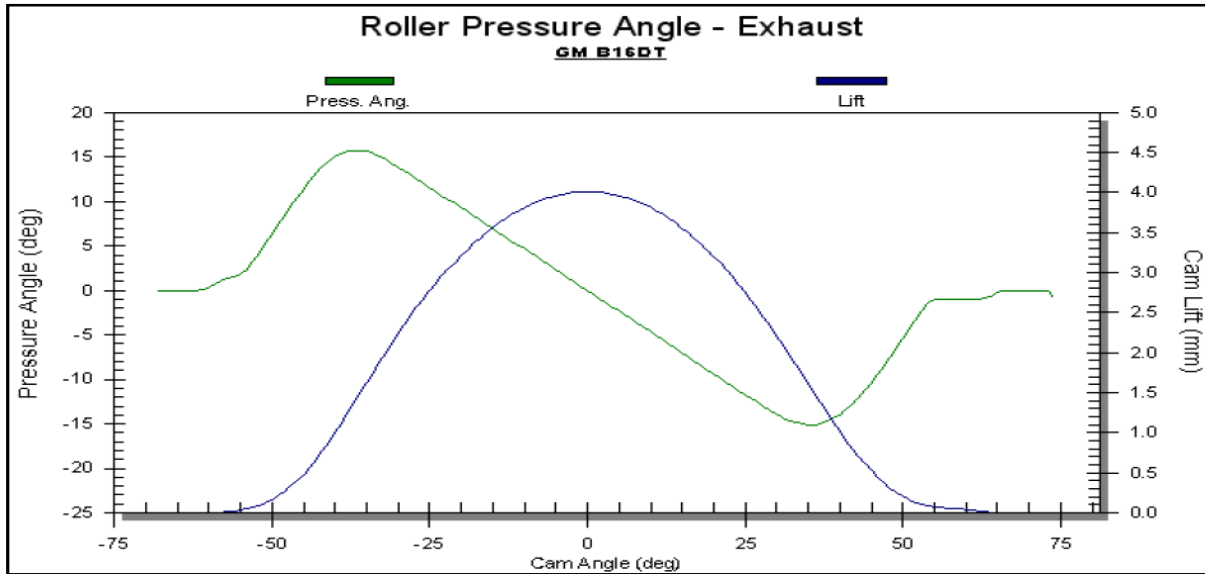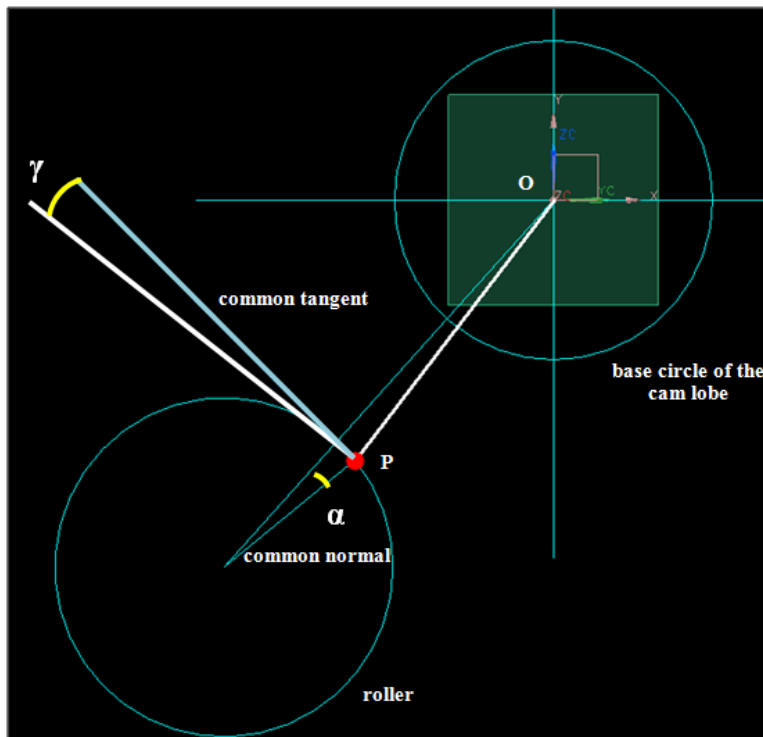

Fig. 42: schematic model of the roller – cam lobe location

The pressure angle α is defined as the angle which the common normal for the cam and follower makes with the path of the follower. Figure 41 shows that the pressure angle α varies within the range 15.75 deg and -15.25 deg; the positive sign means that the angle is measured follows the clockwise direction and correspond to the open event, while the negative sign means that the measured angle follows the counter clockwise direction and correspond to the

New engine concept development-Multi-body dynamic of valvetrain system and friction assessment

Antonio Turturro – Supervisors: Prof. C. Delprete and L. Magro

close event. The normal at the line that links the contact point P to the cam lobe's centre of rotation defines the absolute velocity v_P at point P. On the other hand, the normal at the line that links the centre of the roller and to the contact point P is the tangential velocity of the roller-cam lobe contact v_t. In the other words, it is the tangential velocity of the roller. The reason is that the absolute velocity of the cam lobe v_P produces two effects: the first one is the roller rotation and the second one is the reciprocating movement of the end-pivot rocker arm. The force and the velocity that produce these two motions lie, respectively, on the common tangent and the common normal at the two surfaces in contact at point P. The common normal links the instantaneous centre of the cam lobe to the instantaneous centre of the roller. It is clear that the roller has a constant radius and thus its instantaneous centre is the same as its centre of rotation. The common tangent is traced at contact point P that it is found in a three step procedure: (i)- the first one is to move the roller by a quarter of cam rotation, (ii)- then, the centre of the roller is moved far away about the base radius of the cam lobe plus the cam lift plus the roller radius, and (iii)- finally, a roller radius is traced and shifted by the pressure angle α, as shown in Figure 41. Now, the absolute velocity of the cam lobe v_P is determined by the angle γ in the normal component v_n which produces the reciprocating motion of the end-pivot rocker arm and in the tangential component v_t that produces the rotating motion of the roller. The absolute velocity of the cam lobe v_P is evaluated by the equation (26):

(26) $\qquad v_P = \omega_l \overline{OP}$

where: v_P is the absolute velocity in mm/s, ω_l = 287.98 rad/s the cam lobe angular velocity, $\overline{OP}$ distance between the cam lobe's centre of rotation and the contact point P in mm. Therefore, the normal velocity v_n is calculated by the equation (27):

(27) $\qquad v_n = v_P \sin \gamma$

where: v_n is the normal velocity at contact point P in mm/s. The tangential velocity v_t by the equation (28):

(28) $\qquad v_t = v_P \cos \gamma$

New engine concept development-Multi-body dynamic of valvetrain system and friction assessment

Antonio Turturro – Supervisors: Prof. C. Delprete and L. Magro

where: v_t is the tangential velocity at the contact point P in mm/sec. The angle γ in both the equations (27) and (28) is measured in radians. Finally, the angular velocity of the roller ω_r is calculated by the equation (29):

(29) $$\omega_r = \frac{v_t}{R_r}$$

where: ω_r is the angular velocity of the roller in rad/s, but it could easily convert in rpm or deg/s.

All this values are collected in an Excel file and all of them are plotted in Figure 43, Figure 44, Figure 45, and Figure 46. Figure 43 shows the angle γ that varies within the range 0 deg and 23.25 deg for the open event, and between 0 deg and 22.41 deg for the close one.

Fig. 43: pressure angle α, angle γ, cam lift and the distance OP
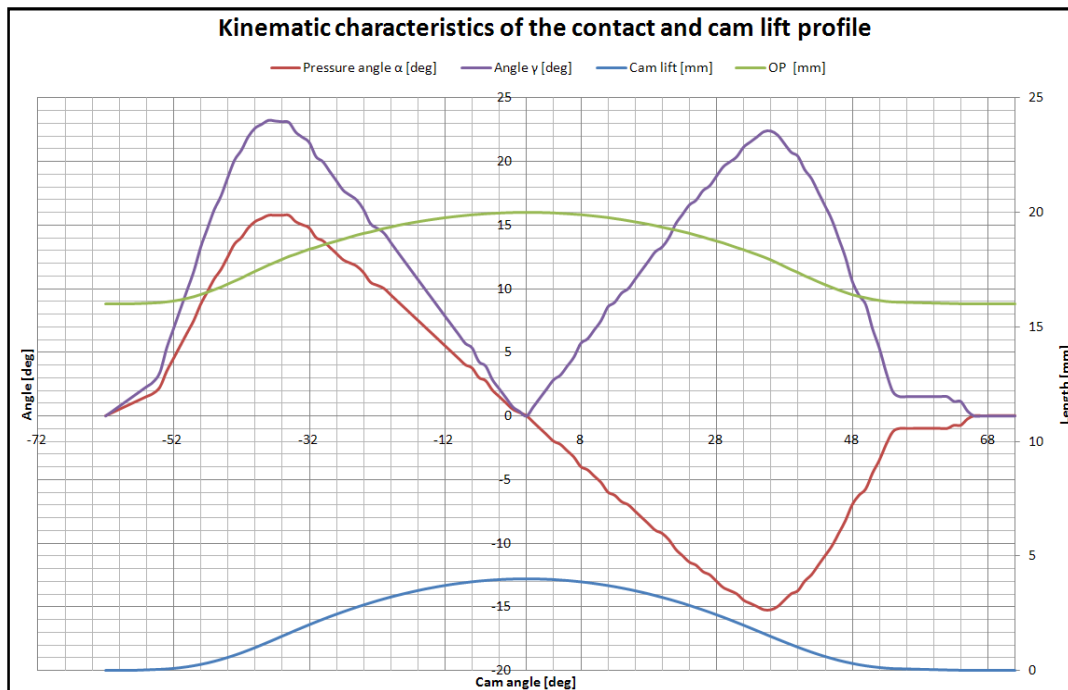
The relative position between the normal at roller radius at the contact point P and the normal at segment $\overline{OP}$ change at 0 cam deg and then the angle γ should change its sign. In this manner, all the velocities will have a negative sign and which does not make sense. So, it is decided to maintain the angle γ as always positive. Figure 43 presents also the cam lift which is related to the valve lift by the rocker ratio. This is 0 mm outside the valve event and reaches 4.01 mm at 0 cam deg, cam nose tip. In the same Figure, the distance $\overline{OP}$ is shown; it

New engine concept development-Multi-body dynamic of valvetrain system and friction assessment

Antonio Turturro – Supervisors: Prof. C. Delprete and L. Magro

varies from 16 mm on the base radius of the cam lobe outside the valve event to 20.01 mm at 0 cam deg. Figure 44 shows the absolute velocity v_P; it varies from 4607.67 mm/sec on the base circle of the cam lobe to 5763.01 mm/sec at maximum cam lift.

Fig. 44: pressure angle α, angle γ, absolute velocity v_P, normal velocity v_n, tangential velocity v_t
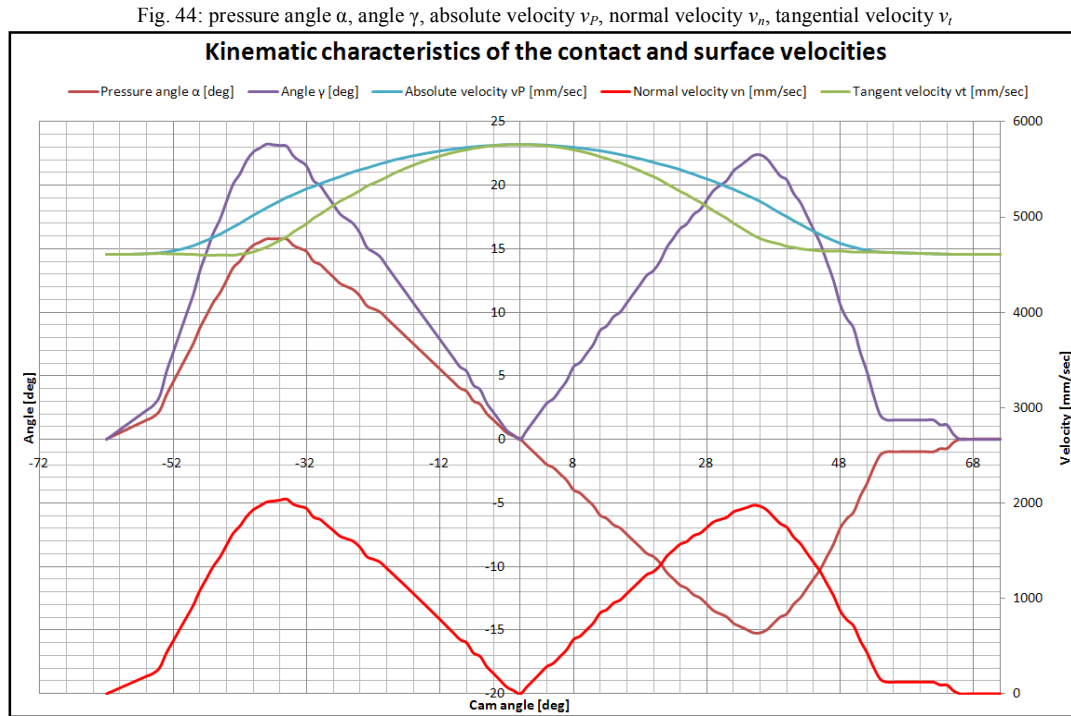
The same Figure shows how the absolute velocity v_P is strongly related to the distance $\overline{OP}$ and the normal v_n and tangential v_t velocities. The values of the tangential velocity v_t on the base circle and at maximum cam lift is the same of absolute velocity v_P because outside the valve event there is no cam lift. On the other hand, the normal velocity v_n varies from 0 mm/s to the maximum velocity on each ramp, because it follows almost the angle γ and the valve velocity trend, in particular, reaches 2042.38 mm/sec at −35 cam deg on the open ramp and 1978.06 mm/s at 35 cam deg on the closed ramp. The most important point to note in Figure 44 is the shape of the normal velocity v_n on the open and closed ramps. The shape of velocity on the height open ramp shows exactly how the height ramp works or rather it boosts the valve velocity from 0 to a maximum slope in a smooth manner. Conversely, the closed ramp drives the valve velocity to 0 through a smooth step. The normal velocity v_n at the end of the height open ramp and at beginning of the closed ramp is, respectively, 215.79 mm/s at −55 cam deg and 123.51 mm/s at 55 cam deg.

New engine concept development-Multi-body dynamic of valvetrain system and friction assessment

Antonio Turturro – Supervisors: Prof. C. Delprete and L. Magro

Figure 45 presents the linear velocity of the rocker pivot which is the same as the normal velocity v_n calculated by the quasi-static model.

Fig. 45: linear velocity of the rocker pivot by quasi-static model
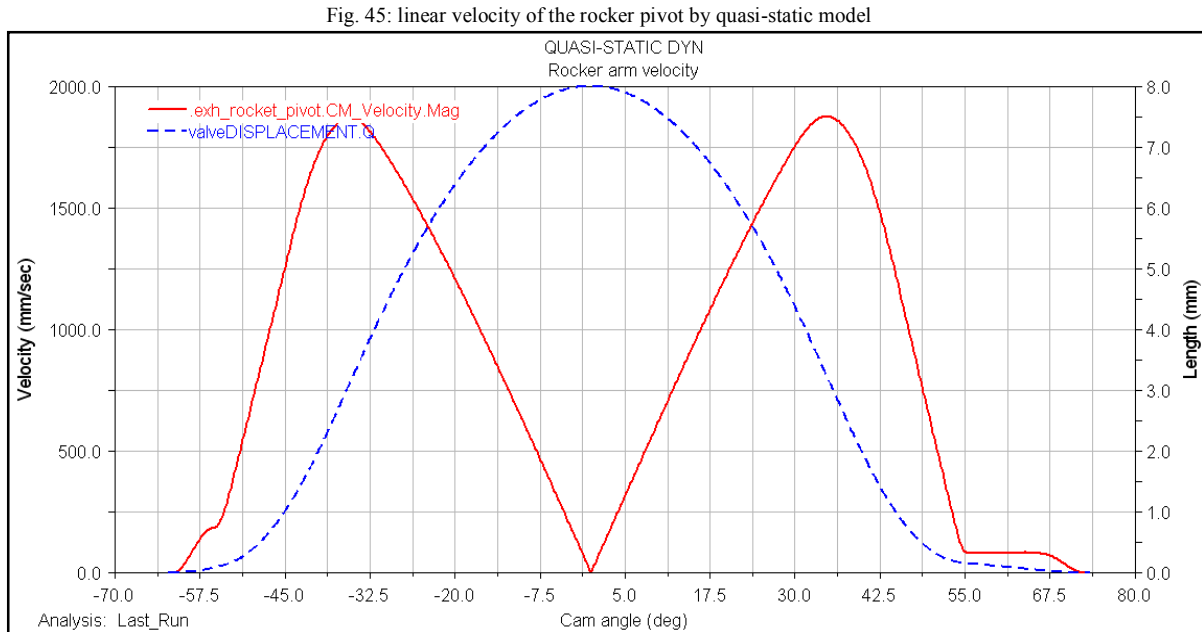
The four velocities to compare the two curves are the maximum velocities on both the open and closed ramp and, as well, at the end of the height open ramp and at the beginning of the closed ramp, and they are, respectively, 1868.48 mm/s at −35.18 cam deg, 1874.57 mm/s at 34.67 cam deg, 180.49 mm/s at −55.60 cam deg, 77.97 mm/s at 55.49 cam deg. The comparison between the kinematic model developed through use of Excel and the result about the normal velocity v_n measured by the ADAMS View 2005 R2 is summed up in Table 11

Tab. 11: normal velocity comparison

Parameter	Excel value [mm/s]	Adams value [mm/s]	Excel angle [cam deg]	Adams angle [cam deg]	Δ value [%]	Δ value [%]
Max height open ramp	215.79	180.49	−55	−55.60	+19.56	−1.08
Max open ramp	2042.38	1868.48	−35	−35	+9.31	0
Max closed ramp	1978.06	1874.57	35	35	+5.52	0
Max height closed ramp	123.51	77.97	55	55.79	+58.41	−1.42

Unfortunately, the accuracy of the Excel model is 1 cam degree and it cannot be compared with the accuracy of ADAMS which is 0.2 cam deg. The normal velocity v_n is good enough

New engine concept development-Multi-body dynamic of valvetrain system and friction assessment

Antonio Turturro – Supervisors: Prof. C. Delprete and L. Magro

on the open and closed ramp with a modest error on the velocities values and no error on the cam angle. For the height ramp the error on the velocities is quite high, but that for the cam angle is acceptable. It is thought that the mismatch on the height ramp is due to the absence of the sliding between the two bodies, which is practice occurs to a certain degree. Figure 46 shows the angular velocity of the roller ω_r in rpm. It follows exactly the tangential velocity v_t scaled to the roller radius as highlighted in the equation (29).

Fig. 46: roller angular velocity
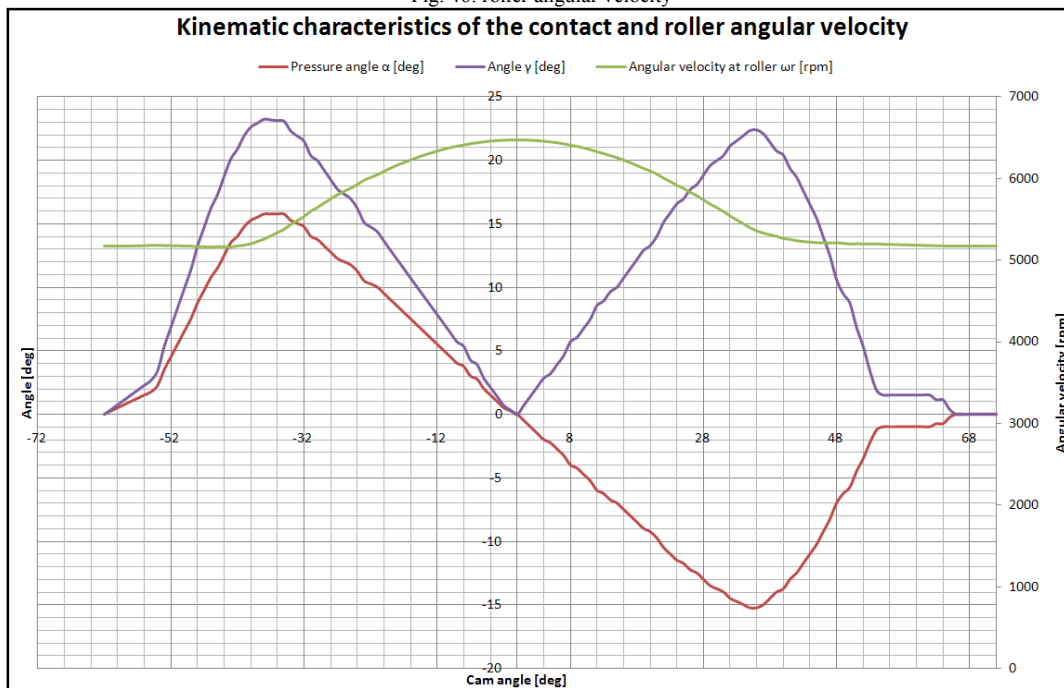
The maximum and minimum angular roller velocities ω_r are, respectively, on the base circle and on cam nose with values 5176.47 rpm and 6474.44 rpm. These constitute all the data required to calculate the entraining velocity of the lubricant into the contact; U in the equation (30):

(30) $$U = \frac{1}{2}\left(v_t^l + v_t^r\right)$$

New engine concept development-Multi-body dynamic of valvetrain system and friction assessment

Antonio Turturro – Supervisors: Prof. C. Delprete and L. Magro

where: v_t^l is the tangential velocity of the cam lobe which means its surface velocity in mm/s; v_t^r is the tangential velocity of the roller that means its surface velocity in mm/s.
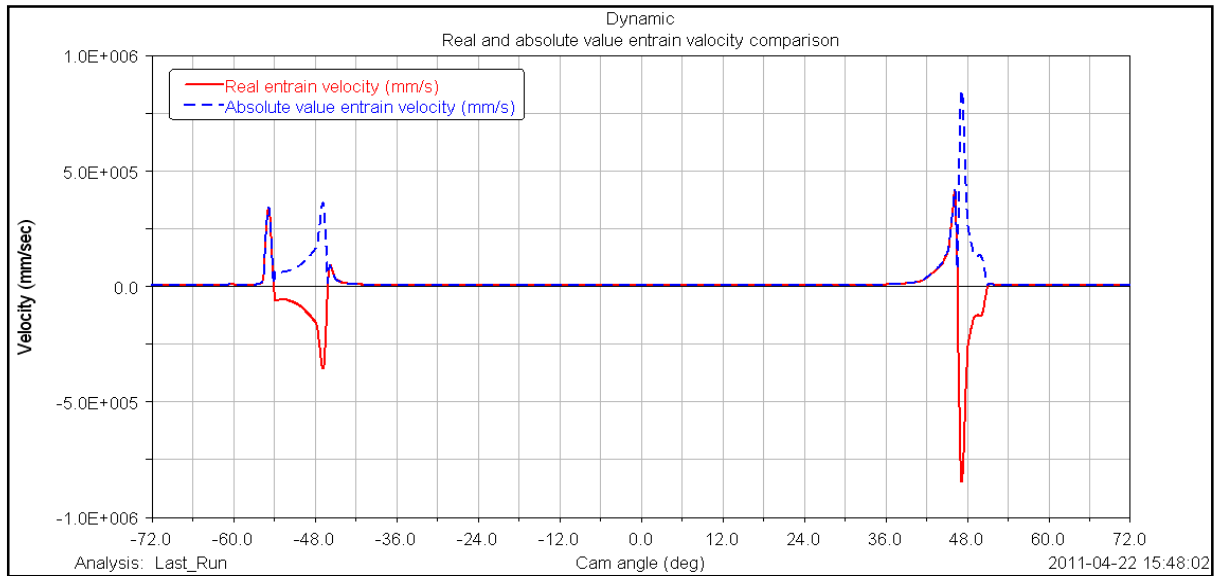
The entraining velocity for the dynamic model is calculated by the equation (30). About the angular velocity of the roller is evaluated directly from the Adams View model and depicts in Figure 47.

Fig. 47: angular velocity of the roller in the dynamic model
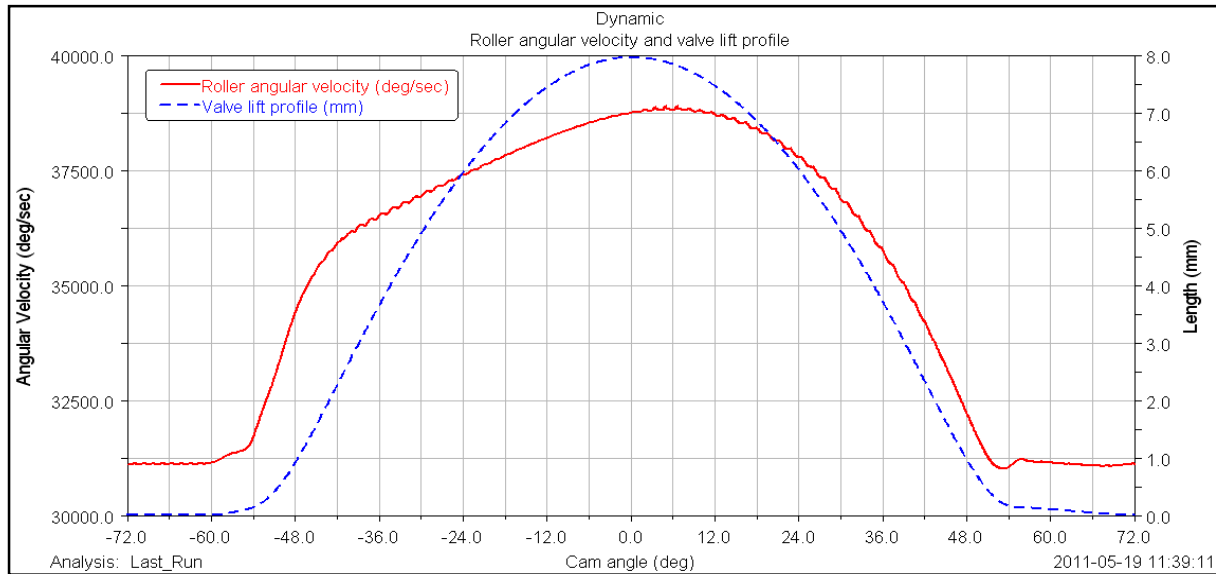
Then, the angular velocity of the roller is multiply with the radius of the roller to obtain the tangential velocity. The shape of the angular velocity follows that one of the valve lift. After the maximum valve lift it is clear the sliding effect on the roller, in particular the peak of the angular velocity is slightly after the peak of the valve lift. On the other hand, the tangential velocity of the cam lobe is evaluated by the radius of curvature of the cam lobe multiply with the angular velocity of the cam lobe. Figure 48 shows the entraining velocity but the concave side of the radius of curvature of the cam lobe produces a negative velocity, and then a negative argument of the first right-side of the equation (25).

New engine concept development-Multi-body dynamic of valvetrain system and friction assessment

Antonio Turturro – Supervisors: Prof. C. Delprete and L. Magro

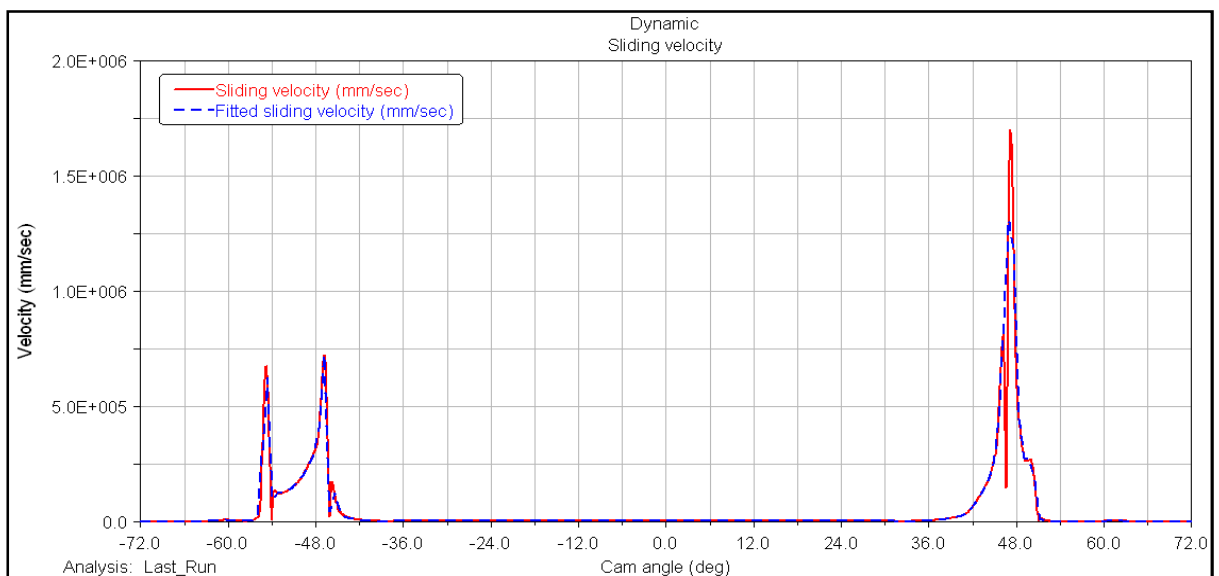Fig. 48: entraining velocity in the dynamic model

So, it is decided to evaluate an absolute value of the entraining velocity and it depicts in Figure 48.

About the sliding velocity, it is used the same velocity components to calculate the entraining velocity in according with the equation (31) and it shows in Figure 49.

(31) $\Delta u = |v_l - v_r|$

Fig. 49: sliding velocity of the roller – cam lobe contact in the dynamic model

New engine concept development-Multi-body dynamic of valvetrain system and friction assessment

Antonio Turturro – Supervisors: Prof. C. Delprete and L. Magro

The sliding velocity follows the radius of curvature of the cam lobe. Figure 49 shows the fitted sliding velocity by the Akima method. The values of the three peaks, from the open side to the closed one, are respectively, 6.21E5 mm/s at −54.63, 7.21E5 mm/s at −46.81 cam deg, 1.31E6 mm/s at −46.96 cam deg.

The sliding between the two bodies produces a decrease of the roller angular velocity ω_r. This decrease of the roller angular velocity is led by the percentage of sliding calculated by the equation (32) proposed by Wang [93] and plotted in Figure 50:

(32) $\qquad \%SLD = \frac{|v_l - v_r|}{\frac{1}{2}|v_l + v_r|} = \frac{\Delta u}{U}$

Fig. 50: percentage of sliding in the roller – cam lobe contact
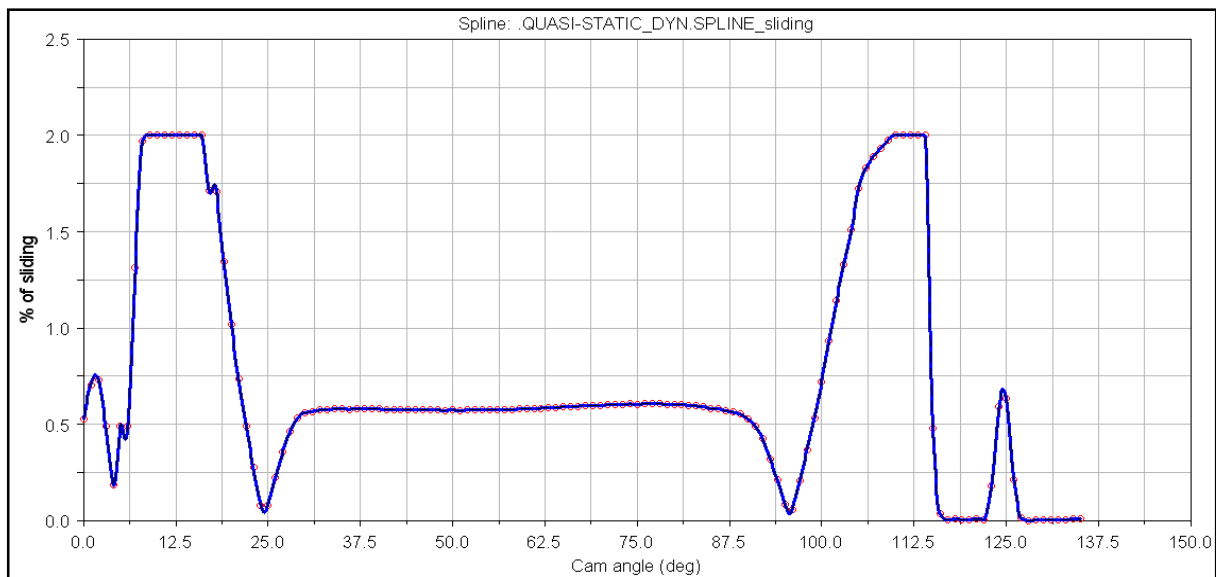
The full length of the EHL contact L is the net length of the roller that means the width of the roller minus the edge chamfer. This is 10.5 mm

The first approach to evaluate the oil film thickness in the dynamic model is to analytically analyse them. First of all, the equivalent or reduced radius of curvature is discussed. The first attempt to analytically evaluate the radius of curvature is through its definition proposed by Chen [96]. The radius of curvature of a curve is a measure of the rate at with which the curve changes direction. Suppose that a curve is given by the equation (33):

New engine concept development-Multi-body dynamic of valvetrain system and friction assessment

Antonio Turturro – Supervisors: Prof. C. Delprete and L. Magro

(33) $\qquad y = f(x)$

and that f has a continuous second derivative. As shown in Figure 51, at a particular point $P_0(x_0,y_0)$ the tangent to the curve makes an angle φ with the positive x direction.

Fig. 51: the definition of the radius of curvature by the derivative
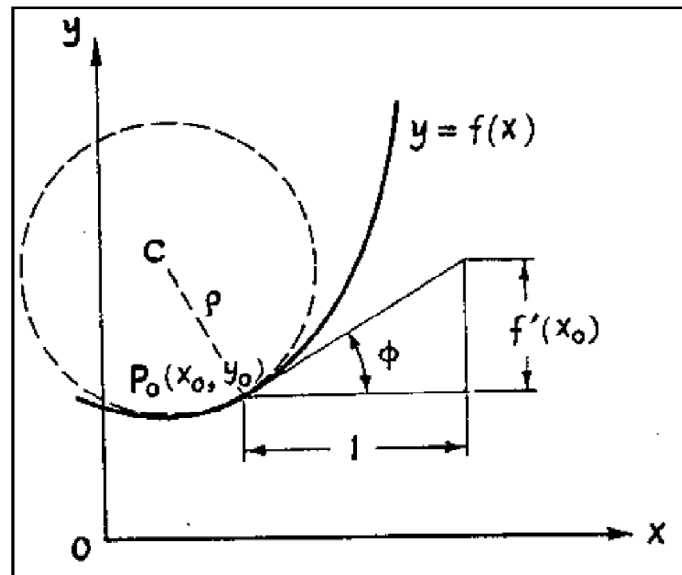
From the definition of a derivative:

(34) $\qquad \varphi = f'(x_0)$

or that at a point $P(x,y)$:

(35) $\qquad \varphi(x) = \tan^{-1}[f'(x)]$

The way φ changes as it moves along a curve is a measure of the sharpness of the curve. Therefore, the curvature k is the rate of change of the angle φ with respect to the arc length s; hence equation (36):

(36) $\qquad k = \dfrac{d\varphi}{ds}$

New engine concept development-Multi-body dynamic of valvetrain system and friction assessment

Antonio Turturro – Supervisors: Prof. C. Delprete and L. Magro

The radius of curvature ρ of an arc at a point is defined as the reciprocal of the absolute value of the curvature at that point, thus:

(37)
$$\rho = \frac{1}{|k|}$$

The circle of curvature of an arc at a point P is the circle which passes through P that has a radius equal to ρ, and whose centre C lies on the concave side of the curve along the normal through P. If the curve is given in the Cartesian coordinates, i.e. equation (33), then radius of curvature is obtained as:

(38)
$$\rho = \frac{\left\{1+[f'(x)]^2\right\}^{\frac{3}{2}}}{f''(x)}$$

In this case, the function under analysis is the cam lift profile depicted in Figure 52.

Fig. 52: cam lift profile
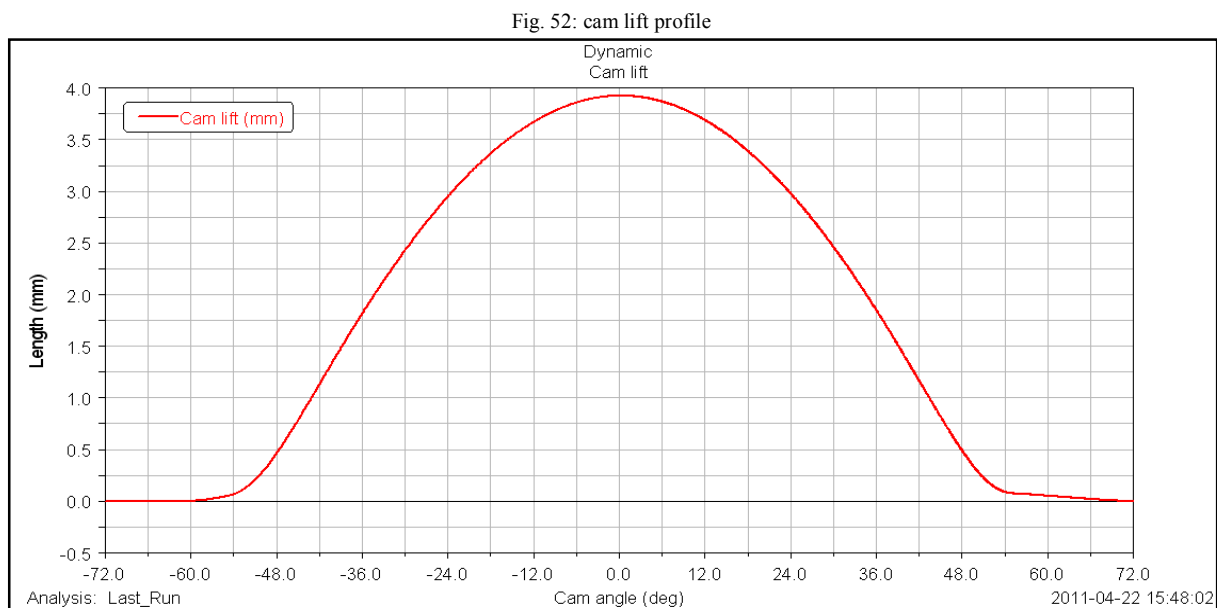
The first derivative and the second derivative of the cam lift profile are, respectively, the cam velocity and the cam acceleration as shown in Figure 53 and Figure 54. For this purpose, cam velocity and acceleration are evaluated by the differentiating the function.

New engine concept development-Multi-body dynamic of valvetrain system and friction assessment

Antonio Turturro – Supervisors: Prof. C. Delprete and L. Magro

Fig. 53: first derivative of the cam lift profile
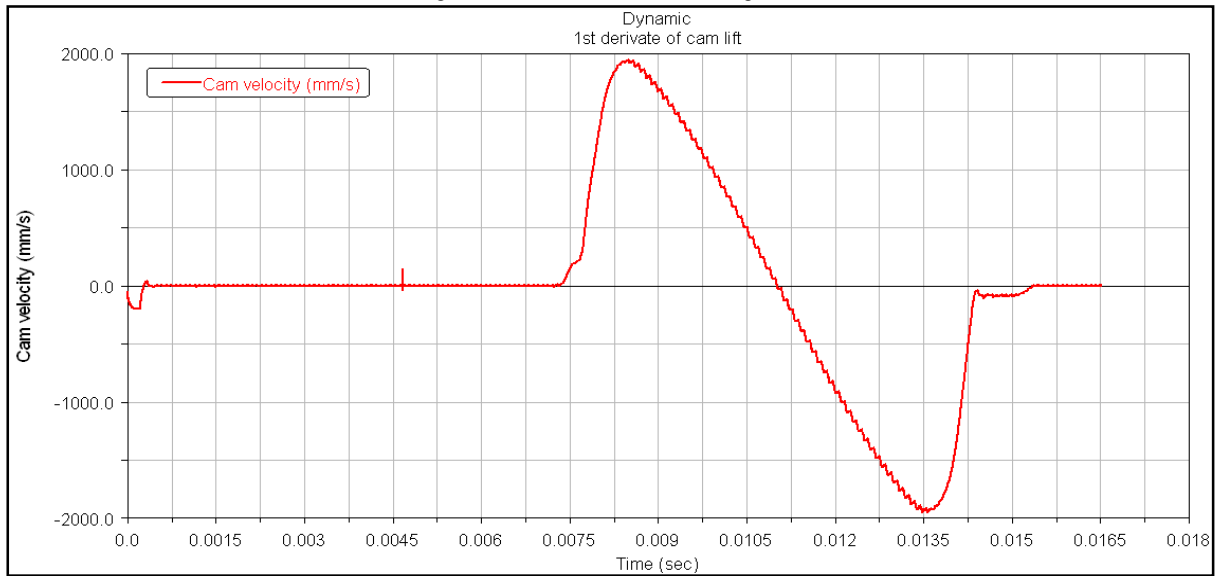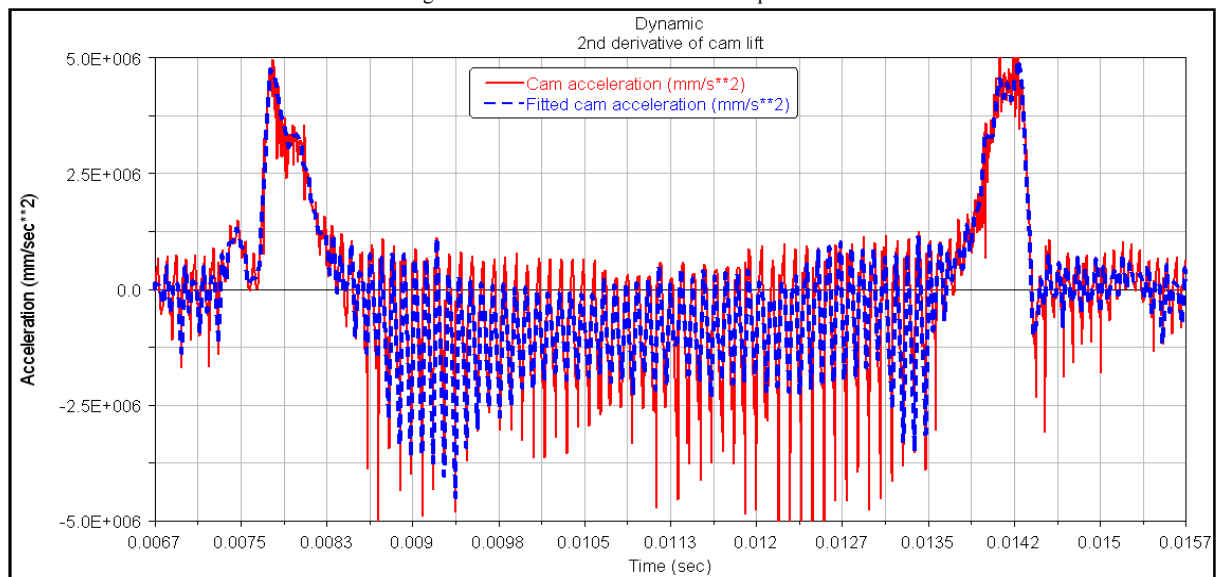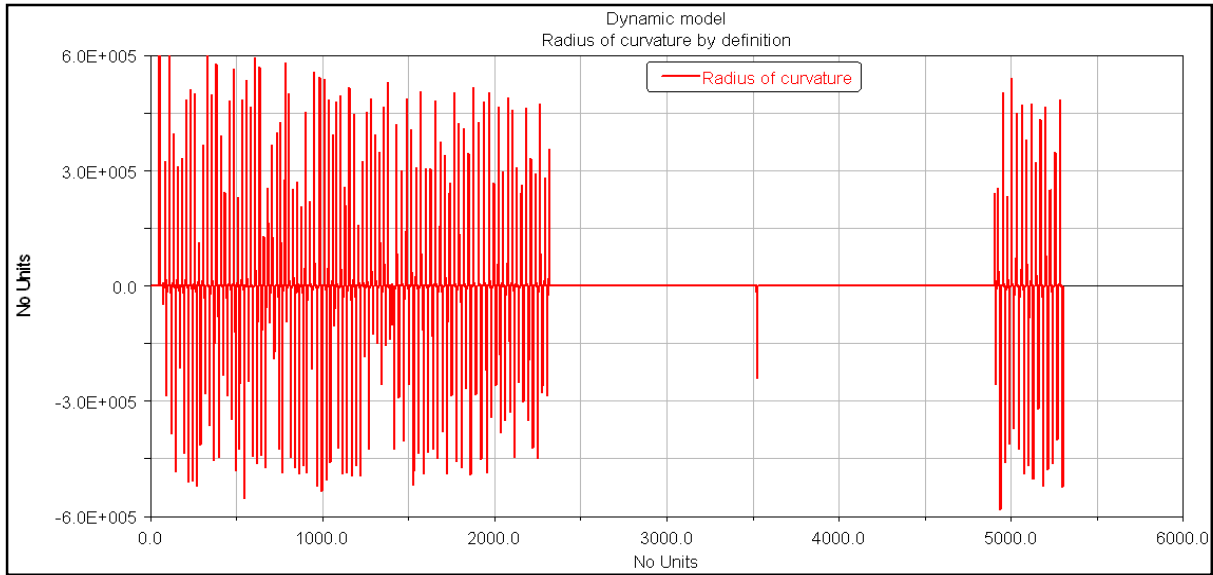

Fig. 54: second derivative of the cam lift profile

Then the radius of curvature is evaluated by equation (38) and plotted in Figure 55.

New engine concept development-Multi-body dynamic of valvetrain system and friction assessment

Antonio Turturro – Supervisors: Prof. C. Delprete and L. Magro

Fig. 55: radius of curvature by definition

Unfortunately, the radius of curvature resulting from this approach is not correct. The reason for this anomaly could be the numerical definition of the function and its derivative.

So, the first attempt to correct this issue it to change the way to read the function and it was decided to use the Stirling interpolation formula presented by Chen [96]. When data are tabulated for uniformly spaced abscissa with increments *h*, it is convenient to express the formulation for interpolation and related processes in terms of a difference table. In connection with the difference table (see Figure 56), Stirling's interpolation formula can be written as the equations (39) and (40):

(39)
$$y = y_i + U \frac{\delta y_{i-1} + \delta y_i}{2} + \frac{U^2}{2} \delta^2 y_{i-1} + \frac{U(U^2-1)}{3!} \frac{\delta^3 y_{i-2} - \delta^3 y_{i-1}}{2} +$$

$$\frac{U^2(U^2-1)}{4!} \delta^4 y_{i-2} + \frac{U(U^2-1)(U^2-2^2)}{5!} \frac{\delta^5 y_{i-3} + \delta^5 y_{i-2}}{2} + \frac{U^2(U^2-1)(U^2-2^2)}{6!} \delta^6 y_{i-3} + \cdots$$

(40)
$$U = \frac{x - x_i}{h}$$

New engine concept development-Multi-body dynamic of valvetrain system and friction assessment

Antonio Turturro – Supervisors: Prof. C. Delprete and L. Magro

Fig. 56: difference table

y	δy	$\delta^2 y$	$\delta^3 y$	$\delta^4 y$	$\delta^5 y$	$\delta^6 y$	$\delta^7 y$	$\delta^8 y$
y_{i-4}								
	δy_{i-4}							
y_{i-3}		$\delta^2 y_{i-4}$						
	δy_{i-3}		$\delta^3 y_{i-4}$					
y_{i-2}		$\delta^2 y_{i-3}$		$\delta^4 y_{i-4}$				
	δy_{i-2}		$\delta^3 y_{i-3}$		$\delta^5 y_{i-4}$			
y_{i-1}		$\delta^2 y_{i-2}$		$\delta^4 y_{i-3}$		$\delta^6 y_{i-4}$		
	δy_{i-1}		$\delta^3 y_{i-2}$		$\delta^5 y_{i-3}$		$\delta^7 y_{i-4}$	
y_i		$\delta^2 y_{i-1}$		$\delta^4 y_{i-2}$		$\delta^6 y_{i-3}$		$\delta^8 y_{i-4}$
	δy_i		$\delta^3 y_{i-1}$		$\delta^5 y_{i-2}$		$\delta^7 y_{i-3}$	
y_{i+1}		$\delta^2 y_i$		$\delta^4 y_{i-1}$		$\delta^6 y_{i-2}$		$\delta^8 y_{i-3}$
	δy_{i+1}		$\delta^3 y_i$		$\delta^5 y_{i-1}$		$\delta^7 y_{i-2}$	
y_{i+2}		$\delta^2 y_{i+1}$		$\delta^4 y_i$		$\delta^6 y_{i-1}$		
	δy_{i+2}		$\delta^3 y_{i+1}$		$\delta^5 y_i$			
y_{i+3}		$\delta^2 y_{i+2}$		$\delta^4 y_{i+1}$				
	δy_{i+3}		$\delta^3 y_{i+2}$					
y_{i+4}		$\delta^2 y_{i+3}$						
	δy_{i+4}							
y_{i+5}								

As shown in Figure 56, the meaning of the terms $\delta^m y_{i\pm n}$ is to consider the m difference of the point backward or forward in n steps from i. Some examples are reported in the equations (41) and (42):

(41) $$\delta y_{i-1} = y_i - y_{i-1}$$

(42) $$\delta y_i = y_{i+1} - y_i$$

Equations (41) and (42) refer to the first difference, but the following differences work in a cascade way as reported in the equations (43) and (44):

(43) $$\delta^3 y_{i-2} = \delta^2 y_{i-1} - \delta^2 y_{i-2}$$

(44) $$\delta^6 y_{i-3} = \delta^5 y_{i-2} - \delta^5 y_{i-3}$$

Differentiating the equation (39) with respect to x gives the equation (45):

(45)
$$\frac{dy}{dx} = \frac{dy}{dU}\frac{dU}{dx} = \frac{1}{h}\frac{dy}{dU}\frac{1}{h}\left[\frac{\delta y_{i-2}+\delta y_i}{2} + U\delta^2 y_{i-2} + \frac{3U^2-1}{3!}\frac{\delta^3 y_{i-2}+\delta^3 y_{i-1}}{2} + \right.$$
$$\frac{3U^2-1}{3!}\frac{\delta^3 y_{i-2}+\delta^3 y_{i-1}}{2} + \frac{4U^3-2U}{4!}\delta^4 y_{i-2} + \frac{5U^4-15U^2+4}{5!}\frac{\delta^5 y_{i-3}+\delta^5 y_{i-2}}{2} +$$
$$\left. \frac{6U^5-20U^3+8U}{6!}\delta^6 y_{i-3} + \cdots\right]$$

New engine concept development-Multi-body dynamic of valvetrain system and friction assessment

Antonio Turturro – Supervisors: Prof. C. Delprete and L. Magro

For the point $x = x_i$, it has $U = O$. Hence, upon substitution of this value of U into the equation (45), it obtains the equation (46) is obtained as:

(46)
$$\left(\frac{dy}{dx}\right)_{x_i} = \frac{1}{h}\left[\frac{\delta y_{i-1}+\delta y_i}{2} - \frac{1}{6}\frac{\delta^3 y_{i-2}+\delta^3 y_{i-1}}{2} + \frac{1}{30}\frac{\delta^5 y_{i-3}+\delta^5 y_{i-2}}{2} + \cdots\right]$$

If equation (45) is differentiated with respect to x another time, equation (47) is obtained as:

(47)

$$\frac{d^2 y}{dx^2} = \frac{1}{h^2}\left[\delta^2 y_{i-1} + U\frac{\delta^3 y_{i-2}+\delta^3 y_{i-1}}{2} + \frac{12U^2-2}{4!}\delta^4 y_{i-2} + \frac{20U^3-30U}{5!}\frac{\delta^5 y_{i-3}+\delta^5 y_{i-2}}{2} + \frac{30U^4-60U^2+8}{6!}\delta^6 y_{i-3} + \cdots\right]$$

The point $x = x_i$, it has $U = O$. Substituting this value of U into equation (47), equation (48) is obtained as:

(48)
$$\left(\frac{d^2 y}{dx^2}\right)_{x_i} = \frac{1}{h^2}\left[\delta^2 y_{i-1} - \frac{1}{12}\delta^4 y_{i-2} + \frac{1}{90}\delta^6 y_{i-3} + \cdots\right]$$

Unfortunately, the Sterling's interpolation formula does not work as well. The main reason is the limitation of the ADAMS View's function builder to build a backward numerical scheme and in particular to implement the difference table. After the previous two attempts, it is understood that a deep numerical strategy is the wrong way to approach the determination of the radius of curvature. So, it is decided to approach this issue in a geometrical manner and the radius of curvature is derived by the method of pole proposed by Chen [96]. In this method there are two important steps: the first one is the evaluation of the pressure angle α and the second one is the derivation of the radius of curvature. In Figure 57 a disc cam rotates clockwise about the camshaft O, imparting motion to an oscillating roller follower of length L which is pivoted at point Q.

New engine concept development-Multi-body dynamic of valvetrain system and friction assessment

Antonio Turturro – Supervisors: Prof. C. Delprete and L. Magro

Fig. 57: (a) radius of curvature derived by the method of pole for the radial cam with swinging roller follower; (b) acceleration polygon
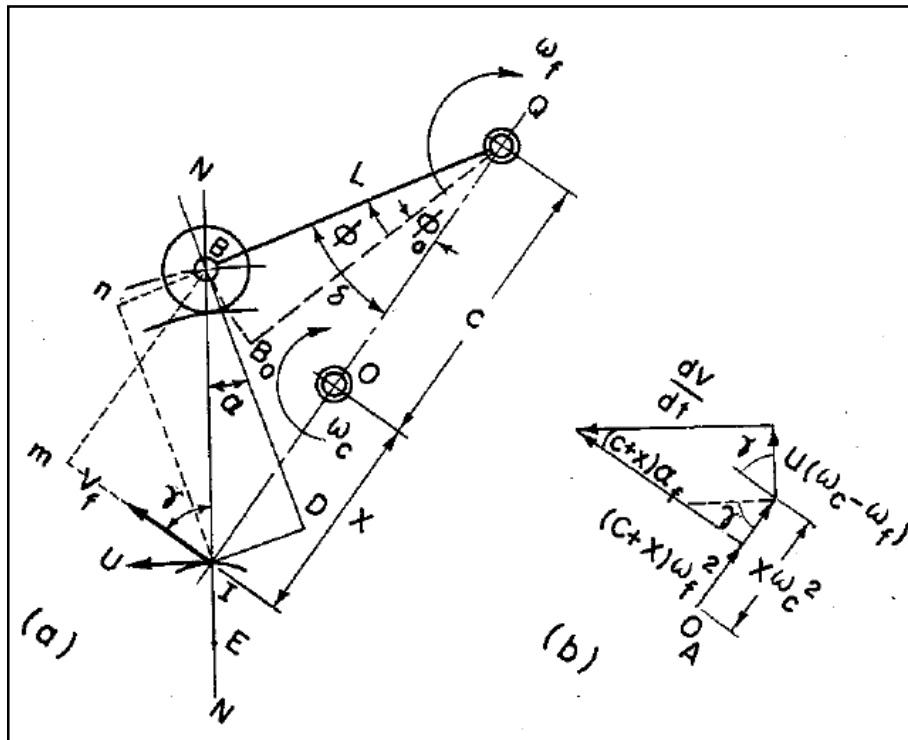
The distance O and Q is c. The fixed angle φ_0 defines the lowest position of the follower. The pressure angle α is between the common normal NN to the curve at the point of roller contact and BD, the normal to the centreline of the follower arm. In the position shown in Figure 57, NN cuts the line of centres OQ at pole I. Since OI and QI are in the same direction, both the cam and the follower will rotate in the same direction. Based in the geometry of Figure 57, the velocity of the follower at point B is as equation (49):

(49)
$$V_f = x\omega_c = (c + x)\omega_f$$

where x is the distance OI. ω_f and ω_c represent the angular velocities of the follower and the cam, respectively. From this equation it obtains as equation (50):

(50)
$$x = \frac{c\omega_f}{\omega_c - \omega_f}$$

Then, equation (51) follows:

New engine concept development-Multi-body dynamic of valvetrain system and friction assessment

Antonio Turturro – Supervisors: Prof. C. Delprete and L. Magro

(51) $$c + x = c\left(1 + \frac{\omega_f}{\omega_c - \omega_f}\right) = \frac{c\omega_c}{\omega_c - \omega_f}$$

or the equation (52):

(52) $$c + x = \frac{c}{1 - \frac{\omega_f}{\omega_c}}$$

Since the angular displacement of the follower is φ, it can be written by the equations (53) and (54):

(53) $$\varphi = f(\theta)$$

(54) $$\frac{d\varphi}{d\theta} = \frac{\frac{d\varphi}{dt}}{\frac{d\theta}{dt}} = \frac{\omega_f}{\omega_c}$$

from which it follows that as the equation (55):

(55) $$c + x = \frac{c}{1 - \frac{d\varphi}{d\theta}}$$

Figure 58 shows equation (53) and, in particular, the angular velocity of the cam lobe, of the end-pivot arm, and the rate between both the velocities.

New engine concept development-Multi-body dynamic of valvetrain system and friction assessment

Antonio Turturro – Supervisors: Prof. C. Delprete and L. Magro

Fig. 58: cam lobe angular velocity, follower angular velocity and the rate of them
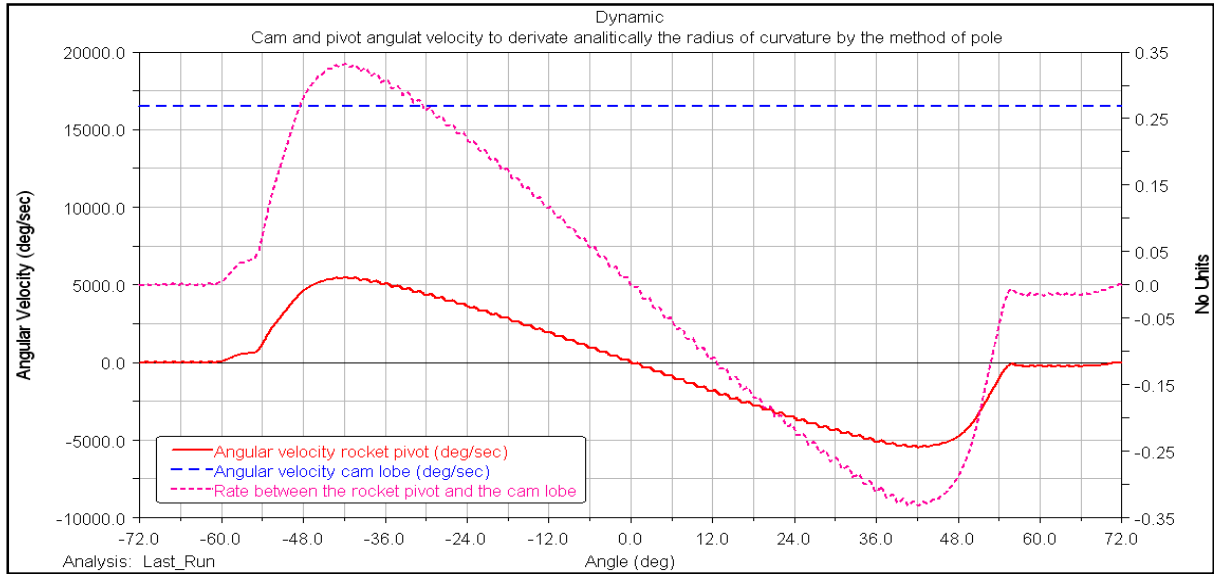
From Figure 57, it can be shown that:

$$(56) \qquad \tan \alpha = \frac{\overline{ID}}{\overline{BD}} = \frac{\overline{nB}}{\overline{nI}} = \frac{(c+x)\cos(\varphi+\varphi_0)-L}{(c+x)\sin(\varphi+\varphi_0)}$$
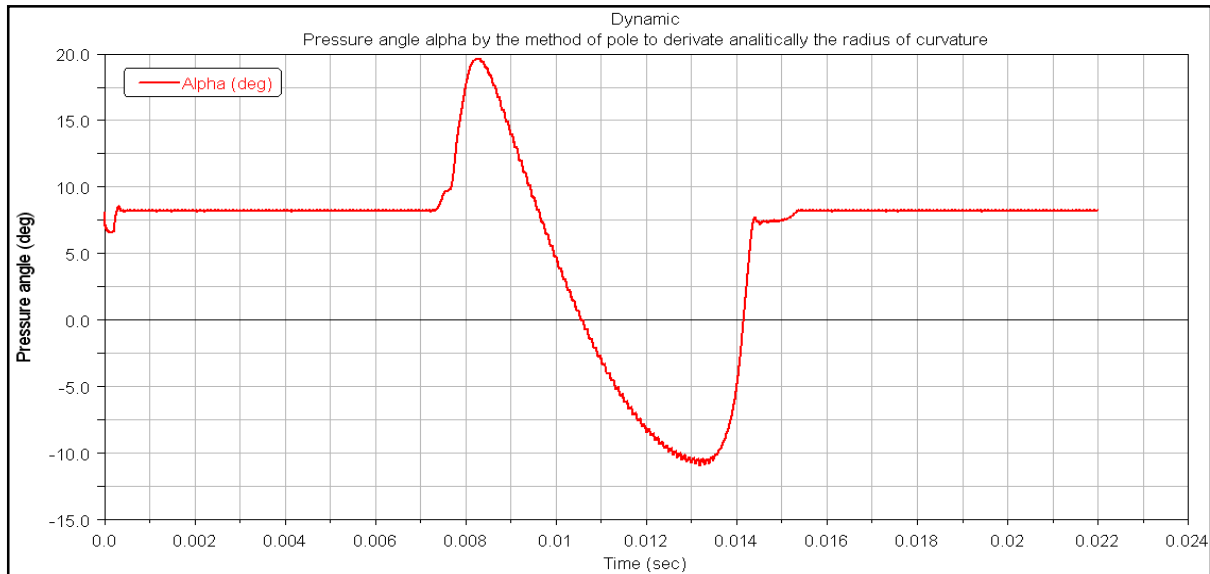
or as:

$$(57) \qquad \tan \alpha = \cot(\varphi + \varphi_0) - \frac{L}{(c+x)\sin(\varphi+\varphi_0)}$$

Using equation (55) yields:

$$(58) \qquad \tan \alpha = \cot(\varphi + \varphi_0) - \frac{L\left(1-\frac{d\varphi}{d\theta}\right)}{c\sin(\varphi+\varphi_0)}$$

Figure 59 shows the pressure angle α calculated by the method of pole. Clearly, the radius of the base circle r_0 is OB_0.

New engine concept development-Multi-body dynamic of valvetrain system and friction assessment

Antonio Turturro – Supervisors: Prof. C. Delprete and L. Magro

Fig. 59: pressure angle derived by the method of pole

The relation between φ_0 and r_0 is as the equation (59):

(59) $$r_0 = \sqrt{l^2 + c^2 - 2\,l\,c\,\cos\varphi_0}$$

In equation (58), $\frac{d\varphi}{d\theta}$ is negative if ω_c is counter clockwise. If *tan α* is negative, it signifies that the common normal *NN* lies on the other side of the perpendicular to the follower arm.

Consider the cam and the follower as two bodies in direct contact. In Figure 64, point *B* is the centre of curvature of the follower roller, and point *E* is assumed to be the centre of curvature of the cam. Note again that these three points (*B*, *E*, *I*) are on the common normal *NN*. Regarding $\rho_f = BI$ and $\rho_c = EI$ as the radii of curvature of the follower roller and the cam, respectively, and note that both are directed quantities. The pole velocity for pure rolling contact in this case is as equation (60):

(60) $$U = \frac{\rho_f(\omega_c - \omega_f)}{1 + \frac{\rho_f}{\rho_c}}$$

where *U* is directed downward and perpendicular to *NN*, as shown in Figure 57. Because ω_c > ω_f, $(\omega_c - \omega_f)$ then it is clockwise. From the acceleration polygon shown in the Figure 57, projection of the acceleration vectors along the common normal results in the relationship as in equation (61)

New engine concept development-Multi-body dynamic of valvetrain system and friction assessment

Antonio Turturro – Supervisors: Prof. C. Delprete and L. Magro

(61) $\qquad (c+x)\dot{\omega}_f \cos\gamma = U(\omega_c - \omega_f) + \left[x\omega_c^2 - (c+x)\omega_f^2\right]\sin\gamma$

In the first term of the right-hand side of the equation (61), it is known from the equation (50) that

(62) $\qquad \omega_c - \omega_f = \omega_c - \dfrac{x}{c+x}\omega_c = \dfrac{c}{c+x}\omega_c$

This together with equation (60), gives

(63) $\qquad U(\omega_c - \omega_f) = \dfrac{\rho_f}{1+\frac{\rho_f}{\rho_c}}(\omega_c - \omega_f)^2 = \dfrac{\rho_f \rho_c}{\rho_f + \rho_c}\left(\dfrac{c}{c+x}\right)^2 \omega_c^2 = \rho_f - \dfrac{\rho_f^2}{\rho_f + \rho_c}\left(\dfrac{c}{c+x}\right)^2 \omega_c^2$

Again using equation (50), the second term of the right-hand side of equation (61) becomes:

(64) $\qquad x\omega_c^2 - (c+x)\omega_f^2 = x\omega_c^2 - x\omega_c\left(\dfrac{x\omega_c}{c+x}\right) = \left(\dfrac{cx}{c+x}\right)\omega_c^2$

Designating the radius of curvature of the cam pitch curve by $\rho = (\rho_f + \rho_c)$ and dividing equation (61) by ω_c^2 after substituting equation (63) and equation (64) into equation (61), it follows that:

(65) $\qquad \dfrac{1}{\rho} = \dfrac{\rho_f\left(\frac{c}{c+x}\right)^2 + \frac{cx}{c+x}\sin\gamma - (c+x)\frac{d^2\varphi}{d\theta^2}\cos\gamma}{\omega_f^2\left(\frac{c}{c+x}\right)^2}$

in which the following relationship is used:

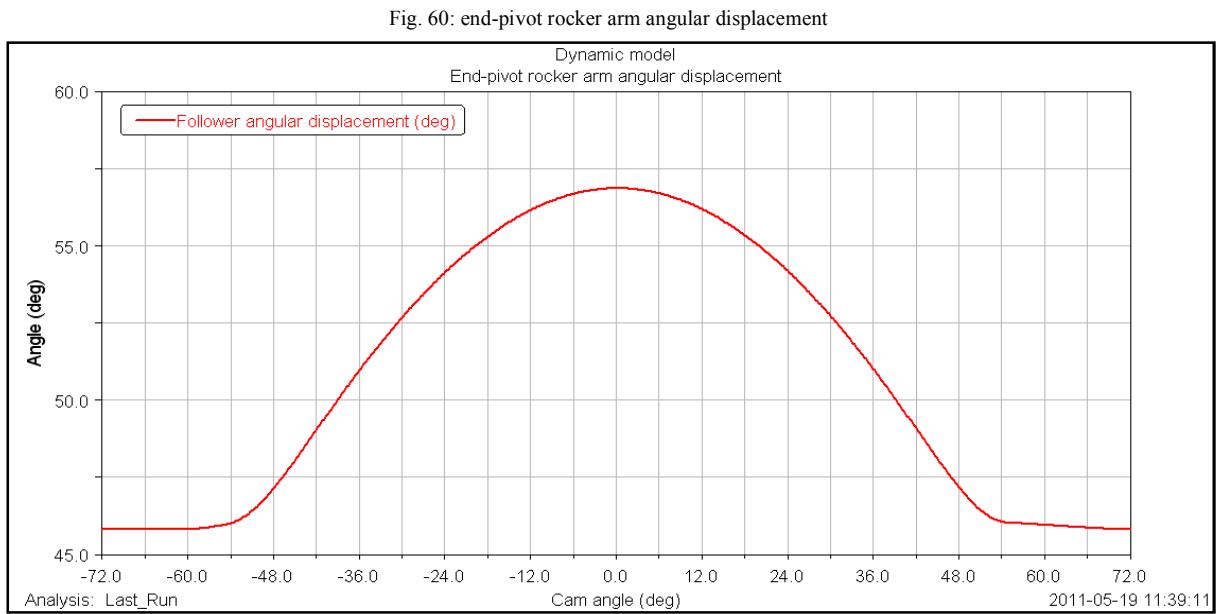(66) $\qquad \dfrac{\dot{\omega}_f}{\omega_c^2} = \dfrac{d^2\varphi}{d\theta^2}$

Designating the angle $(\varphi_0 + \varphi) = \delta$, with the aid of the triangle QIn in Figure 57, it can be written as:

New engine concept development-Multi-body dynamic of valvetrain system and friction assessment

Antonio Turturro – Supervisors: Prof. C. Delprete and L. Magro

(67) $\qquad BI = \rho_f = \dfrac{(c+x)\sin\alpha}{\cos\alpha}$

and also

(68) $\qquad \rho_f = \dfrac{(c+x)\cos\delta - L}{\sin\alpha}$

Figure 60 shows the angle δ.

Fig. 60: end-pivot rocker arm angular displacement

Equating this with equations (67) and (68) gives:

(69) $\qquad L = (c+x)[\cos\delta - \sin\delta\tan\alpha]$

Referring to the triangle *BIm* in Figure 56 and using equation (67) yields:

(70) $\qquad \cos\gamma = \dfrac{L\sin\delta}{\rho_f} = \dfrac{L\sin\delta\cos\alpha}{(c+x)\sin\delta} = \dfrac{L\cos\alpha}{c+x}$

where:

(71) $\qquad \gamma = \delta + \alpha$

New engine concept development-Multi-body dynamic of valvetrain system and friction assessment

Antonio Turturro – Supervisors: Prof. C. Delprete and L. Magro

(72) $$\sin \gamma = \sin \delta \cos \alpha + \cos \delta \sin \alpha$$

Substituting equations (67), (69), (70), and (72) into the equation (65) leads to:

(73) $$\frac{1}{\rho} = \frac{\cos \alpha}{c \sin \delta} + \frac{Lx}{c(c+x)^2} \frac{\sin \alpha \cos^2 \alpha}{\sin^2 \delta} - \frac{L\frac{d^2\varphi}{d\theta^2}\cos^3 \alpha}{c^2 \sin^2 \delta}$$

Finally, substituting equations (50) and (55) into equation (65) results in:

(74) $$\frac{1}{\rho} = \lambda\{1 + \lambda[(1 - \varphi')\varphi' \sin \alpha - \varphi'' \cos \alpha]\}$$

where

(75) $$\lambda = \frac{\cos \alpha}{c \sin \delta}$$

(76) $$\varphi' = \frac{d\varphi}{d\theta}$$

(77) $$\varphi'' = \frac{d^2\varphi}{d\theta^2}$$

Figure 61 and Figure 62 show, respectively, *sin δ* and the parameter λ. In equation (74), the following sign convention should be observed: *φ'* is $\begin{pmatrix}negative \\ positive\end{pmatrix}$ when the cam and the follower are in the $\begin{pmatrix}same \\ opposite\end{pmatrix}$ direction of rotation during the outward motion stroke; *sin α* is $\begin{pmatrix}positive \\ negative\end{pmatrix}$ when *tan α* in the equation (58) is $\begin{pmatrix}positive \\ negative\end{pmatrix}$. When ρ is positive, the pitch curve is convex and the converse is true for a negative curvature. In the end, the radius of curvature derived by the method of pole is depicted in Figure 63.

New engine concept development-Multi-body dynamic of valvetrain system and friction assessment

Antonio Turturro – Supervisors: Prof. C. Delprete and L. Magro

Fig. 61: sine of end-pivot rocker arm angular displacement
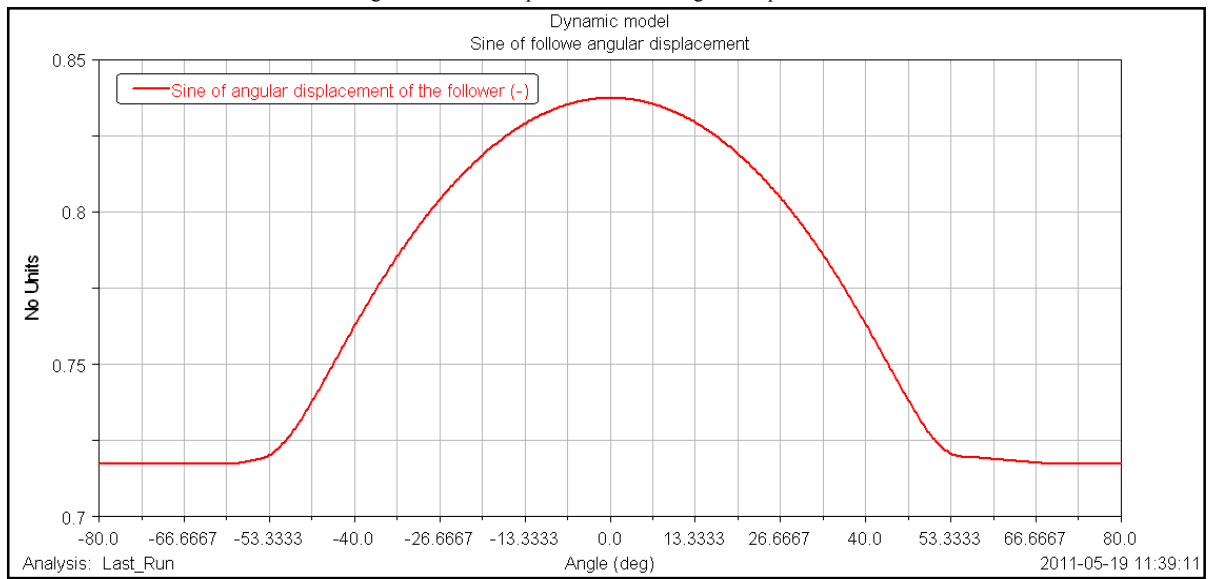
Fig. 62: lambda parameter of the method of pole

New engine concept development-Multi-body dynamic of valvetrain system and friction assessment

Antonio Turturro – Supervisors: Prof. C. Delprete and L. Magro
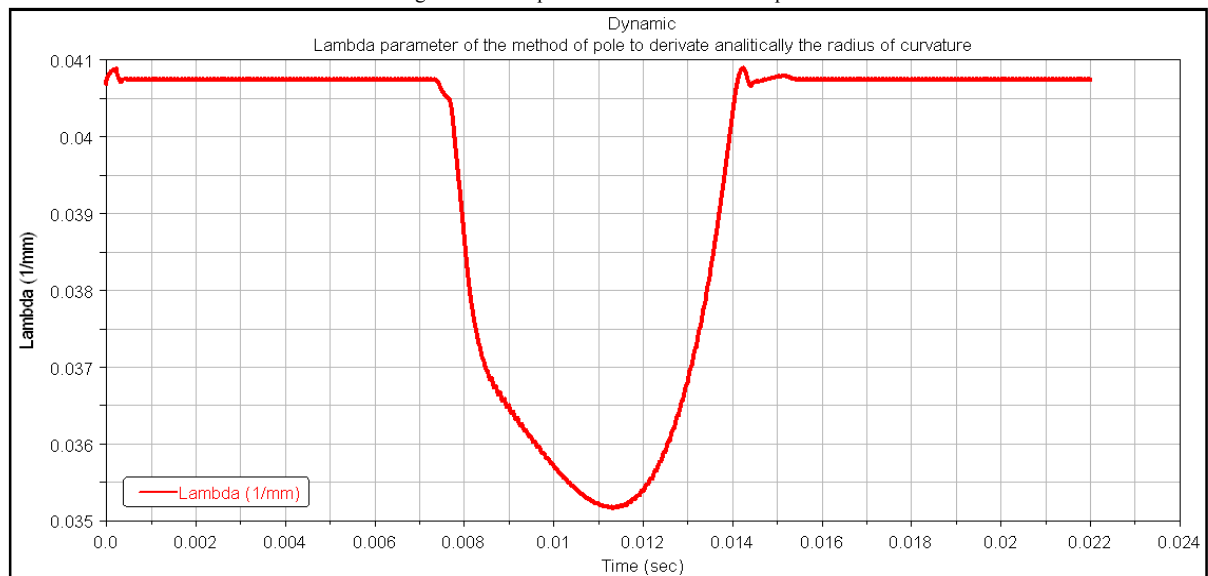
Fig. 63: radius of curvature derived by method of pole
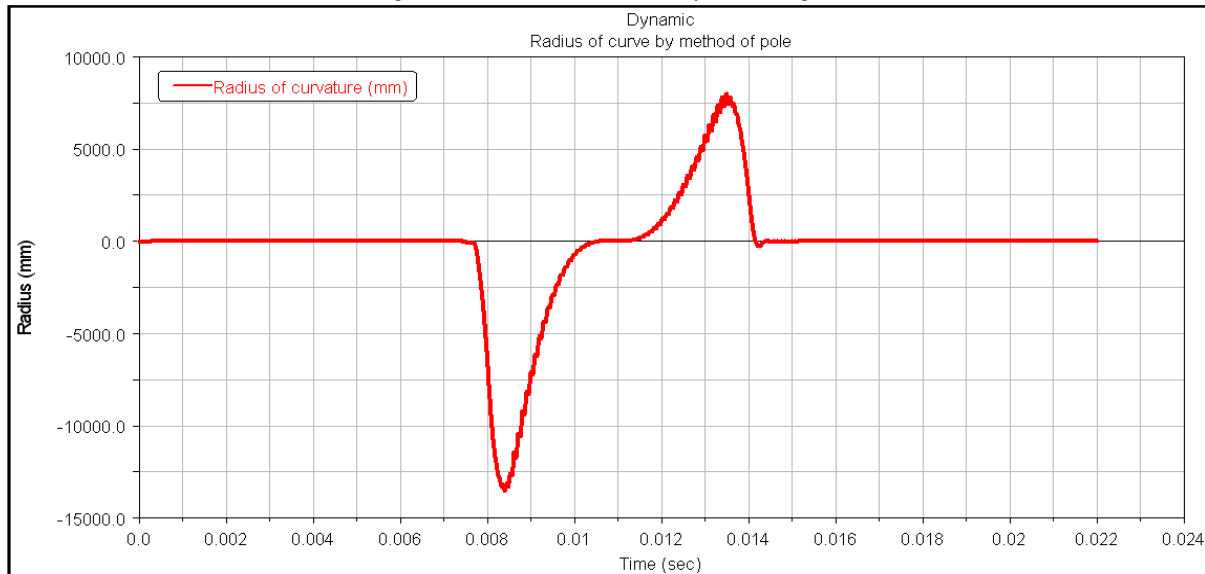
The shape of the radius of curvature by the method of pole is affected by different factors. First of all, this mathematical synthesis model does not take into account the sliding effect that leads to the imbalance of the pressure angle, the lambda parameter and the radius of curvature shape. Secondly, the method of pole derives the radius of curvature from a kinematic point of view, but nowadays, the radius of curvature and, consequently the cam lift profile are designed by the shape of acceleration curve and further considering the jerk, the third derivative of the cam lift, and the ping, the forth derivative of the cam lift. At the end, the radius of curvature shape derived by the method of pole could be correct in accord with the cam radius of curvature proposed by Wang [93] (see the Figure 64) but is contrary to that proposed by Norton [97] (see the Figure 65).

Fig. 64: instantaneous cam radius of curvature

New engine concept development-Multi-body dynamic of valvetrain system and friction assessment

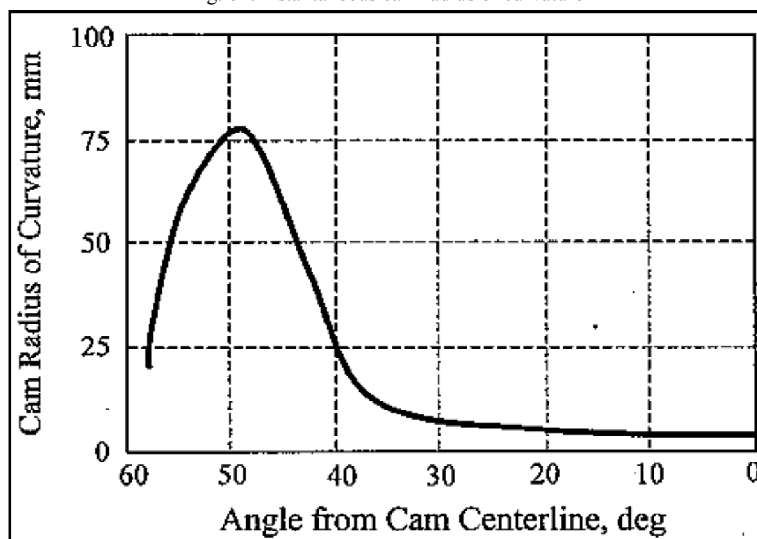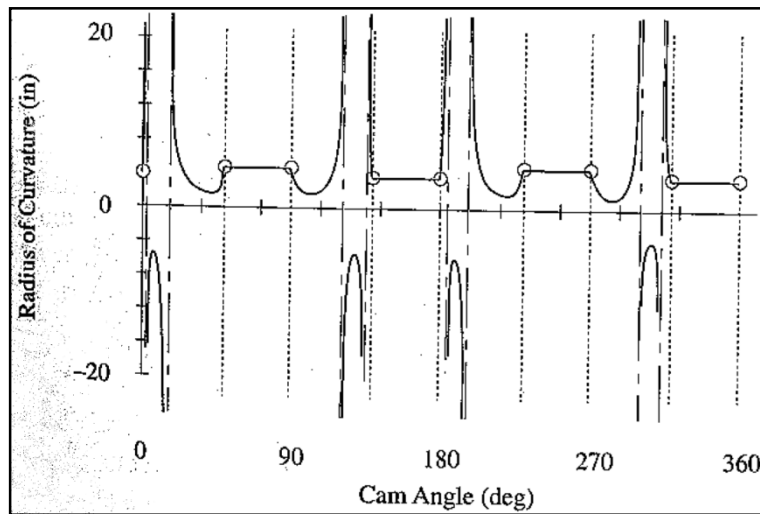Antonio Turturro – Supervisors: Prof. C. Delprete and L. Magro

Fig. 65: radius of curvature of a four-dwell radial cam with translating roller follower

The reason for this conflict is the description of the cam profile that has a strongly influence on the radius of curvature profile. In this project, it is probably used as a double-dwell radial cam and the method of pole is not able to describe correctly the radius of curvature of this type of cam and if it is used the radius of curvature in Figure 63, the valve acceleration profile will not conform to that evaluated by ADAMS View. Therefore, for this reason it is decided to use the radius cam profile in Figure 23. Then, the equivalent radius of contact is evaluated in the same way as for the quasi-static model and is shown in Figure 66.

Fig. 66: equivalent radius of contact for the cam lobe – roller coupling in the dynamic model
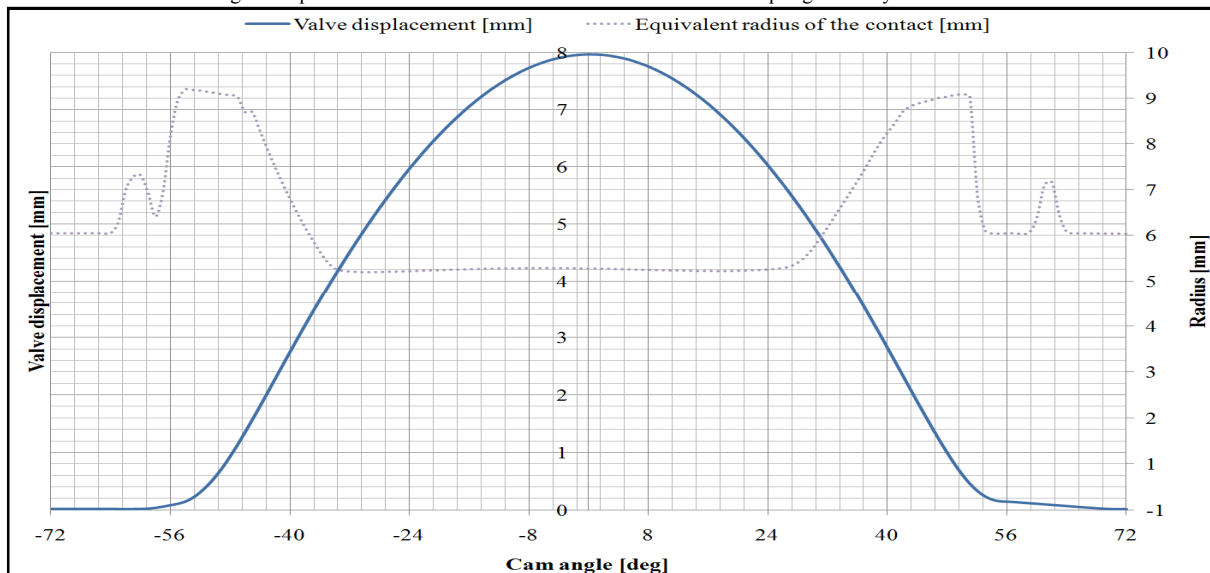

Figure 66 presents both the equivalent radius of contact and the cam lift profile for comparison purposes. The equivalent radius of curvature at maximum valve lift is 4.78 mm at

New engine concept development-Multi-body dynamic of valvetrain system and friction assessment

Antonio Turturro – Supervisors: Prof. C. Delprete and L. Magro

0 cam deg and it remains almost constant, while the maximum radii of curvature of both the opening and closing ramps are, respectively, 8.92 at −53.97 cam deg and 8.88 at 50.83 cam deg. Indeed, the maximum equivalent radii of contact, respectively, at height opening ramp and at height closing ramps are: 6.84 mm at −60.29 cam deg and 6.73 mm at 61.58 cam deg. Table 12 sums up the relevant equivalent radii of the roller/cam contact.

Tab. 12: relevant equivalent radius of roller - cam lobe contact for the dynamic model

Reduced radius of curvature	Value [mm]	Angle [cam deg]
Max radius at height open ramp	6.84	−60.29
Max radius at open ramp	8.92	−53.97
Radius at max cam lift	4.78	0
Max radius at closed ramp	8.88	50.83
Max radius at height closed ramp	6.73	61.58

Finally the oil film thickness is evaluated by the Grubin's equation proposed by Gohar and Rahnejat [73] (see equation (25)) and depicts in Figure 67.

Fig. 67: oil film thickness by Grubin's equation in the dynamic model
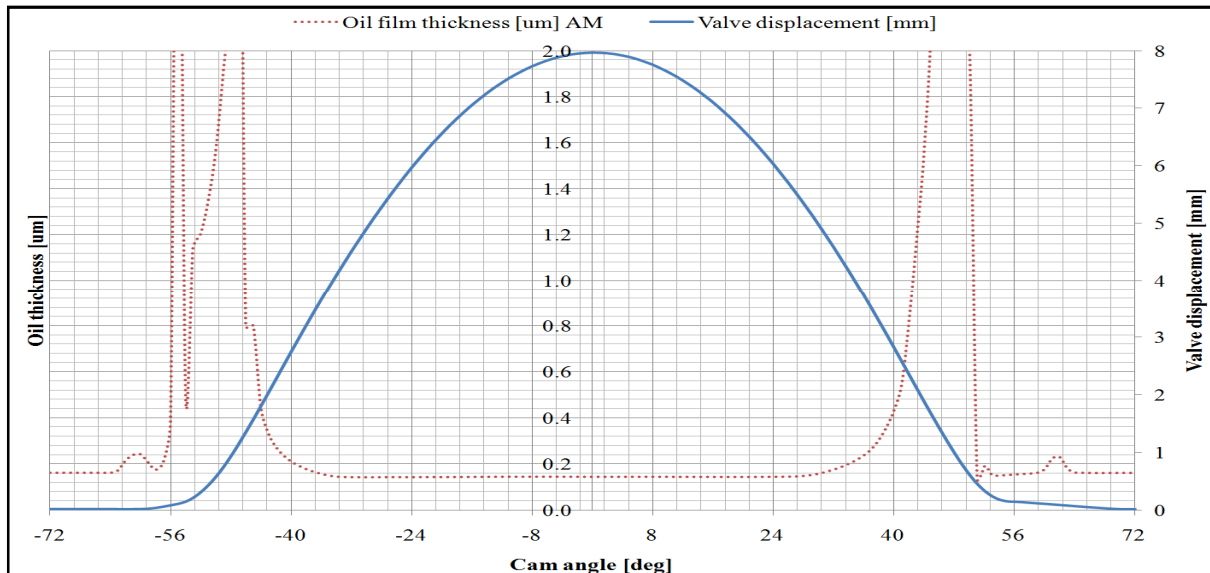
The oil film thickness is fitted with the Akima method and it is possible highlight three peaks that derive from the radius of curvature trend of the cam lobe. Actually, there are 4 peaks but the Akima method fuse that of the closed side. The peaks values of the open and closing side are, respectively, 3.73 μm at −54.63 cam deg, 4.01 μm at −46.81 cam deg, and 6.96 μm at
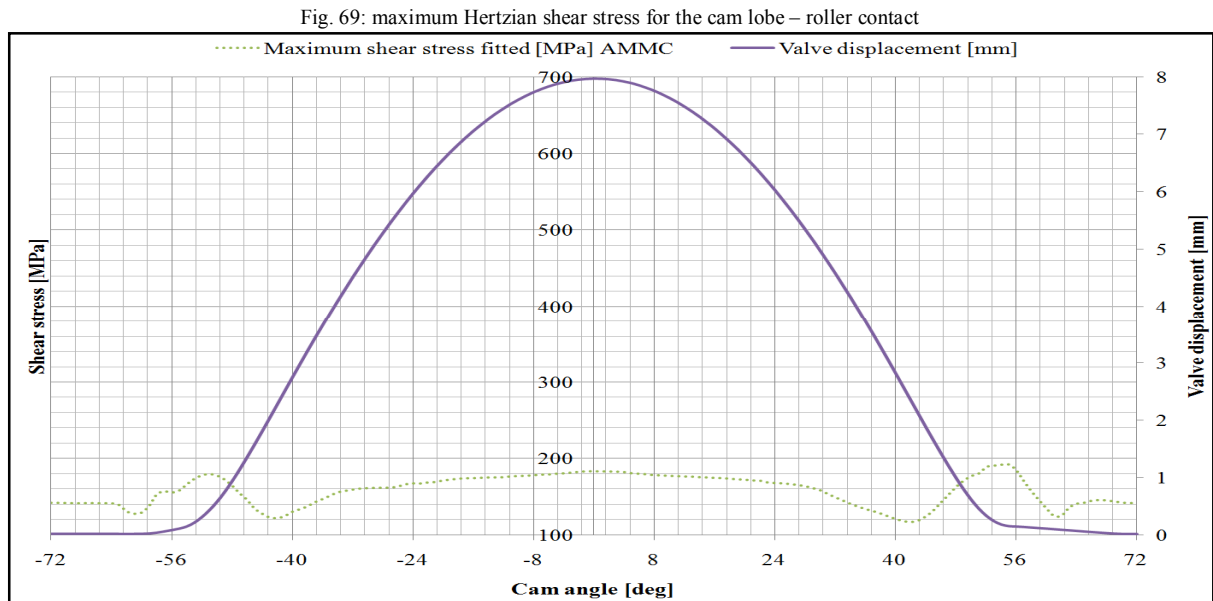
New engine concept development-Multi-body dynamic of valvetrain system and friction assessment

Antonio Turturro – Supervisors: Prof. C. Delprete and L. Magro

46.96 cam deg. On the height opening and closing ramp, the values of the oil thickness are, respectively, 0.24 μm at −60.31 cam deg, and 0.24 μm at 61.87 cam deg. On the opening and closing side of the cam lobe, the oil film thickness is around 0.15 μm.

The next group of parameters are related to the Hertzian stress on the contact [73, 93, 94]. For the dynamic model, it is used the same approach explain in the quasi-static one. The maximum Hertzian contact pressure $\bar{p}_0$ is evaluated by the equation (15) and depicts in Figure 68.

Fig. 68: maximum Hertzian pressure for the cam lobe – roller contact
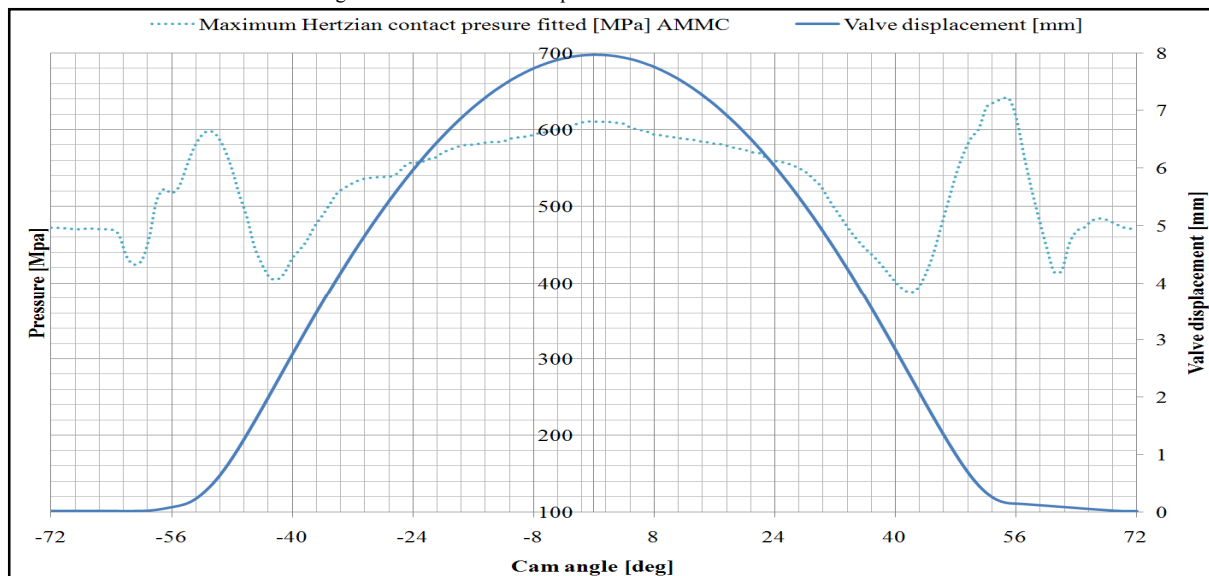
Inside the material the Hertzian pressure produces a stress system composed by a tensile stress with the same value of the Hertzian pressure and a shear stress τ_{max} evaluated by the equation (16) and depicts in Figure 69.

New engine concept development-Multi-body dynamic of valvetrain system and friction assessment

Antonio Turturro – Supervisors: Prof. C. Delprete and L. Magro

Fig. 69: maximum Hertzian shear stress for the cam lobe – roller contact

The maximum shear stress τ_{max} acts in the centreline of the contact at a depth of 0.786 *a*. The maximum Hertzian pressure and the maximum Hertzian shear stress trends could be described through three key points: the two transition area between the height ramps and the main ramps, and the value at maximum cam lift. The values of the maximum Hertzian pressure, from the open side to the closed one, are respectively: about 598 MPa at −51.02 cam deg, about 611 MPa at maximum cam lift, and about 641 MPa at 53.00 cam deg. About the maximum Hertzian shear stress the values are respectively, from the open side to the closed one: about 180 MPa at -51.02 cam deg, about 183 MPa at maximum cam lift, and about 183 MPa at 53.00 cam deg. The reasons for the different peaks dimension is the difference slopes of the height opening and closing ramp as depicted in Figures 33 and 34; and the different shape of the radius of curvature in the transient area between the height and the main ramps as shown in Figure 23 and Figure 66. The material of the cam lobe and the roller in contact on this project is assumed to be iron steel. According with Wang [93] and other literature material, an average Hertzian limit for this kind of material is 1724 MPa for the Hertzian pressure and 862 MPa for the Herztian shear stress. So, the cam lobe and the roller respect that limit.

In Elasto-Hydro Dynamic - EHD cam to follower contact the lubricant properties play a very important role from the point of view of film formation and friction. Lubricant viscosity greatly depends on pressure. In EHD cam-follower contact the lubricant experience extreme

New engine concept development-Multi-body dynamic of valvetrain system and friction assessment

Antonio Turturro – Supervisors: Prof. C. Delprete and L. Magro

large pressure. Although most of the studies considered a Newtonian model of the lubricant, the severity of working conditions at cam to follower conjunction makes this assumption questionable. Limiting shear stress and various models of non-Newtonian models in terms of effective viscosity were proposed in the literature. The most commonly used empirical formulas describing the dependence of lubricant viscosity on pressure. Roeland equation is one of the most commonly used relation describing dependence of viscosity on pressure and is shown in equation (78):

$$(78) \qquad \eta_p = \eta_0 exp\left\{\frac{\alpha p_0}{z}\left[-1 + \left(1 + \frac{p}{p_0}\right)^z\right]\right\}$$

where: η_p is the oil viscosity at contact pressure; η_0 the oil viscosity at ambient pressure; z the oil viscosity index; α the pressure-viscosity coefficient; p_0 the pressure constant typically $1.98 \cdot 10^8$ Pa; p the contact pressure.

The oil viscosity index is described in equation (79):

$$(79) \qquad z = \frac{\alpha p_0}{\ln\frac{\eta_0}{\eta_\infty}} = 0.4205$$

where η_∞ is viscosity at infinite pressure [98] typically $6.315 \cdot 10^{-5}$ Pa s. The oil viscosity related to the maximum Hertzian pressure is shown in Figure 70.
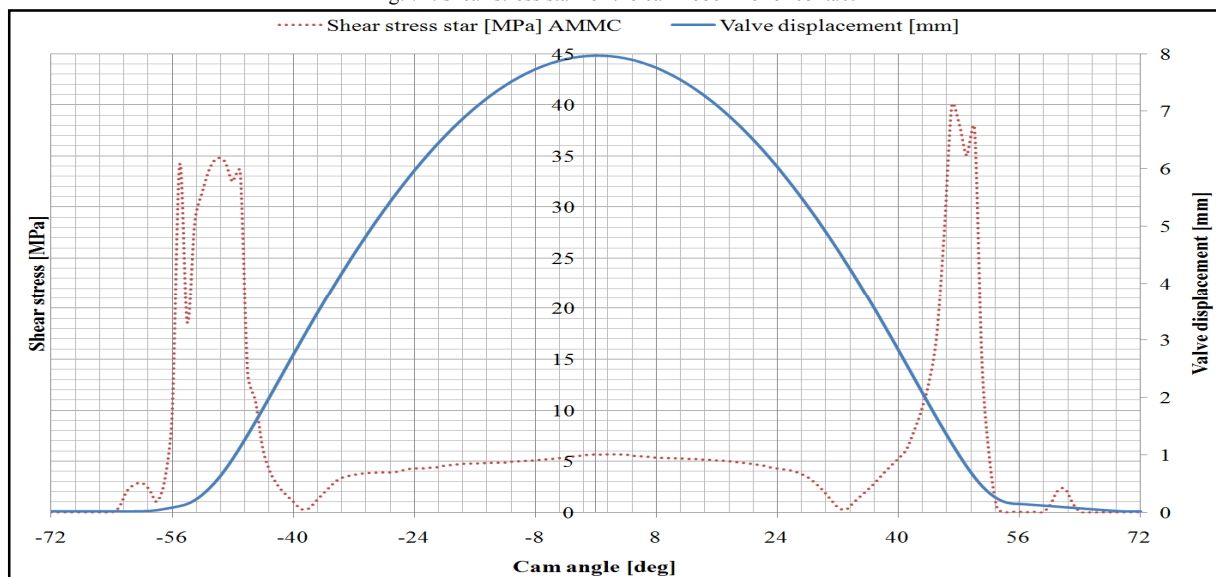
Fig. 70: oil viscosity at Hertzian maximum pressure by Roeland rehology model for the cam lobe – roller contact

New engine concept development-Multi-body dynamic of valvetrain system and friction assessment

Antonio Turturro – Supervisors: Prof. C. Delprete and L. Magro
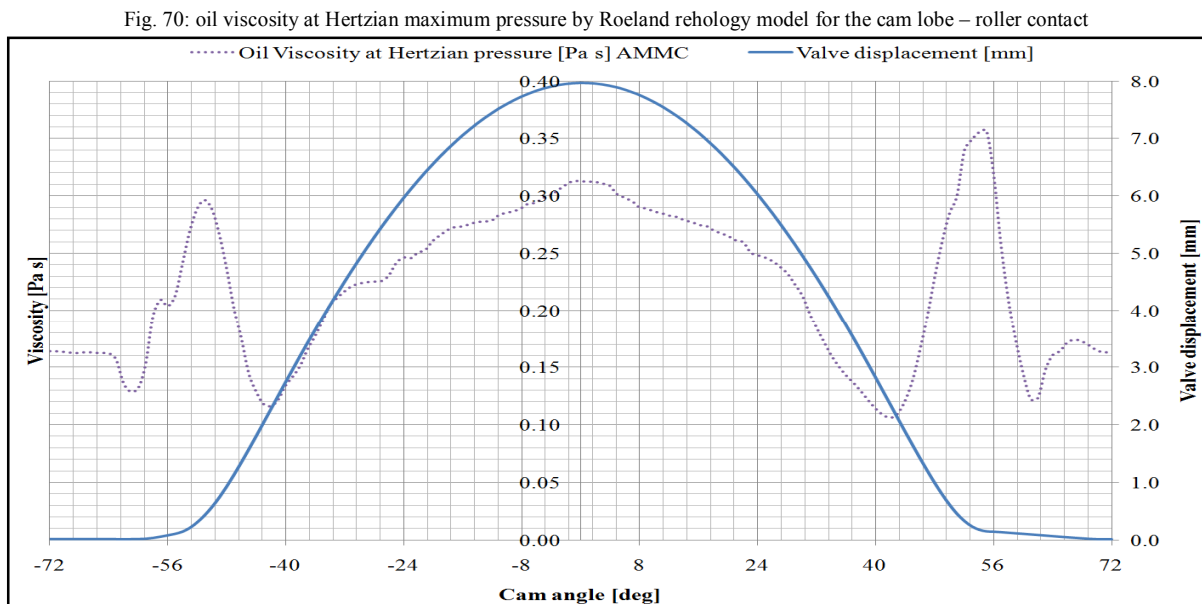
The oil viscosity follow the Hertzian maximum pressure and one could be notice the variation from the base circumference or the transition area between the height and the main ramp, and the peaks of this parameter. In particular, on the base circumference the oil viscosity is around 0.16 Pa s; while the three peaks, one at cam tip nose and the others two on the transition areas, are respectively: 0.31 Pa s, 0.30 Pa s at −51 cam deg, and 0.36 Pa s at 55 cam deg. The effect of Hertzian pressure is not extremely visible if the oil viscosity value is considered alone. If the ambient viscosity, 0.007 Pa s, is taken account and compared with the above value, the effect of Hertzian pressure is highlight.

Roeland equation shows good correlation for pressures up to 1 GPa. In valvetrain, however, pressures up to 2GPa are common and in a general EHD contact pressures can reach 3GPa.

Depending on the oil film thickness, Newtonian or non-Newtonian behaviour oil film will occur. The Eyring shear strength separates the two domains. So, a quantity called τ^* is defined as equation (80) and plotted in Figure 71:

(80) $$\tau^* = \frac{\eta_p \Delta U}{h_0}$$

Fig. 71: shear stress star for the cam lobe – roller contact

New engine concept development-Multi-body dynamic of valvetrain system and friction assessment

Antonio Turturro – Supervisors: Prof. C. Delprete and L. Magro

If the shear stress star is lower than the Eyring limit τ_0, the oil film has a Newtonian behaviour and it is equal to the shear stress star. Otherwise, the oil film has a non-Newtonian behaviour and shear stress is evaluated with the follow general relation:

$$(81) \qquad \tau = \tau_0 + c\,p$$

where: τ_0 is Eyring limit, typically 2MPa; p the contact pressure related to the generating force; and c the slope of the oil limiting shear stress-pressure relation related to the generating force. Equation (81) has to be characterized both in the case of boundary and viscous friction force. In the roller-cam lubricated conjunction, the oil behaviour is almost non-Newtonian but there are different region of Newtonian behaviour, so the final shear stress will be a mixed of both.
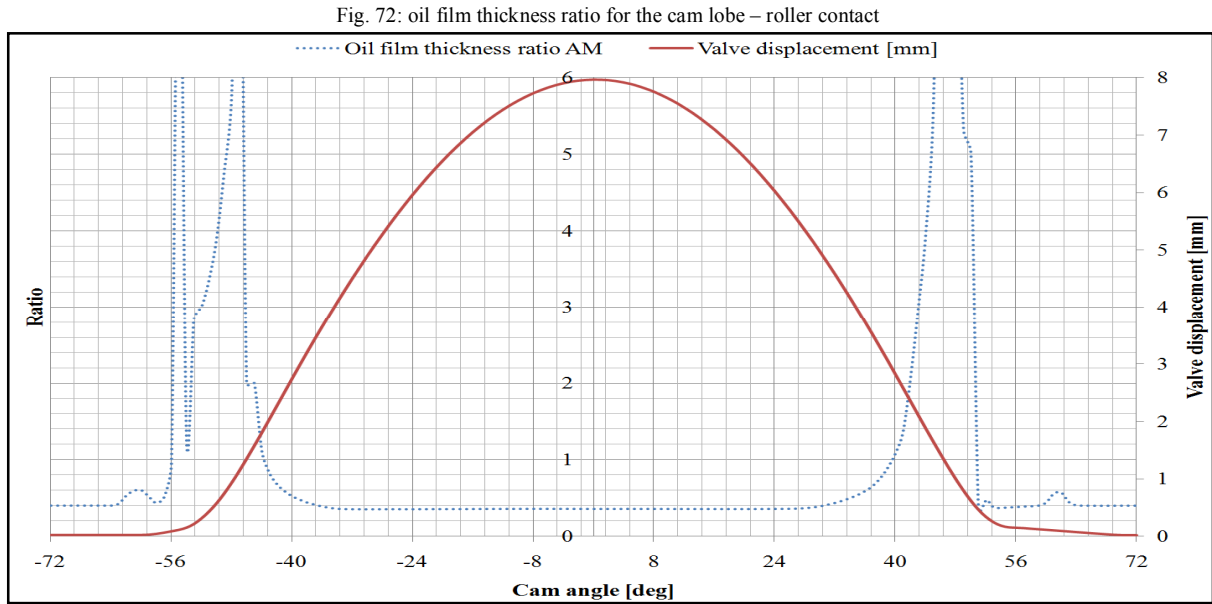
The combined asperity of the two surfaces is evaluated as:

$$(82) \qquad \sigma = \sqrt{\sigma_r^2 + \sigma_c^2}$$

where σ_r and σ_c are, respectively, the RMS asperity height of the roller surface and the cam surface; typically combined asperity is 0.4 µm.

The oil film thickness parameter is defined as (83) and plotted in Figure 72:

$$(83) \qquad \lambda = \frac{h_0}{\sigma}$$

New engine concept development-Multi-body dynamic of valvetrain system and friction assessment

Antonio Turturro – Supervisors: Prof. C. Delprete and L. Magro

Fig. 72: oil film thickness ratio for the cam lobe – roller contact

The behaviour of the oil film thickness ratio is almost constant, except the transition regions between the height and the main ramp, where the high oil film thickness produces high values of this parameter. In particular, the value of the cam is about 0.36.

Two statistical function $F_2(\lambda)$ and $F_{5/2}(\lambda)$ evaluate the part of the asperity that, respectively, participate to generate the asperity contact area and the load carried by the asperity according with (84).

$$(84) \qquad F_n(\lambda) = \frac{1}{\sqrt{2\pi}} \int_\lambda^\infty (s-\lambda)^n \, e^{-\frac{s^2}{2}} ds$$

These functions, describing a Gaussian distribution of the asperity heights, are defined according to Teodorescu et al. [99] and their least square fitting are shown in equation (85) and (86), and plotted in Figure 73.

$$(85) \qquad F_{5/2}(\lambda) = -0.1922\lambda^3 + 0.721\lambda^2 - 1.0649\lambda + 0.6163$$

New engine concept development-Multi-body dynamic of valvetrain system and friction assessment

Antonio Turturro – Supervisors: Prof. C. Delprete and L. Magro

(86)
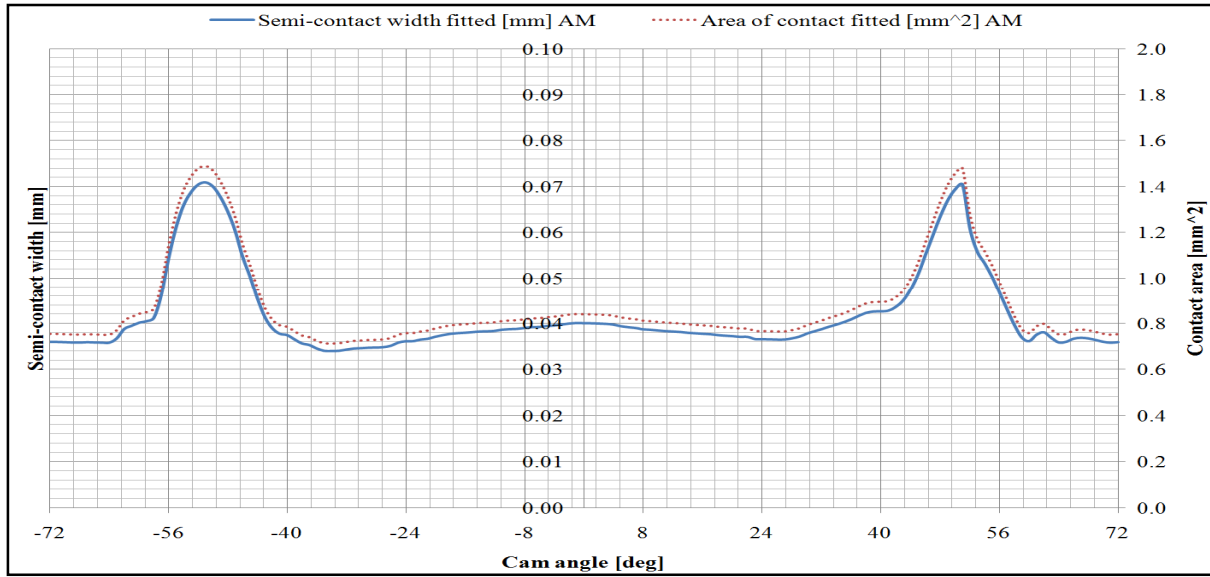$$F_2(\lambda) = -0.116\lambda^3 + 0.4862\lambda^2 - 0.7949\lambda + 0.4999$$

Fig. 73: statistical functions and oil film thickness ratio the cam lobe – roller contact
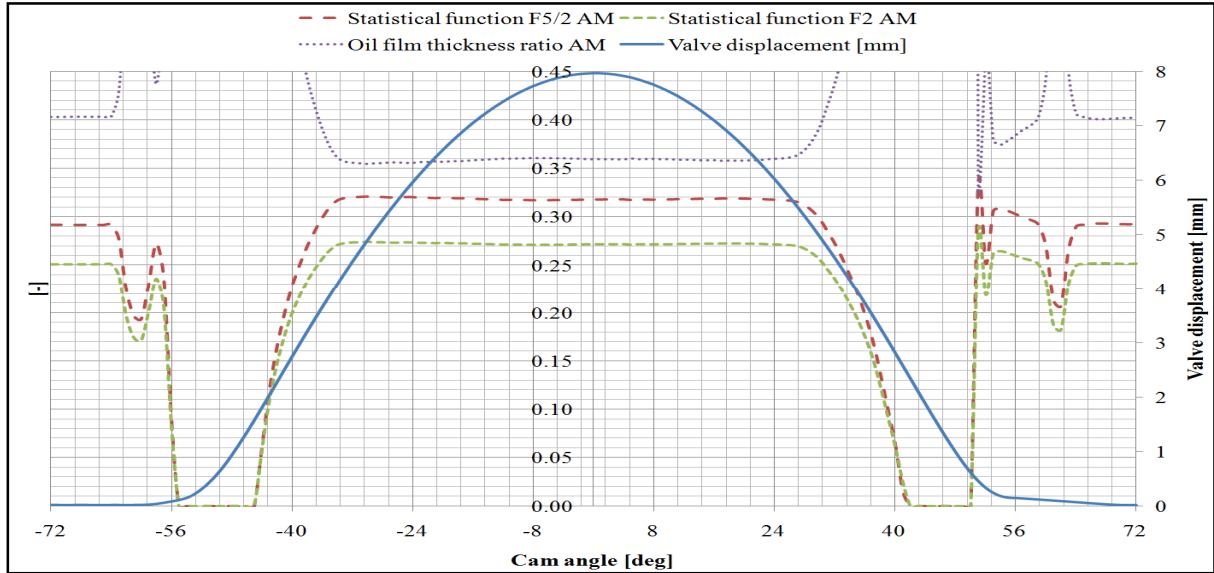
The statistical functions $F(\lambda)$ have a negative proportional behaviour respect to oil film thickness ratio. In fact, where the oil film thickness is high the value of $F(\lambda)$ is 0. On the cam nose the value of $F_{5/2}(\lambda)$ and $F_2(\lambda)$ are respectively around 0.32 and 0.27.

The next group of parameters are related with the contact area A in according with all assumptions described in the quasi-static model. The semi width dimension a, area of contact A are evaluated respectively by the equation (11) and (12). Figure 74 shows the semi-contact width and the contact area of the cam lobe-roller interface.

New engine concept development-Multi-body dynamic of valvetrain system and friction assessment

Antonio Turturro – Supervisors: Prof. C. Delprete and L. Magro

Fig. 74: semi width and area of the roller – cam lobe contact in the dynamic model

There are three characteristic points in the shape of both the semi width contact dimension and the contact area. These points are the transition area between the height and the main ramp, and the maximum cam lift. The values of the semi width dimension in these points are respectively: about 0.071 mm at −50.00 cam deg; about 0.040 mm at 0 cam deg; and about 0.070 mm at 50.03 cam deg. About the contact area the values are, respectively, about 1.49 mm^2 at −50.00 cam deg; about 0.84 mm^2 at 0 cam deg; and 1.48 mm^2 at 50.03 cam deg.

Considering the model proposed by Greenwood and Tripp [100] with a Gaussian distribution of the asperity height and a constant radius of curvature of the asperities, the actual area of the asperity contact A_a and the load carried by the asperities P_a may be estimated according to the following formulas [99]:

$$A_a = \pi^2 (\zeta \beta \sigma)^2 A F_2(\lambda) \tag{87}$$

$$P_a = \frac{8\sqrt{2}}{15} \pi (\zeta \beta \sigma)^2 \sqrt{\frac{\sigma}{\beta}} A F_{5/2}(\lambda) \tag{88}$$

New engine concept development-Multi-body dynamic of valvetrain system and friction assessment

Antonio Turturro – Supervisors: Prof. C. Delprete and L. Magro

where: A is the Hertzian contact area, ζ the surface density of asperity peaks and β the radius of curvature at the peak.

According with Greenwood [100] and Teodorescu [99], assuming $\sigma_r = \sigma_c$, results in an average value of the group $\zeta\beta\sigma = 0.055$; moreover assuming $\frac{\sigma}{\beta} = 0.001$, the asperity contact area and the load carried by the asperities become respectively (89) and (90), and they are plotted in Figure 75 and 76.

(89) $$A_a = 0.0298 F_2(\lambda) A$$

(90) $$P_a = 0.000227 F_{5/2}(\lambda) E A$$

Fig. 75: asperity contact area of roller – cam lobe coupling in the dynamic model

New engine concept development-Multi-body dynamic of valvetrain system and friction assessment

Antonio Turturro – Supervisors: Prof. C. Delprete and L. Magro
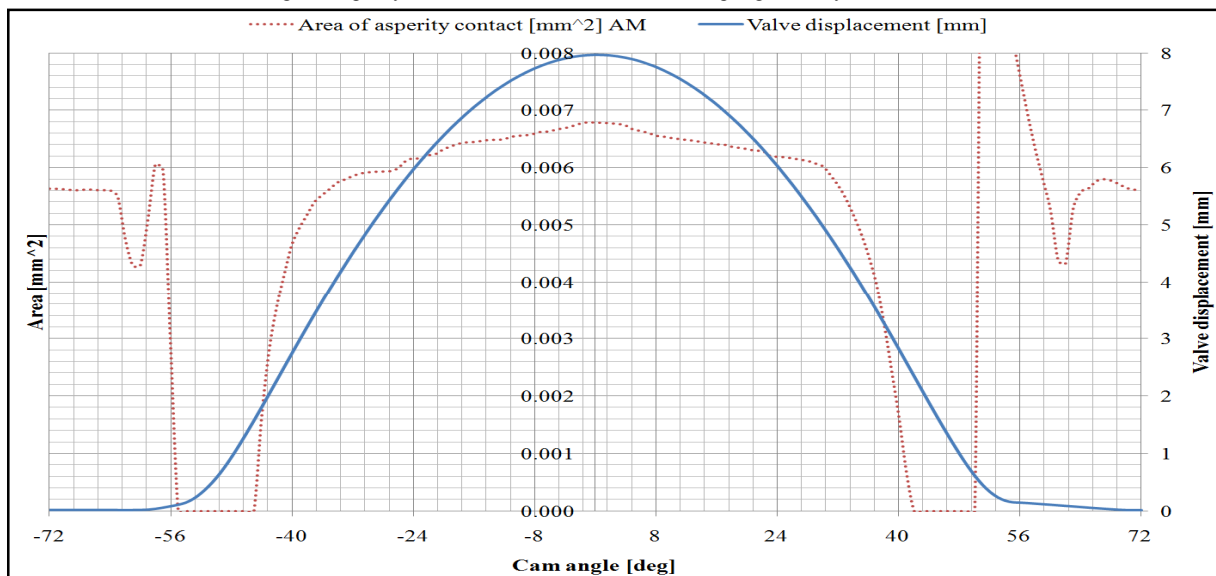
Fig. 76: load carried by the asperity at roller – cam lobe coupling in the dynamic model
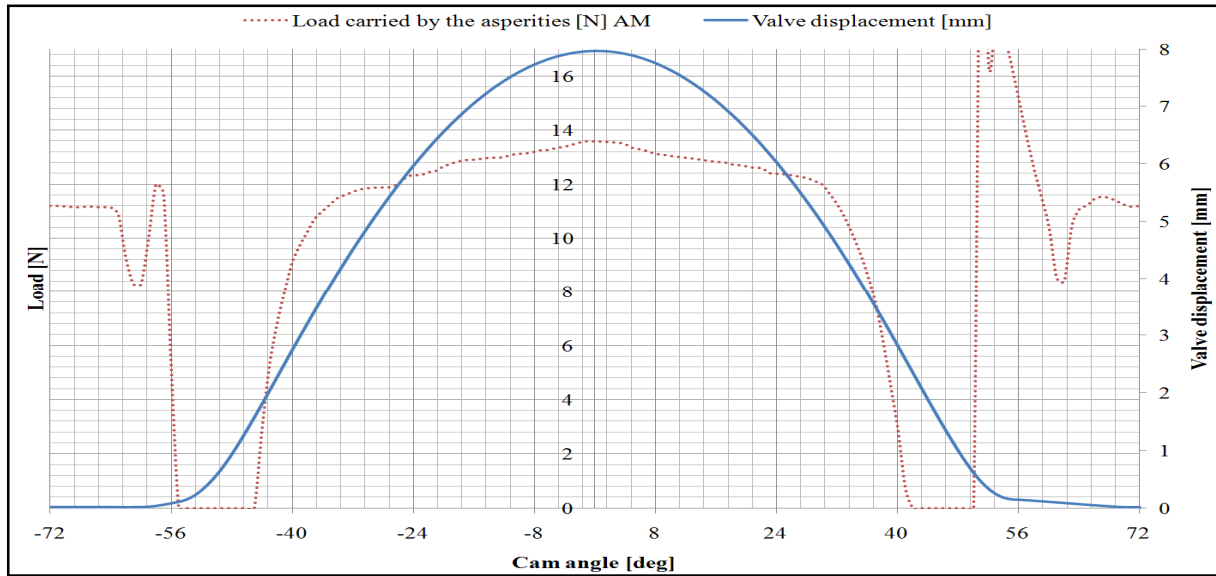
The value of area of asperity contact and the load carried by the asperities are zero where the oil film is thick enough to avoid the boundary interaction or respectively about 0.0065 mm^2 and 13 N both at cam nose.
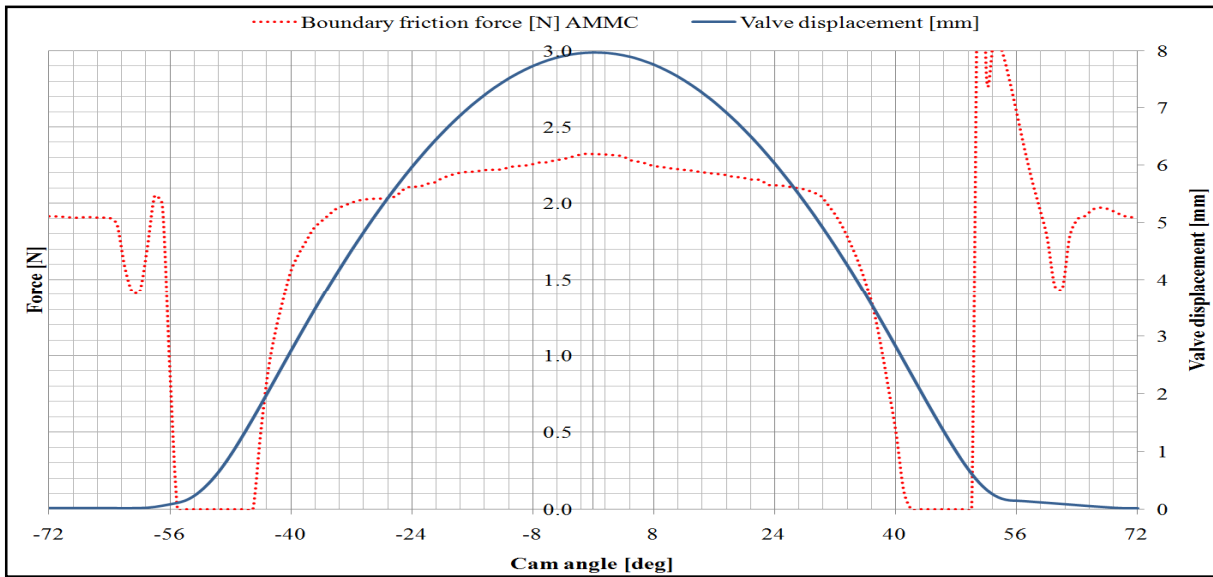
The boundary friction force will result from the shearing of a very thin oil film and the non-Newtonian behaviour will prevail. The shear strength τ could be expressed as [99-101] according with equation (81):

$$(91) \qquad \tau = \tau_0 + m\, p_a^*$$

where: m is pressure coefficient of the boundary shear strength, typically 0.17; and p_a^* the pressure applied on the asperities contact area. Integrating over the asperities contact area, the boundary friction force could be calculated by the following formula and plotted in Figure 77:

$$(92) \qquad F_b = \tau_0 A_a + m P_a$$

New engine concept development-Multi-body dynamic of valvetrain system and friction assessment

Antonio Turturro – Supervisors: Prof. C. Delprete and L. Magro

Fig. 76: boundary friction force of roller – cam lobe coupling in the dynamic model

The contribution of the boundary friction force is around 2 N with an increase on the cam nose in comparison to the base circumference and a shock drop to 0 in the transition area where the thick of the oil film is enough to avoid boundary interaction.

The viscous friction force is produced by the shearing of the oil film trapped between the two contacting surfaces. Depending on the oil film thickness, Newtonian or non-Newtonian behaviour oil film occur. The two domains are separated by the Eyring shear strength, typically value is 2 MPa. In case of Newtonian behaviour the shear stress is equal to the shear stress star. While, in case of non-Newtonian behaviour for the viscous friction evaluation, according with equation (81) the shear stress is:

(93) $$\tau = \tau_0 + \gamma\, p^*$$

where: γ is the slope of the oil limiting shear stress-pressure relation, and p^* the pressure on the oil film in according with equation (94) and plotted in Figure 78:

287

New engine concept development-Multi-body dynamic of valvetrain system and friction assessment

Antonio Turturro – Supervisors: Prof. C. Delprete and L. Magro

(94) $$p^* = \frac{W_R - P_a}{A}$$

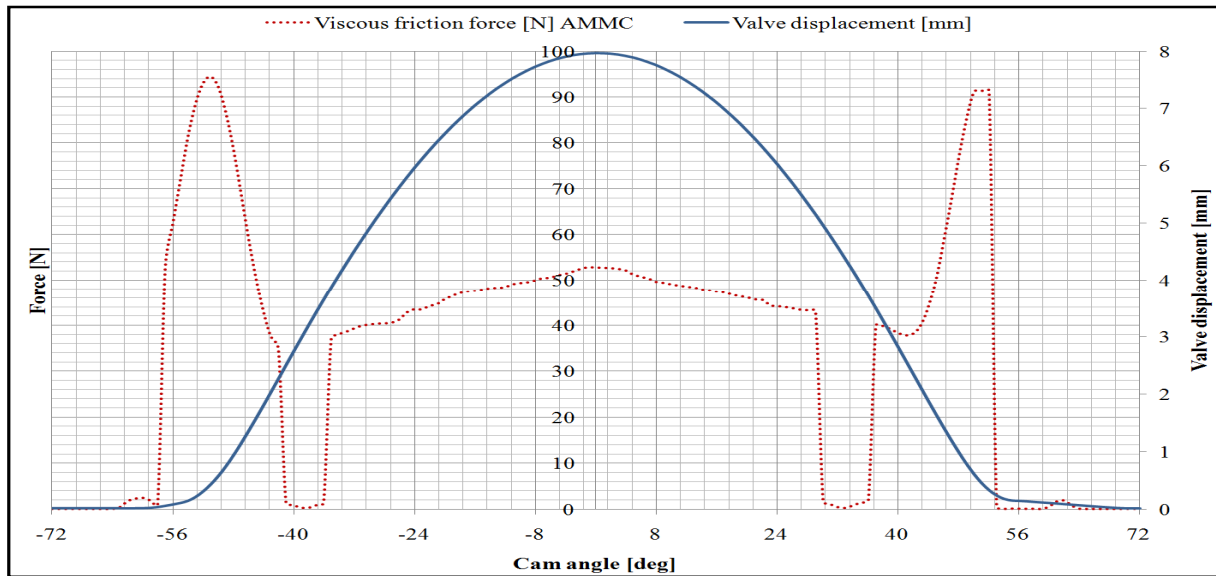Fig. 78: pressure on the oil film at roller – cam lobe coupling in the dynamic model
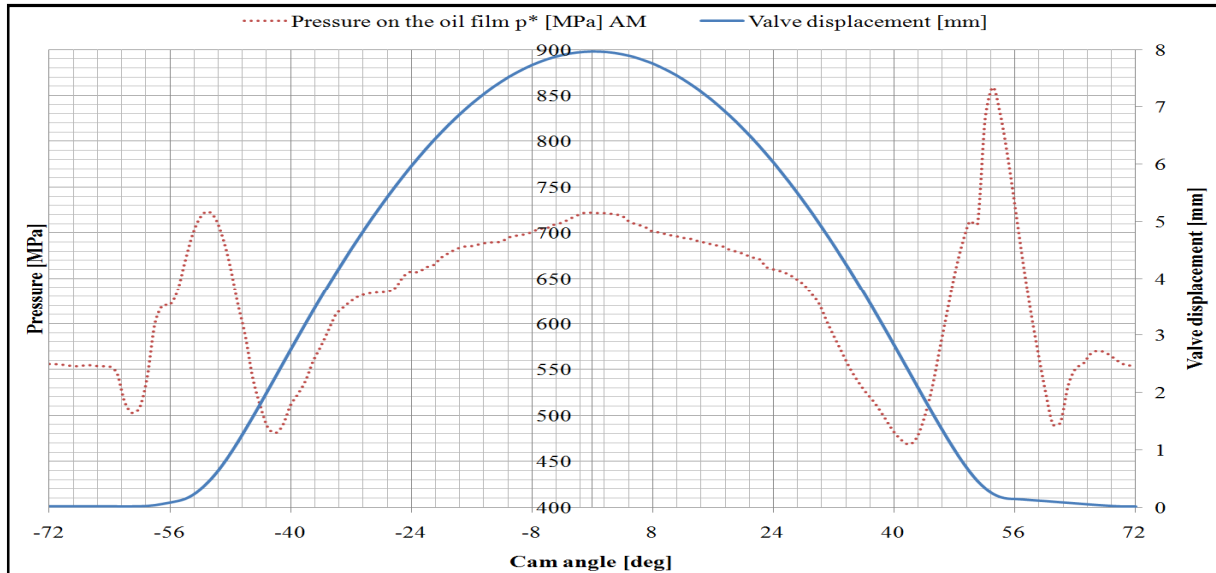
For the effect of the high pressure due to the high contact load at cam-roller conjunction, the pressure on the oil film has high values. In particular, on the base circumference it is around 550 MPa while on the cam nose, it could be notice three peaks: on the transition areas and on the cam nose tip. The three values are respectively: 730 MPa both on the opening side and on the cam tip nose; indeed 860 MPa on the closed side.

Depending of the oil film behaviour, the viscous friction force could be calculated using either equation (80) or (93) and it plots in Figure 79:
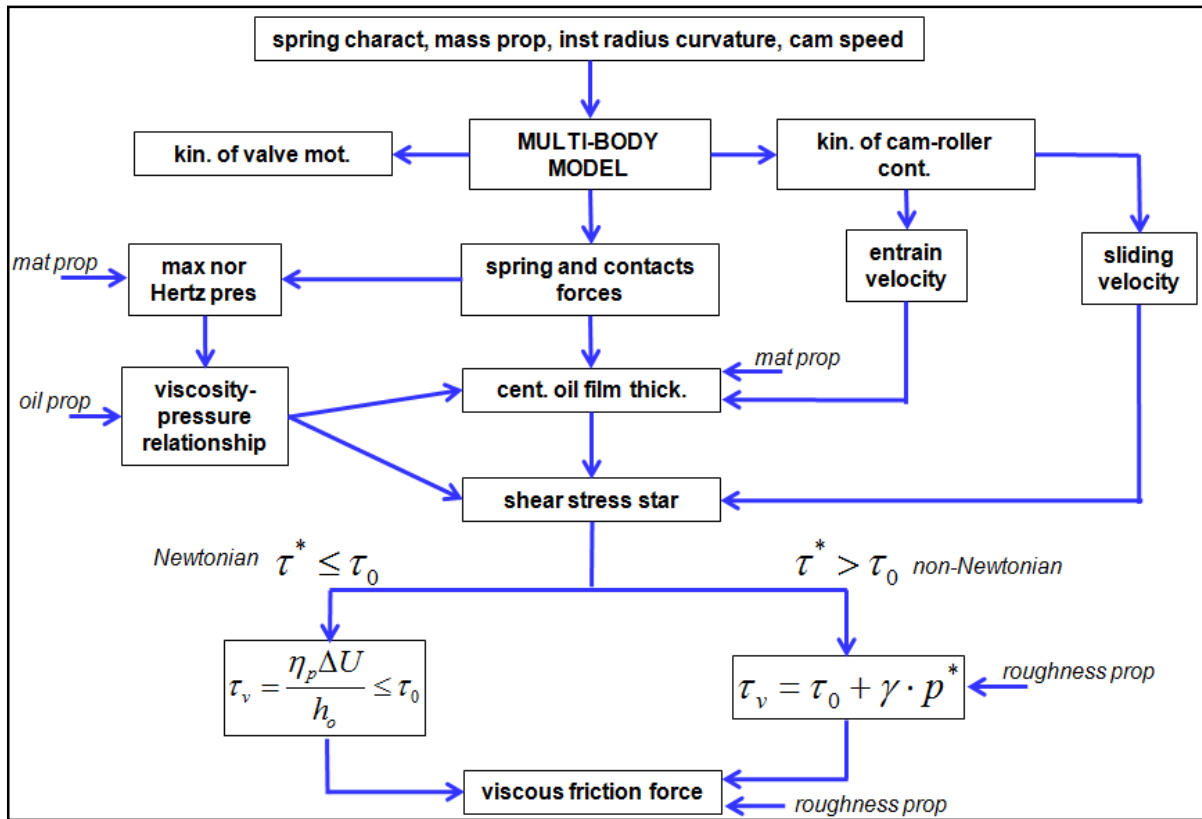
(95) $$F_v = \tau(A - A_a)$$

New engine concept development-Multi-body dynamic of valvetrain system and friction assessment

Antonio Turturro – Supervisors: Prof. C. Delprete and L. Magro

Fig. 79: viscous friction force of roller – cam lobe coupling in the dynamic model

As shown in Figure 79, the viscous friction force is two order of magnitude higher of the boundary friction force. In particular, the three key points are around 95 N on the transition area on the opening side; around 45 N on the cam nose; and around 90 N on the transition area on the closing side. The high values of the viscous friction force is due to two main factors: the high sliding velocity between the cam and roller surfaces and the high Hertzian pressure from the high load at roller-cam conjunction. Figure 80 sums up the core of elasto-hydrodynamic lubrication model.

New engine concept development-Multi-body dynamic of valvetrain system and friction assessment

Antonio Turturro – Supervisors: Prof. C. Delprete and L. Magro

Fig. 80: core of EHL model

The friction force F_f between the roller and the cam, shown in Figure 81, has two components, a boundary friction F_b and a viscous friction component F_v.
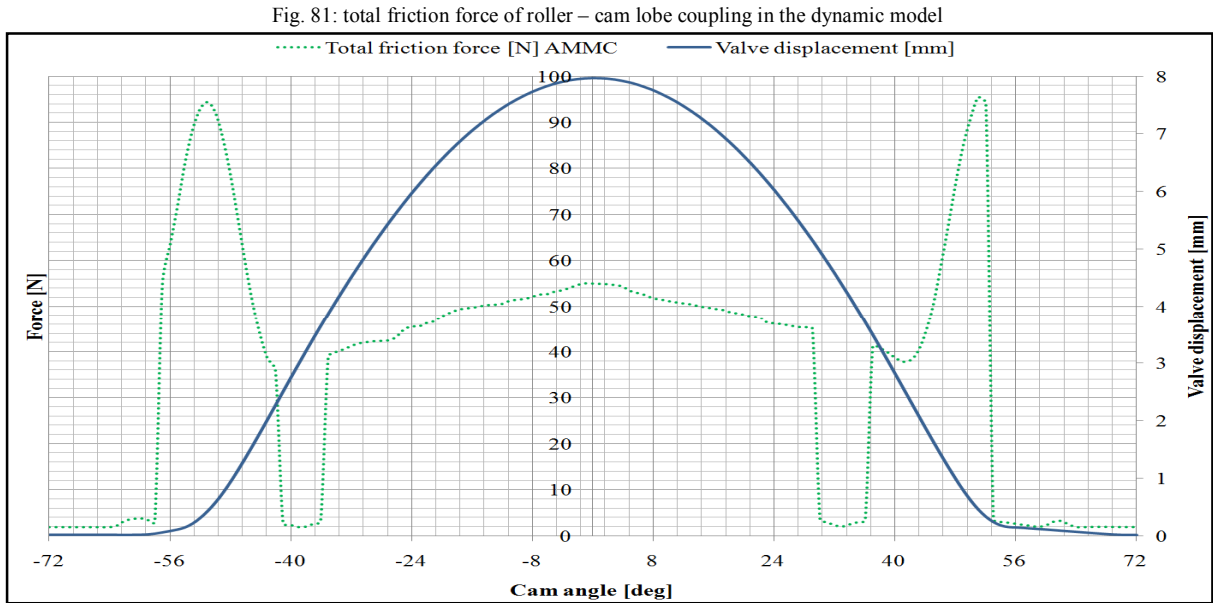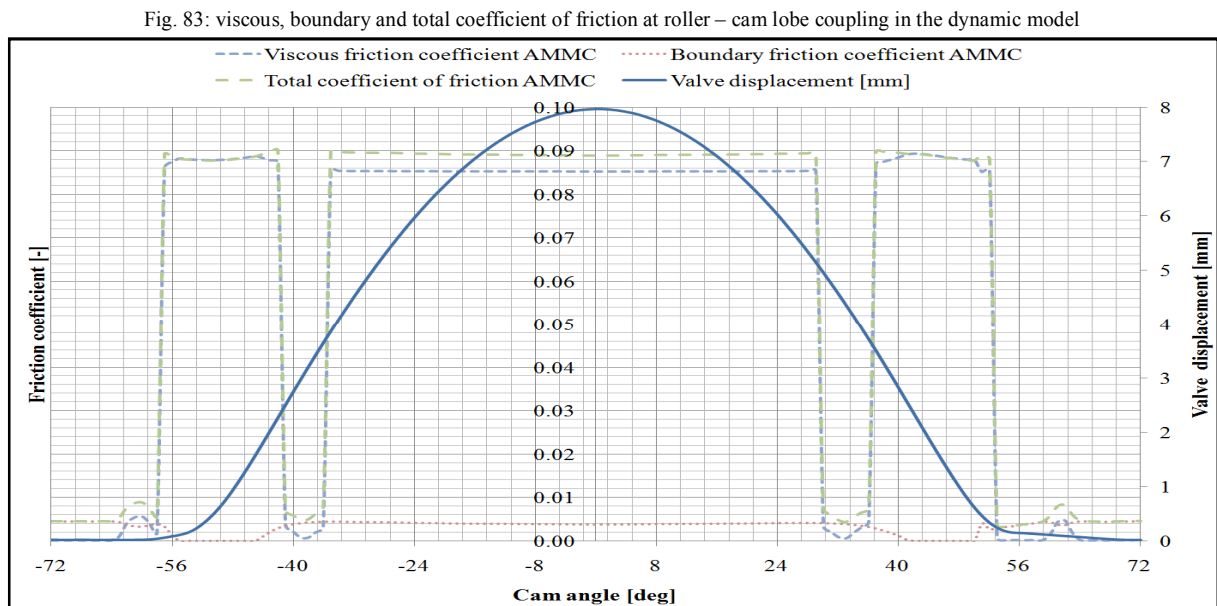
(96)
$$F_f = F_b + F_v$$

New engine concept development-Multi-body dynamic of valvetrain system and friction assessment

Antonio Turturro – Supervisors: Prof. C. Delprete and L. Magro

Fig. 81: total friction force of roller – cam lobe coupling in the dynamic model

Figure 82 shows the total friction force and its components. The Figure below highlights the negligible contribution of the boundary friction.

Fig. 82: viscous, boundary and total friction force of roller – cam lobe coupling in the dynamic model
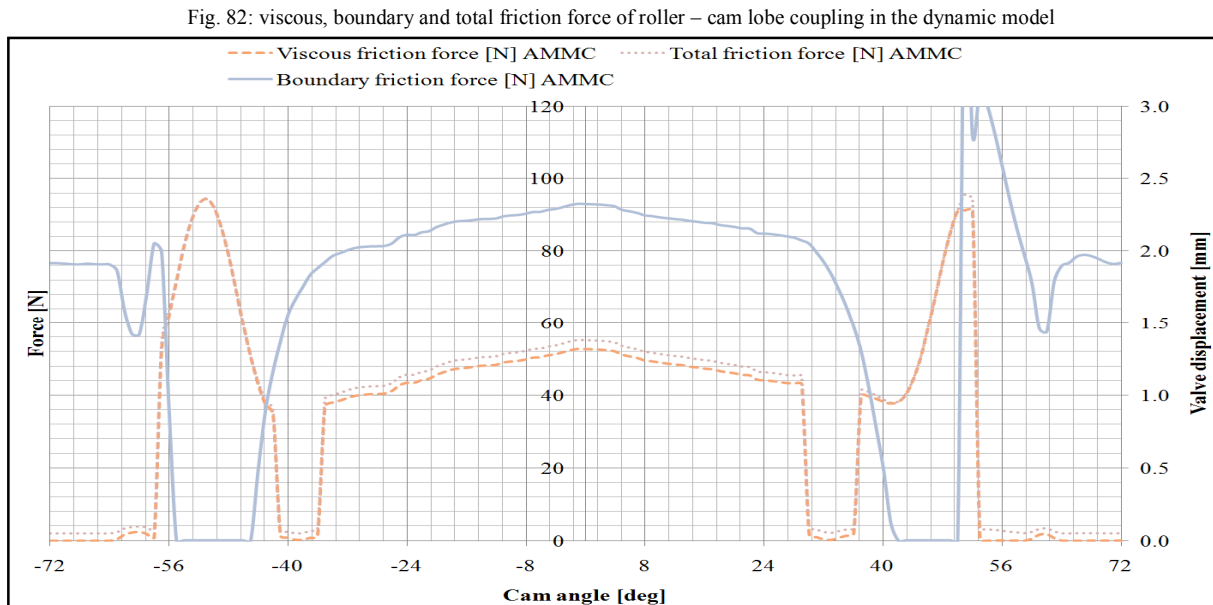
The coefficient of friction f_f between the roller and the cam has two components as well, a boundary friction coefficient f_b and a viscous friction coefficient f_v.

$$(97) \qquad f_f = f_b + f_v = \frac{F_b + F_v}{W_R}$$

New engine concept development-Multi-body dynamic of valvetrain system and friction assessment

Antonio Turturro – Supervisors: Prof. C. Delprete and L. Magro

Figure 83 shows the coefficient of friction and its components.

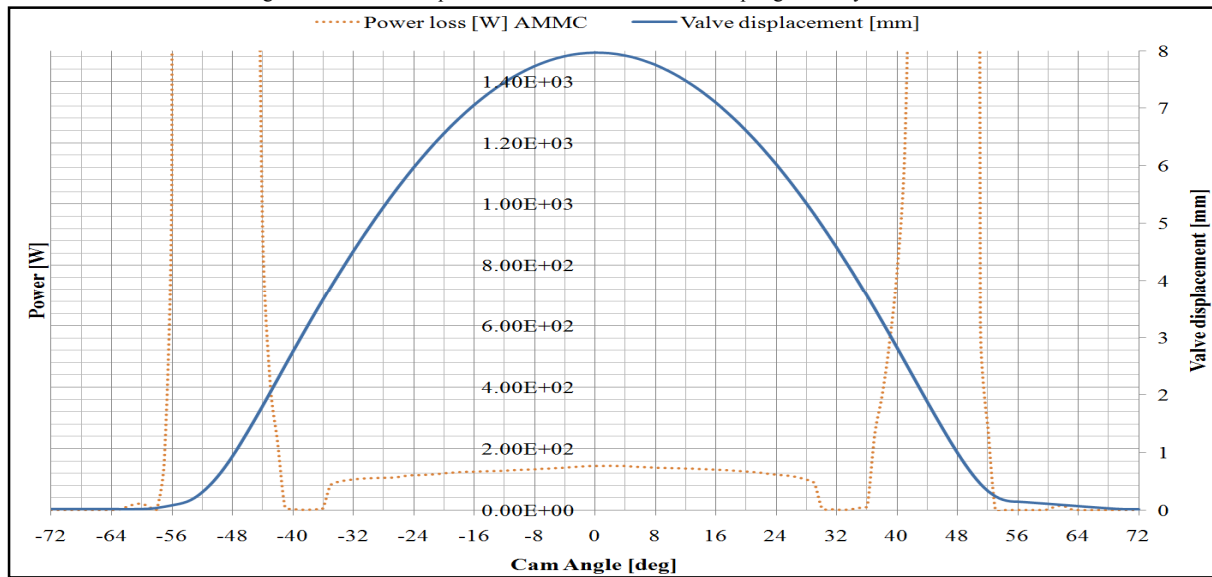Fig. 83: viscous, boundary and total coefficient of friction at roller – cam lobe coupling in the dynamic model

The total friction coefficient follows strictly the viscous friction coefficient due the high contribution of the viscous friction force. The value of the total coefficient of friction is around 0.09 with two exceptions in two areas of the flanks where the viscous friction force is almost 0.

The power loss of the system P_l could be evaluated by equations (98) and is plotted in Figure 84:

(98) $\qquad P_l = F_f \Delta U$

New engine concept development-Multi-body dynamic of valvetrain system and friction assessment

Antonio Turturro – Supervisors: Prof. C. Delprete and L. Magro

Fig. 84: instantaneous power loss of roller – cam lobe coupling in the dynamic model

The major cause of generated instantaneous power loss is the viscous friction force. The average power loss is 1.33 kW. In comparison with experimental data, on this particular engine regime where the system is in the highest overspeed regime, there are an over estimation of the friction of the cam – roller lubricated conjunction. The difference from the model analyzed and the experimental data extracted from Calabretta[7] and other GM industrial report highlights an overestimation of 13%.

The next group of parameters are related to the viscous friction torque on the roller T_r and on the cam lobe T_c [73]. The viscous friction torques on roller T_r and on cam T_c are evaluated respectively by the equation (99) and (100), and depicted in the Figure 85 and Figure 86.

(99) $$T_r = FR_r$$

(100) $$T_c = FR_c$$

New engine concept development-Multi-body dynamic of valvetrain system and friction assessment

Antonio Turturro – Supervisors: Prof. C. Delprete and L. Magro

Fig. 85: instantaneous total friction torque on roller and the valve lift profile for the dynamic model
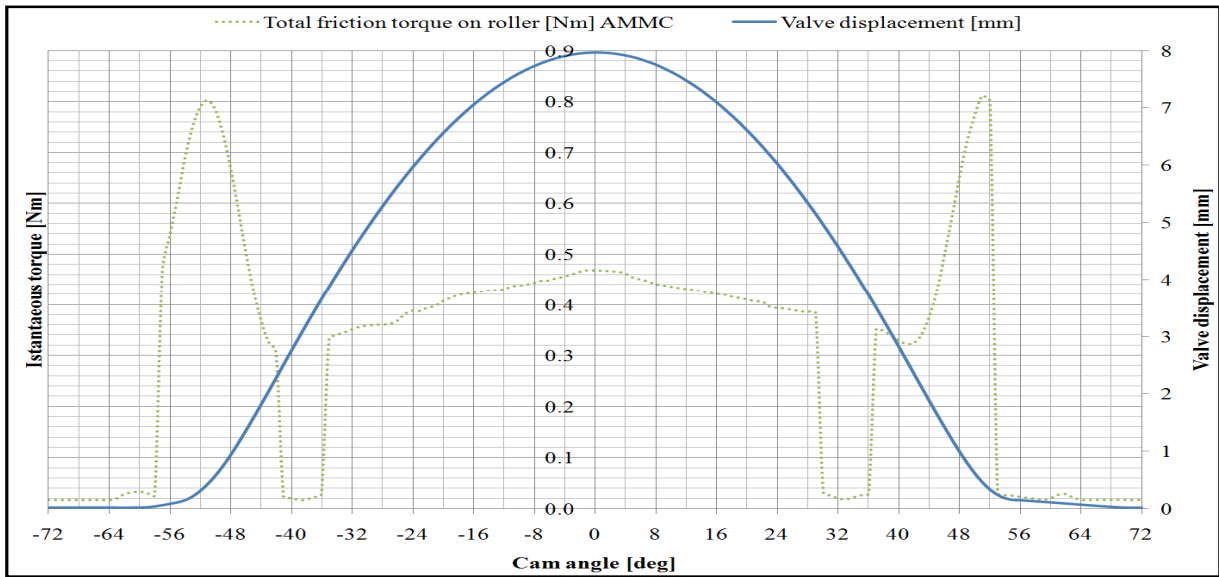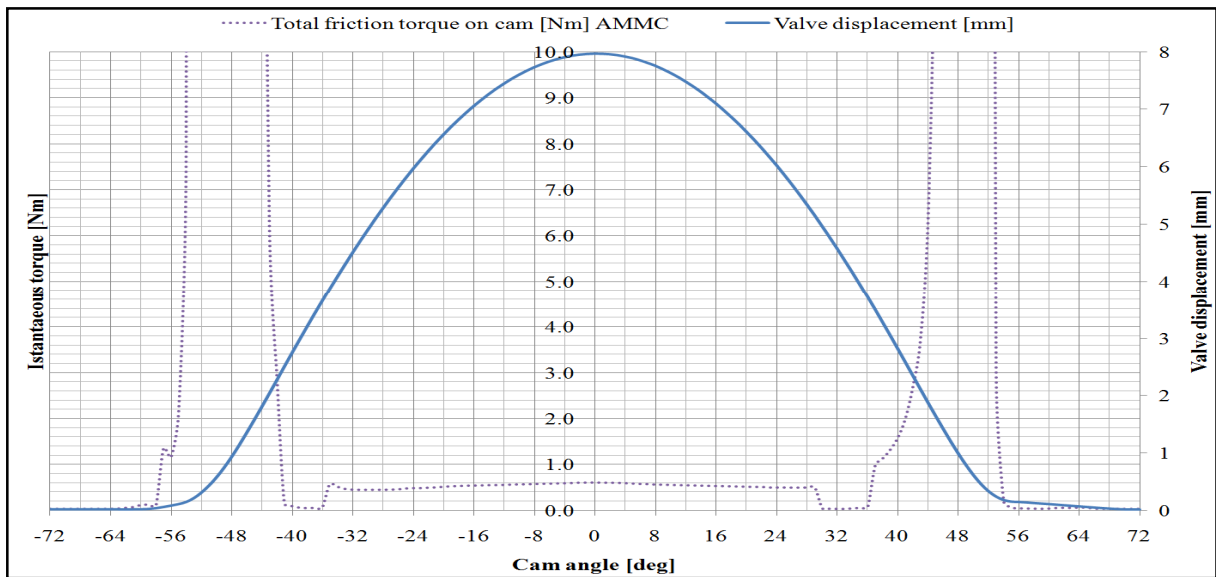

Fig. 86: instantaneous total friction torque at cam

The instantaneous total friction torque at roller follow strictly the total friction force trend because the roller has constant radius of curvature of 8.5 mm. On the other hand, the total friction torque at cam follows the total friction force as well but only on the cam nose where the instantaneous radius of cam curvature is in the same magnitude of the roller. In the transition area where for lubrication reasons the instantaneous radius of cam curvature is quite high, the total friction force is amplifier. It happens because in that region of the valve ramp there is both a high value of viscous friction force F and an enormous value of the

New engine concept development-Multi-body dynamic of valvetrain system and friction assessment

Antonio Turturro – Supervisors: Prof. C. Delprete and L. Magro

radius of curvature of the cam lobe R_l. Pay attention that it is instantaneous torque absorption or an instantaneous torque request of the system.

The next group of parameters for the dynamic model are related to the contact centre deflection δ and the contact stiffness K_C [73]. According with the elasticity theory by Hertz and the elastic line contact theory, the total deflection at the centre of the contact δ is evaluated by the equation (13) and depicts in the Figure 87.

Fig. 87: total central deflection in micron at cam lobe – roller contact
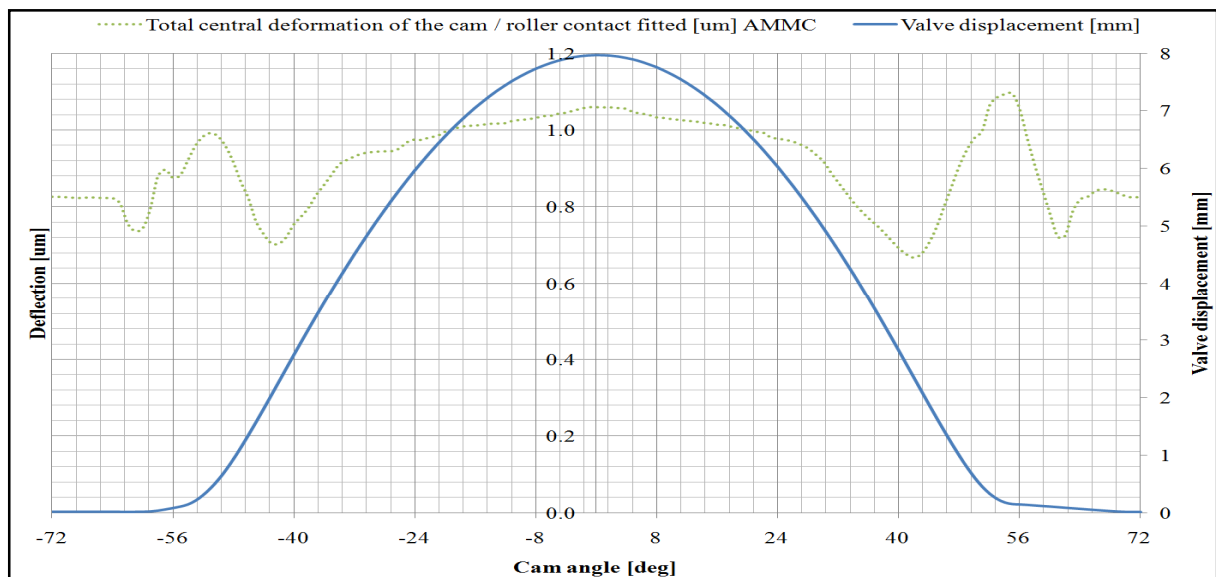
About the fitted total central deformation of the cam lobe-roller contact, depicted in the Figure 87, is possible highlight three key points: the peaks at transition area between the height ramps and the main ramps, and the value at maximum cam lift. The values of the central total deformation in these points, from the open side to the closed one, are respectively: about 0.99 µm at −51.02 cam deg, about 1.59 µm at 0 cam deg, and about 1.94 µm at 52.00 cam deg.

While the contact stiffness K_C is evaluated by the equation (14) and depicts in the Figure 88.

New engine concept development-Multi-body dynamic of valvetrain system and friction assessment

Antonio Turturro – Supervisors: Prof. C. Delprete and L. Magro

Fig. 88: fitted contact stiffness for the cam lobe – roller coupling
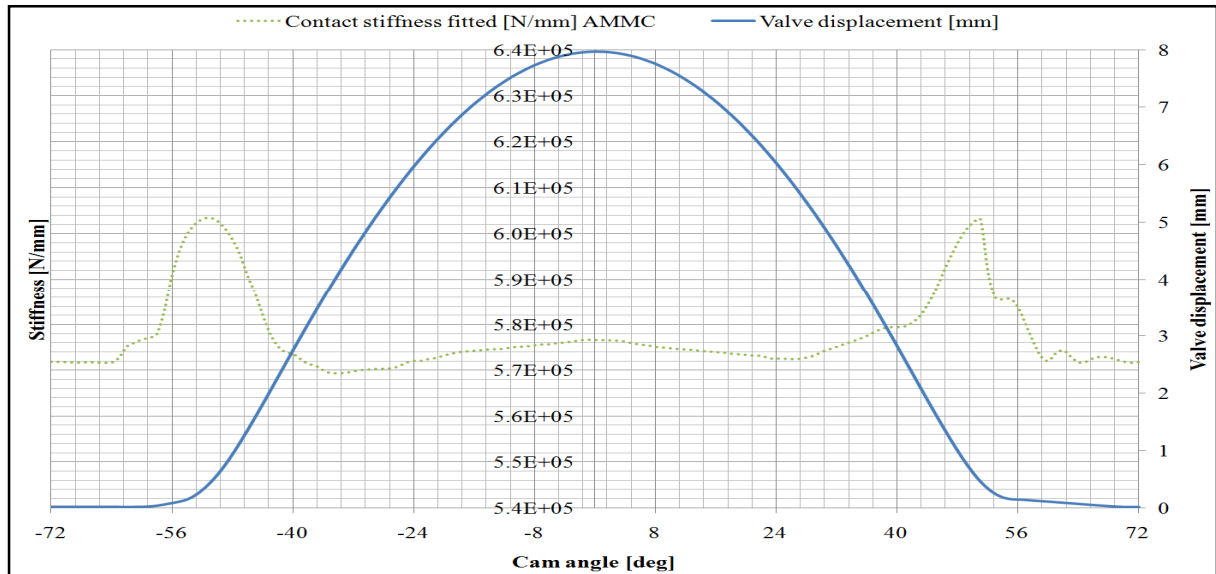
As the total central deformation, the fitted contact stiffness shape has three key points: the transition area between the height open ramp and the main open ramp where the contact stiffness value is about 6.04E5 N/mm at −51.02 cam deg, about 5.77E5 N/mm at maximum cam lift, and about 6.03E5 N/mm at 49.00 cam deg.

III-VIII Quasi-static and dynamic model – Results discuss and comparison

After analysed the quasi-static model and the dynamic model, it is the time to compare the results to highlight the dynamic effects on the valve train system, how the key parameters change from the quasi-static and the dynamic model, and when and how work the lift off effect.

The first argument of comparison is the valve and cam lift profile shown in Figures 89 and 90.

New engine concept development-Multi-body dynamic of valvetrain system and friction assessment

Antonio Turturro – Supervisors: Prof. C. Delprete and L. Magro

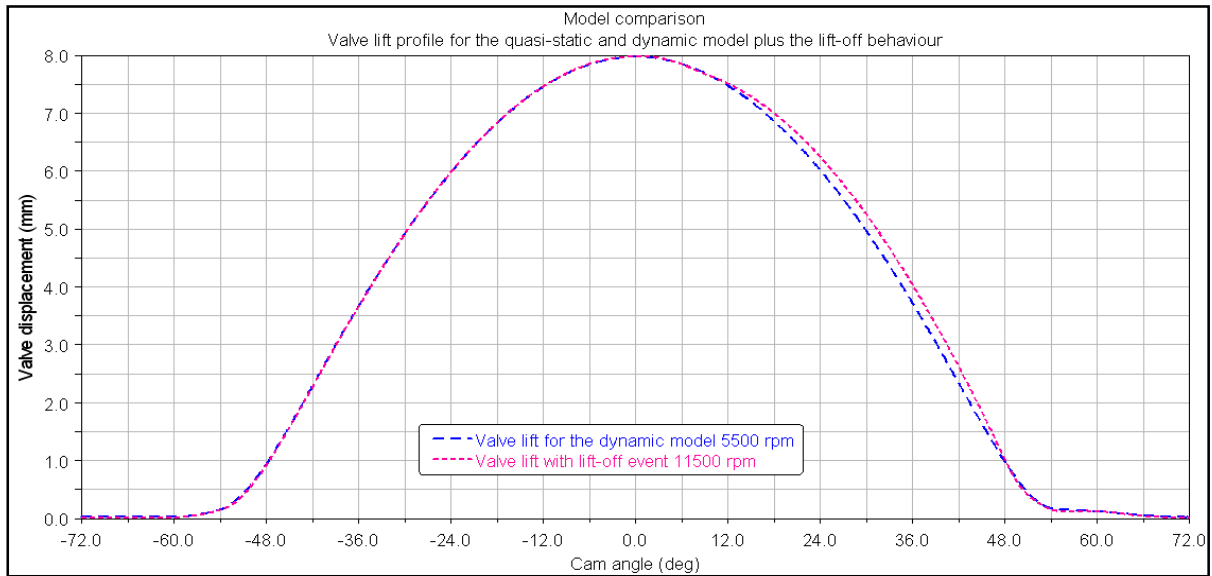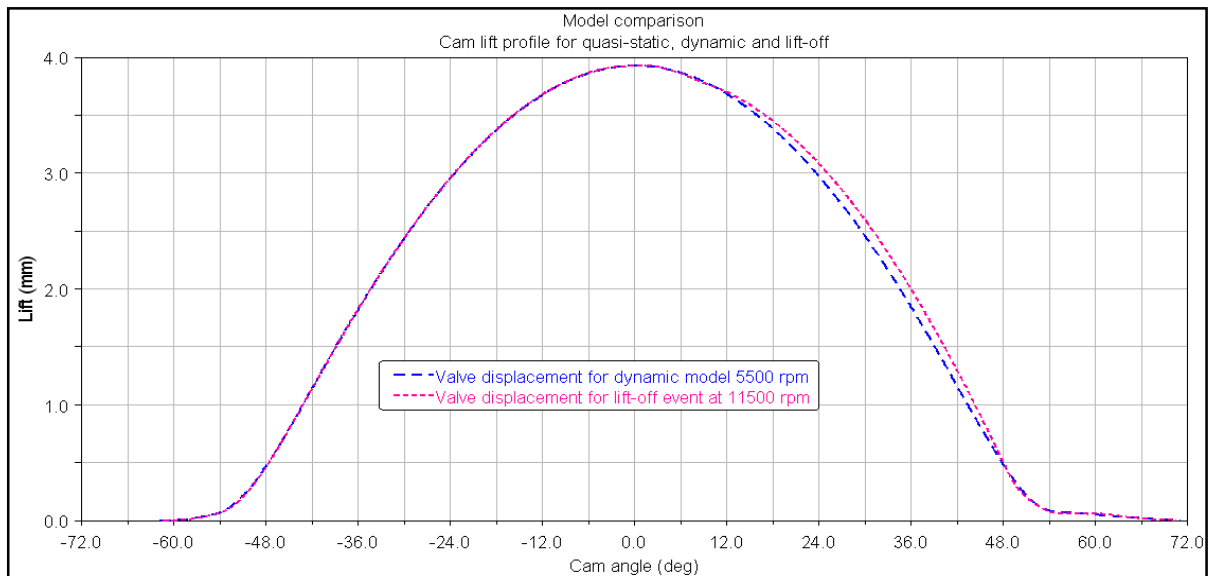Fig. 89: valve lift profile comparison

Fig. 90: cam lift profile comparison

About the lift-off event, Figures 89 and 90 shows how the follower lose the contact and the close event is not control by the cam lobe. Figures 89 and 90 shows the lift-off event at 11500 rpm engine, while Figure 91 shows the spring force trend. The experimental data about the lift-off of this system is not available. Probably, it is slightly lower because to reduce the surface roughness of the cam lobe, the stiffness of the solid-to-solid force contact feature is a little bit much higher than the material one.

New engine concept development-Multi-body dynamic of valvetrain system and friction assessment

Antonio Turturro – Supervisors: Prof. C. Delprete and L. Magro

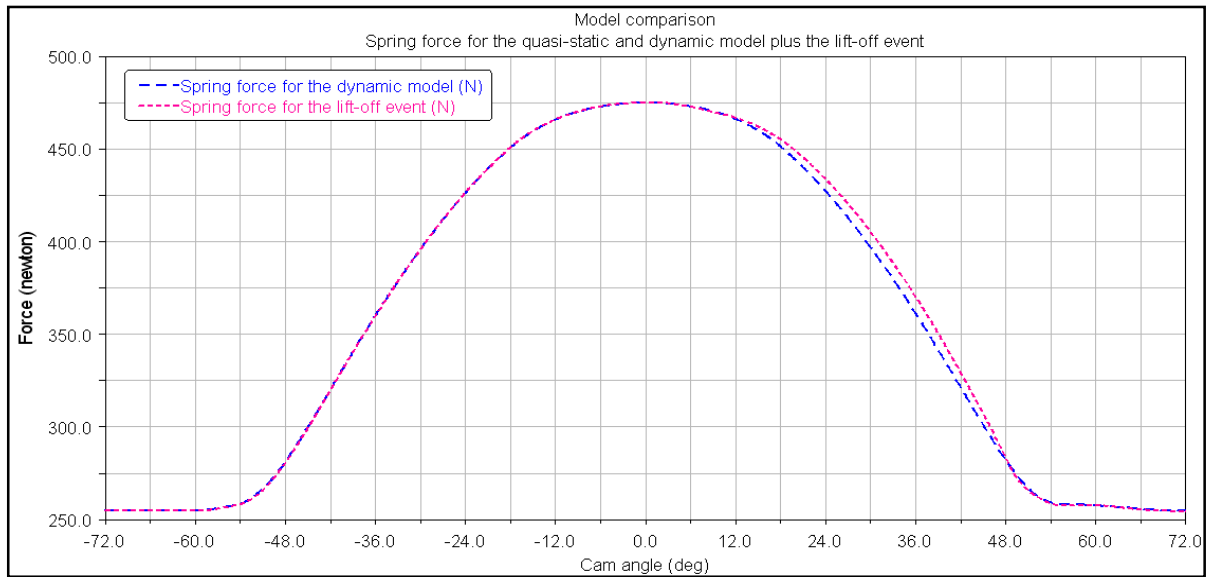Fig. 91: spring force for dynamic and lift-off cases

Figure 92 shows the resultant force at valve body or, in the other words, the tip contact load comparison for both the model. In according to Wang [93] and the industrial reports, the rising of the engine speed increase the peaks values in the transition area between the height ramps and the main ramps, but, in the opposite way, it decreases the tip contact load around the nose and in general on the flanks as well.

Fig. 92: contact load at valve tip – rocker pad interface for the quasi-static and dynamic cases
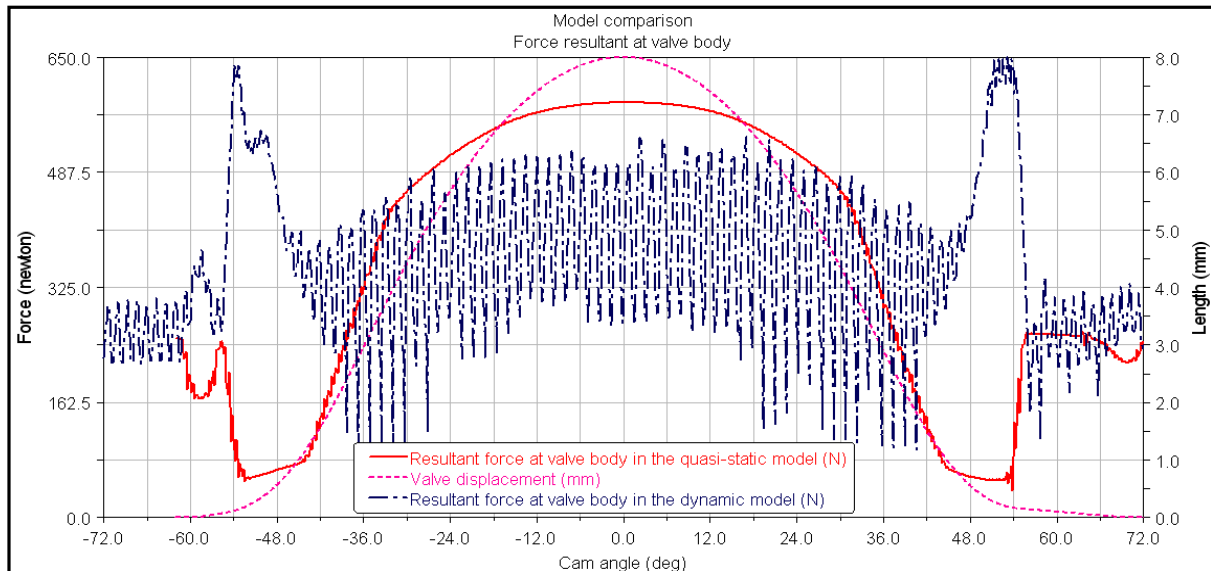
The reason for this behaviour is the effect of the dynamic-inertia phenomena which the quasi-static model does not take account. In fact, usually in the industrial world the quasi-static

New engine concept development-Multi-body dynamic of valvetrain system and friction assessment

Antonio Turturro – Supervisors: Prof. C. Delprete and L. Magro

model is called "0 rpm" model, to highlight the static environment in which the model works. At the end, there is not the right model and the wrong model but the quasi-static model takes a picture of the system at very low speed and the dynamic model takes a picture of the system at 5500 rpm. This behaviour is shown in the Figure 93 as well, where the contact load at roller – cam lobe interface is compared for both the models.

Fig. 93: contact load at roller – cam lobe interface for the quasi-static and dynamic cases
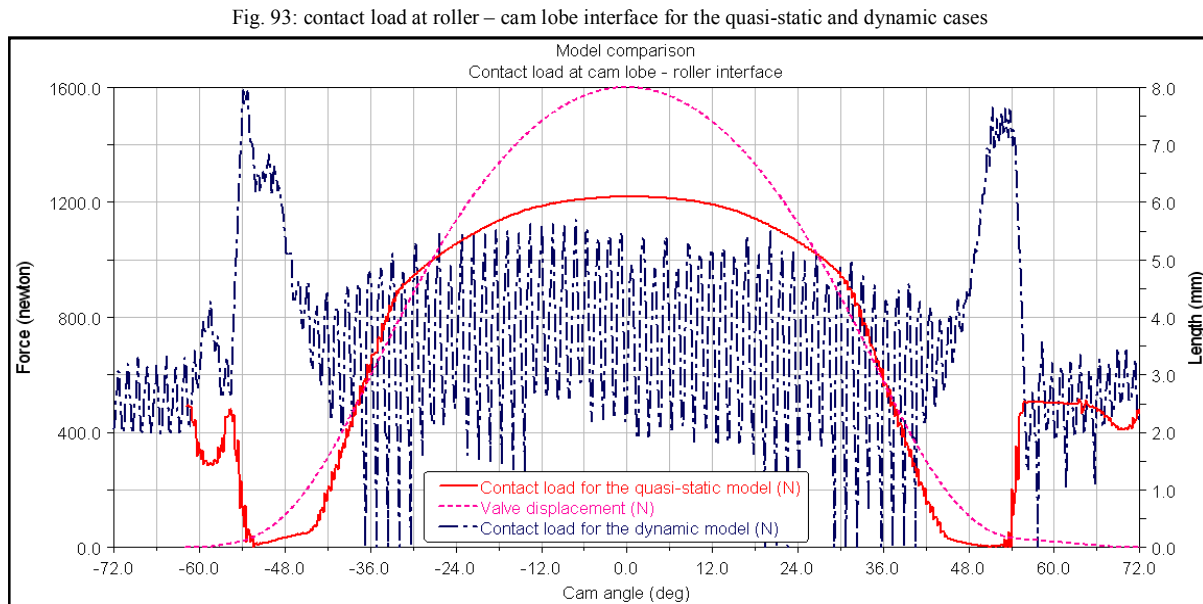

Figure 94 depicts the comparison of the semi-width dimension of the contact area in the roller-cam lobe interface. As shown in Figure 92, the semi-width dimension is strongly affected by the contact load and so, by the dynamic effects that the quasi-static does not consider. On the other hand, the comparison of Figure 92 shows how the semi-width at low speed is and how it changes in the meantime that the engine reaches the speed of 5500 rpm.

New engine concept development-Multi-body dynamic of valvetrain system and friction assessment

Antonio Turturro – Supervisors: Prof. C. Delprete and L. Magro

Fig. 94: semi-width dimension of the contact area at roller – cam lobe interface for the quasi-static and dynamic cases
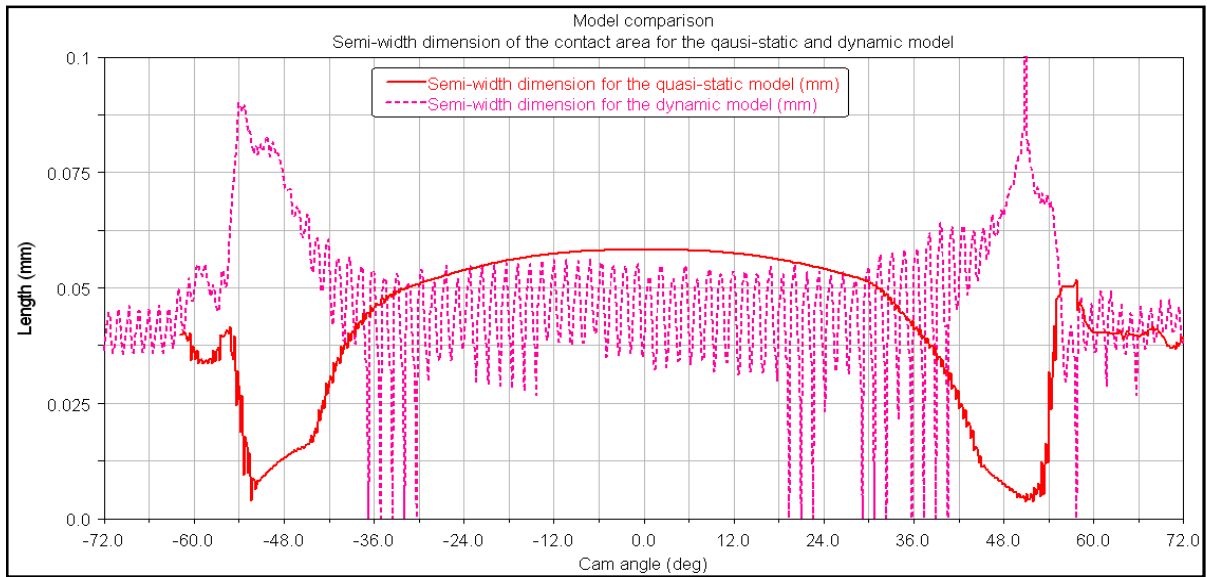

Figure 95 shows the total central deflection at roller-cam lobe contact for the quasi-static and dynamic model.

Fig. 95: total central deflection at roller – cam lobe contact for the quasi-static and dynamic cases
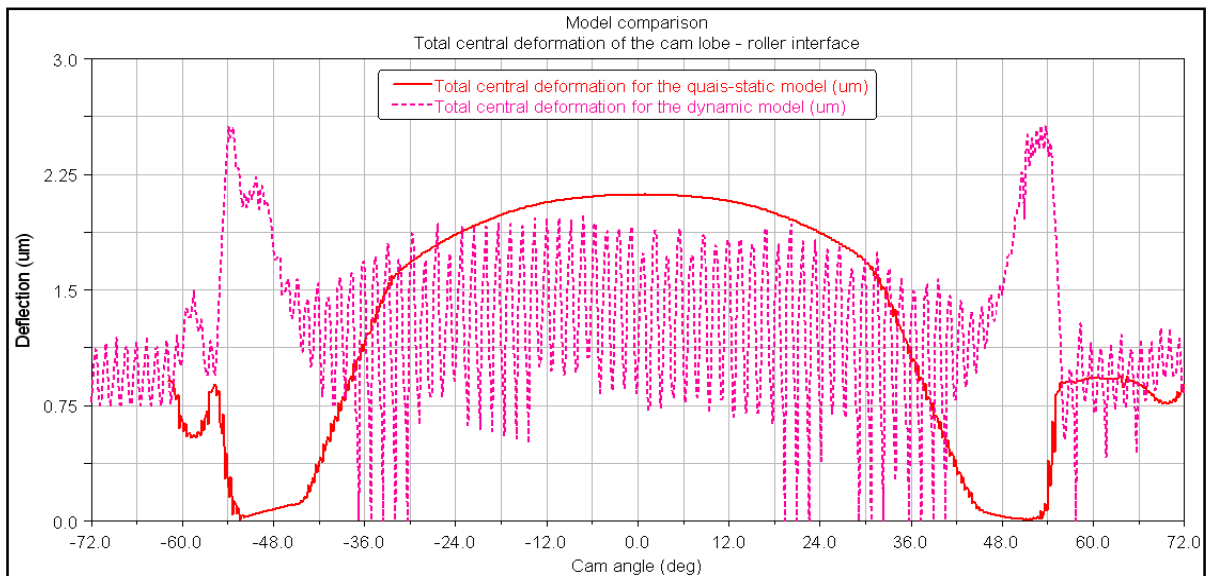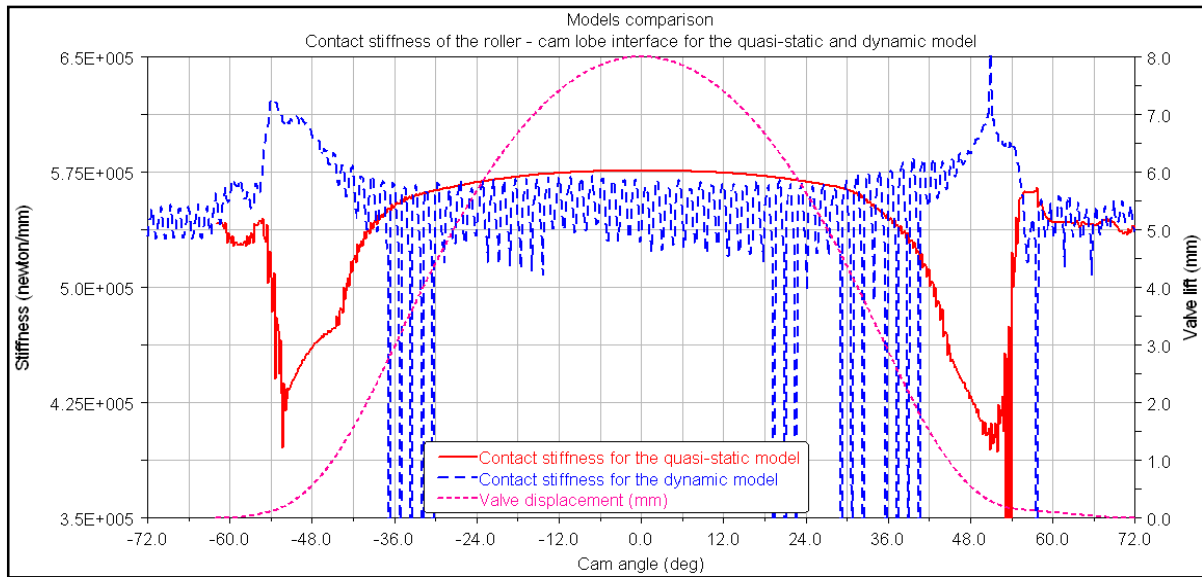

Figure 95 highlights the effect of the dynamic behaviour or in other words the extreme important contribution of the inertia force that rise up with the engine speed.

This dynamic effect is present in the contact stiffness of the roller – cam lobe interface shown in Figure 96.

New engine concept development-Multi-body dynamic of valvetrain system and friction assessment

Antonio Turturro – Supervisors: Prof. C. Delprete and L. Magro

Fig. 96: contact stiffness at roller – cam lobe contact for the quasi-static and dynamic cases

The maximum Hertzian contact pressure and the maximum Hertzian shear stress shown in Figures 97 and 99, highlights the strong linked with the contact load at roller-cam lobe interface which in the dynamic model is affected by the inertia factor.

Fig. 97: maximum Hertzian contact pressure at roller – cam lobe contact for the quasi-static and dynamic cases
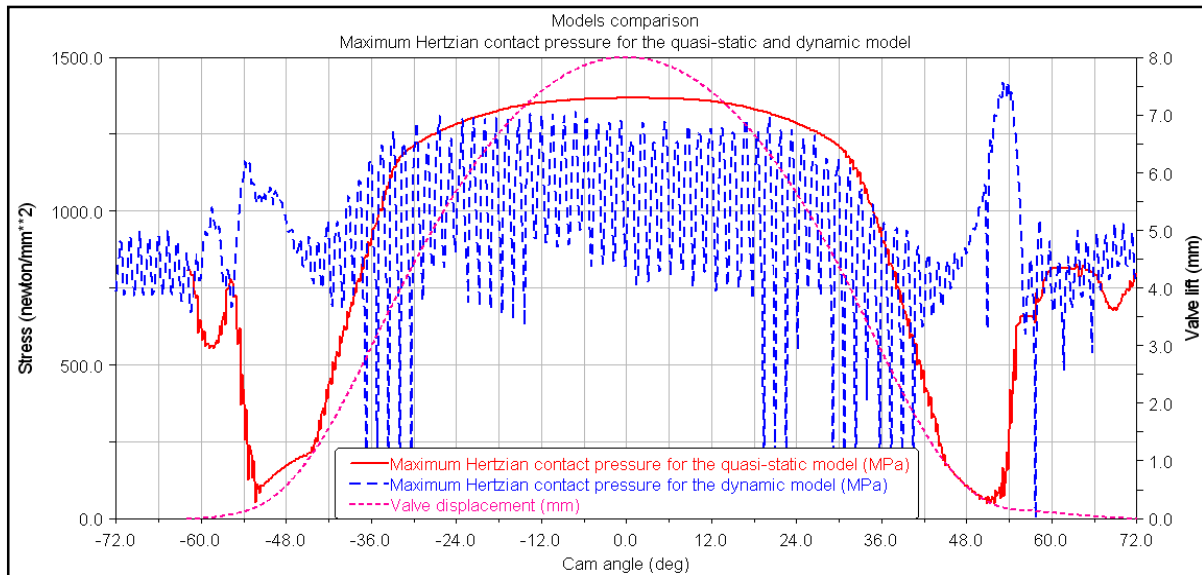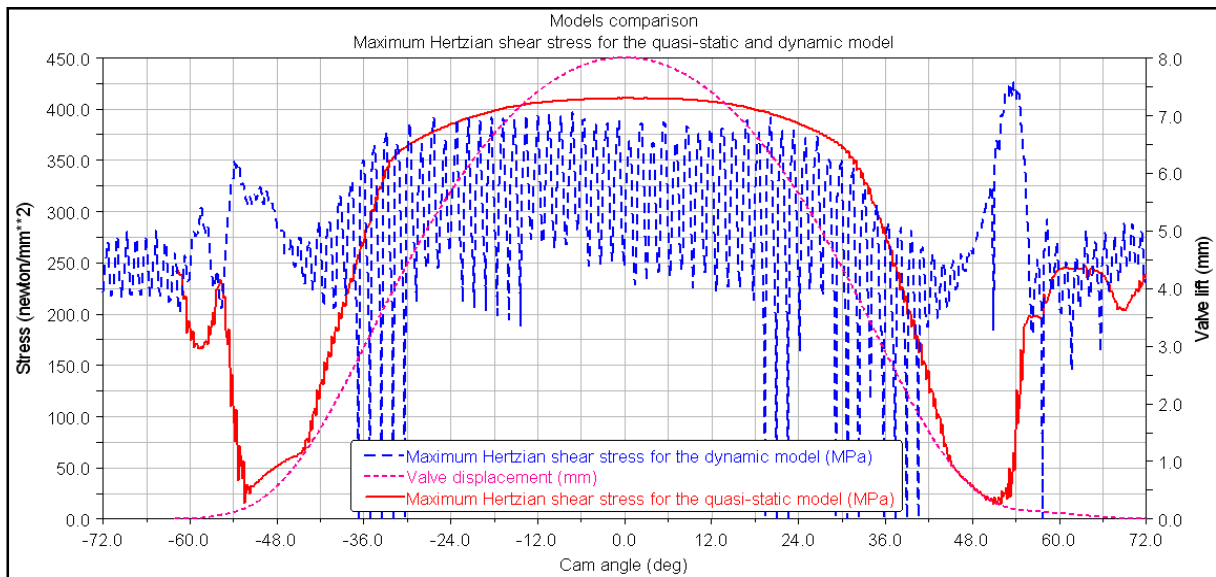
New engine concept development-Multi-body dynamic of valvetrain system and friction assessment

Antonio Turturro – Supervisors: Prof. C. Delprete and L. Magro

Fig. 98: maximum Hertzian shear stress at roller – cam lobe contact for the quasi-static and dynamic cases

III-IX Reference

1. Taylor C. M., "Engine Tribology", Tribology Series, 26, 1993, pp. 301

2. Taylor C. M., "Fluid Film Lubrication in Automobile Valve Trains", Proc. Instn. Mech. Engrs., Part J: J. Engng. Trib., 1994, Vol. 208, pp. 221-234

3. Anderson B. S., "Company Perspectives in Vehicle Tribology – Volvo", 17th Leeds – Lyon Symposium on Tribology, 1991, pp. 306-503

4. Parker D. A., Adams D. R., "Friction Losses in Reciprocating Internal Combustion Engine", IMech Conference on Tribology: Key to the efficient engine, Mechanical Engineering Publications, 19th January 1982, pp. 31-39

5. Eichhorn U., Schonfeld H., "The Valve Train of Internal Combustion Engines as a Source of Vibration – Experimental Results and Methods of Calculations", Proc. XXIII FISITA Congress, Torino (Italy), May 1990, pp. 389-395